Experimental and Numerical Investigation for the Effect of Graphite Fins and Magnets on the Thermal Performance of the Single Slope Solar Still

A Thesis

Submitted to the College of Engineering at University of Kerbela

in Partial Fulfillment of the Requirements for the Degree of Master Science in the

Mechanical Engineering

By

Ali Bani Khassaf

(B.Sc. in the mechanical engineering / University of Technology 2003)

Supervised by

Prof. Dr. Abbas Sahi Shareef   and   Asst. Prof. Dr. Hayder Jabbar Kurji

بِسْمِ اللَّهِ الرَّحْمَنِ الرَّحِيمِ

الرَّحْمَنُ ﴿1﴾ عَلَّمَ الْقُرْآنَ ﴿2﴾ خَلَقَ الْإِنْسَانَ ﴿3﴾ عَلَّمَهُ الْبَيَانَ

صَدَقَ اللهُ العَلِيُّ العَظِيمُ (4)

Supervisor' Certificate

We hereby certify that this thesis entitled " **Experimental and Numerical Investigation for the Effect of Graphite Fins and Magnets on the Thermal Performance of the Single Slope Solar Still**" prepared by the student (**Ali Bani Khassaf**), had been carried out completely under my supervision at the University of Kerbela/Mechanical Engineering Department, in the partial fulfillment of the requirements for the degree of Master Sciences in the Mechanical Engineering

Signature:

Prof. Dr. Abbas Sahi Shareef

Mechanical Engineering Department

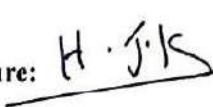**University of Kerbela**

Date: /   / 2023

Signature:

Asst. Prof. Dr Hayder Jabbar Kurji

Mechanical Engineering Department

University of Kerbela

Date: /   / 2023

Examination Committee' Certificate

We certify that we have read this thesis entitled " Experimental and Numerical Investigation for the Effect of Graphite Fins and Magnets on the Thermal Performance of the Single Slope Solar Still "and, as an examination committee, we examined the student (Ali Bani Khassaf) in its contents and in our opinion, it meets the standard of a thesis and is adequate for the award of the degree of Master Sciences in Mechanical Engineering.
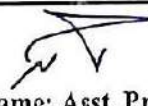
Signature:

Name: Prof. Dr. Abbas Sahi Shareef

(Supervisor)

Date: / / 2023

Signature: H . J. K

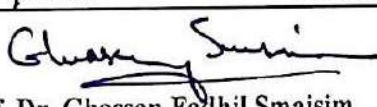Name: Asst. Prof. Dr. Hayder Jabbar Kurji

(Supervisor)

Date: 5 7 / 2023

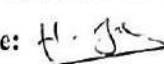Signature:

Name: Asst. Prof. Dr. Haider N. Azziz

(Member)

Date: 5 / 7 / 2023

Signature:

Name: Asst. Prof. Dr. Farhan Lafta Rashid

(Member)

Date: 5 / 7 / 2023

Signature:

Name: Prof. Dr. Ghassan Fadhil Smaisim

Date: 5 / 7 / 2023

Approval of the Head of the Mechanical Engineering Department

Signature: H . J. K

Name: Asst. Prof. Dr. Hayder Jabbar Kurji

Date: 5 / 7 / 2023

Approval of Deanery of the Engineering College

Signature:

Name: Prof. Dr. Laith Shakir Rasheed

(Dean of the Engineering College)

II

Linguistic' certificate

       I certify that the thesis entitled " **Experimental and Numerical Investigation for the Effect of Graphite Fins and Magnets on the Thermal Performance of the Single Slope Solar Still**", which has been submitted by (**Ali Bani Khassaf**) has been proofread, and its language has been amended to meet the English style.

Signature:

Name: Dr. wajde Alyhya

Date: / / 2023

Undertaking

     I certify that this research work entitled " **Experimental and Numerical Investigation for the Effect of Graphite Fins and Magnets on the Thermal Performance of the Single Slope Solar Still**" is my own work. The work has not been presented elsewhere for assessment. Where material has been used from other sources, it has been properly acknowledged / referred.

Signature:

Ali Bani Khassaf

Date: /   / 2023

<u>Acknowledgements</u>

<u>Dedication</u>

To All Whom I Love

I Dedicate This Modest Effort

To my loyal teachers, my children, my brothers and sisters and all my relatives and friends…

Ali Bani Khassaf

Date: /   /2023

Abstract

A Modified system, which was created and produced locally was used in the current investigation as an experimental setup. The primary component of the system is a solar still, along with auxiliary components, including measuring tools. The investigation was carried out numerically using ANSYS software. Solar distillation with magnets and a fin were utilized to enhance the performance of the solar distiller. Experimental and numerical investigations were performed for the temperatures of water, distiller base, steam, and the internal and external distiller glass cover. This is in addition to the efficiency and productivity of the solar distiller. The results of the experiments and the mathematical analysis showed that all the methods utilized in this study might enhance the performance of the solar distiller. This can be done by boosting the temperature of the water in the distiller, which will produce steam more quickly. Using the fins was superior to using magnets for achieving the research goal. At the same time, the use of magnets had a lesser role compared to the fins. Most important, using all these techniques collectively (solar distillation with fins and fins with magnetics) can raise the water temperature, still base temperature, steam temperature, and internal temperature of the distiller cover by roughly (24, 26, 34 and 55) %. Thus, the use of all techniques collectively can improve the efficiency and productivity, of the solar distiller by 33%, 38%, and 55% respectively in comparison to the usual case of the solar distiller (without any modification). To show the reliability degree of the software used in the current work and the accuracy and validity of the numerical results of this thesis, the results were verified by comparing these results with previous studies in the same field and under almost the same conditions. It was concluded that the software was built correctly and gave acceptable results to a large degree The highest error percentage between them was 10%, which is relatively acceptable. By comparing the experimental results of the present study with the numerical ones, a good agreement was noted between them.

This indicates that the current work was conducted according to what was planned and in a way that ensures that errors were avoided as much as possible. This was achieved by repeating the experimental tests several times and days until stable and realistic results were obtained.

Table of Contents

List of Tables

List of Figures

NOMENCLATURES

Symbol	_Description_	_Units_
A	Area of the solar still	m^2
Cp	Specific heat	kJ/kg. K
E	Energy	W
t	Time	s
g	Gravity	m/s^2
I	Incident solar energy	W/m^2
Gr	Grashof number	-
h	Heat transfer coefficient	W/m^2. K
hb	Back loss coefficient	W/m^2. K
L	Latent heat	kJ/kg
K	Thermal conductivity	W/m. K
M	Hourly productivity	kg
Q	Heat transfer rate	kJ
Ac	Area of solar collector	m^2
m	Mass	kg
P	Pressure	N/m^2
Pr	Prandtl number	-
Ra	Rayleigh number	-
T	Temperature	C^0
Ub	Overall bottom loss coefficient	W/m^2
Ut	Top loss coefficient	W/m^2
UL	Overall heat transfer coefficient	W/m^2
V	Wind speed	m/s

Greek Symbols

Symbol	Description	Units
α	Absorptivity	-
α'	Fraction of solar energy absorbed	-
ε	Emissivity	-
εeff	Effective emissivity	-
δ	Incremental rise	C^0
τ	Transmittance coefficient	-
γ	Kinematic viscosity	-
η	Efficiency	(%)
σ	Stefan-Boltzmann constant	$W/m^2.K^4$
β	Slope angle of collector	degrees
μ	Dynamic viscosity	Pa. s
ρ	Density	kg/m^3

Abbreviation

Abbreviation	Description
a	Ambient air
b	Basin
eva	Evaporation
g	Glass
gp	Graphite plate
in	Input (embodiment) energy
ins	Insulation
mg	Magnet

o	Overall
r	Radiation
s	Sun
ss	Solar still
st	Stored energy
w	Water
CSS	Conventional solar still
GPLF	Graphite plate fins solar still
GCYF	Graphite cylindrical fins solar still
GREF	Graphite rectangular fins solar still
MSS	Magnet solar still
ANSYS	Analysis of System
mg	Magnet
MF	Magnetic field
R	Thermal resistance

C
H
A
P
T
E
R

1

Introduction

CHAPTER ONE

1. INTRODUCTION

The available fresh water on earth is limited. Over two-thirds of the earth's surface is covered with water, but more than 97% of the available water is either salty or polluted. The rest, nearly around 2.6%, is fresh water. Less than 1% of freshwater is within reach of humans and other organisms. Even this tiny fraction is believed to be adequate to support life on earth, but fresh water demand is increasing daily due to the increasing population. Polluted water cannot be used directly for drinking as it has harmful microbes and dissolved substances. Many developed and developing countries of the world are facing the problem of the supply of drinking and fresh water. The methods for the production of freshwater used nowadays are as follows: reverse osmosis, multi-effect distillation, mechanical vapor compression, etc. These methods involve Signified energy drawbacks consumption in purification. The solar thermal desalination method is best suited for low-cost fresh drinking water production. Interest in solar distillation systems is increasing because they are easy to operate and have less maintenance cost [1].

	2010	2011	2012	2013	2014	2015	2016	2017	2018
Solar photovoltaic	40	72	102	136	172	217	291	384	483
Concentrated solar power	1.3	1.7	2.6	3.8	4.5	4.8	4.9	5.0	5.7
Total renewable energy	1223	1329	1442	1563	1693	1846	2009	2182	2361
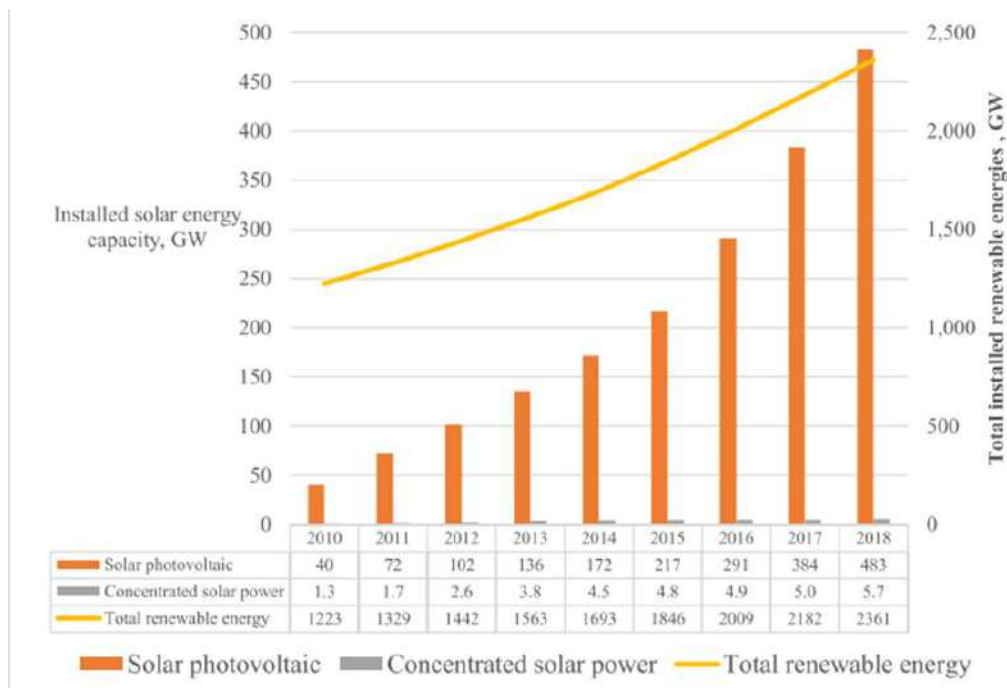
Figure (1.1) Renewable and solar energy capacity trends installed during

(2010-2018) [1]

1.1 Solar desalination

Solar distillation is classified into two primary categories based on the configuration of the manufacturing facility. In addition, the first type is the direct type, which uses a solar collector inside a solar-powered basin to heat and evaporates the basin's water directly from the sun. The second category, which is known indirectly because solar collectors and solar still are distinct, includes humidification-dehumidification as an example (HDH) [5]. The upper layer of a saltwater pond is heated using solar thermal energy that has arrived. The water evaporates and condenses on the cover due to the heated top layer of the pond. While the concentration of salts in the pond stays high, contaminants and salts are separated during water evaporation, and the water condenses to become useable [6].

1.1.1 Conventional solar stills

Solar stills mimic the natural hydrogen cycle and are one of the simplest ways to desalinate water. The basis for how it functions is how water evaporates when exposed to air. The top layer of the solar still water basin releases hot water vapor, which, as a result of the difference in temperature between the boundary of the lid, rises and condenses, creating water devoid of pollutants and salt. The solar still typically consists of a basin filled with undrinkable water, an outer covering made of transparent glass or plastic that allows sunlight to fluid through, and a conduit that collects the water produced after distillation [5].

1.1.2 Humidification-Dehumidification Technique (HDH)

In the specific assembly region, efficiency has increased and decreased depending on the principle utilized in the indirect type of solar water desalination. This is caused by several things, including the turbulent fluid of water and air mass transfer coefficients, huge vaporization surfaces, increased heat, and energy recovery strategies [6].

1.2 Solar Distillation Mechanism

The solar water purification system operates similarly to rain, with water-absorbing heat, evaporating, and condensing. Solar water distillation processes provide a closed-loop system that is more efficient due to the system's total administration, which allows it to be adjusted according to the conditions. As illustrated in Figure (1.2), the solar still unit has a glass cover, a water-resistant basin, and a black liner to maximize solar energy absorption. The basin is filled with salt or somewhat saline water, letting it heat naturally under the sun. The steam then rises and falls on the glass cover, slanted at an angle and accumulates in a bowl. The residual salty water and suspended materials are left in the basin and will be removed later [7]. As indicated in Figure (1.2) there are various classic

distillates, including (single slope, double slope glazing cover, V-shape and spherical solar still).
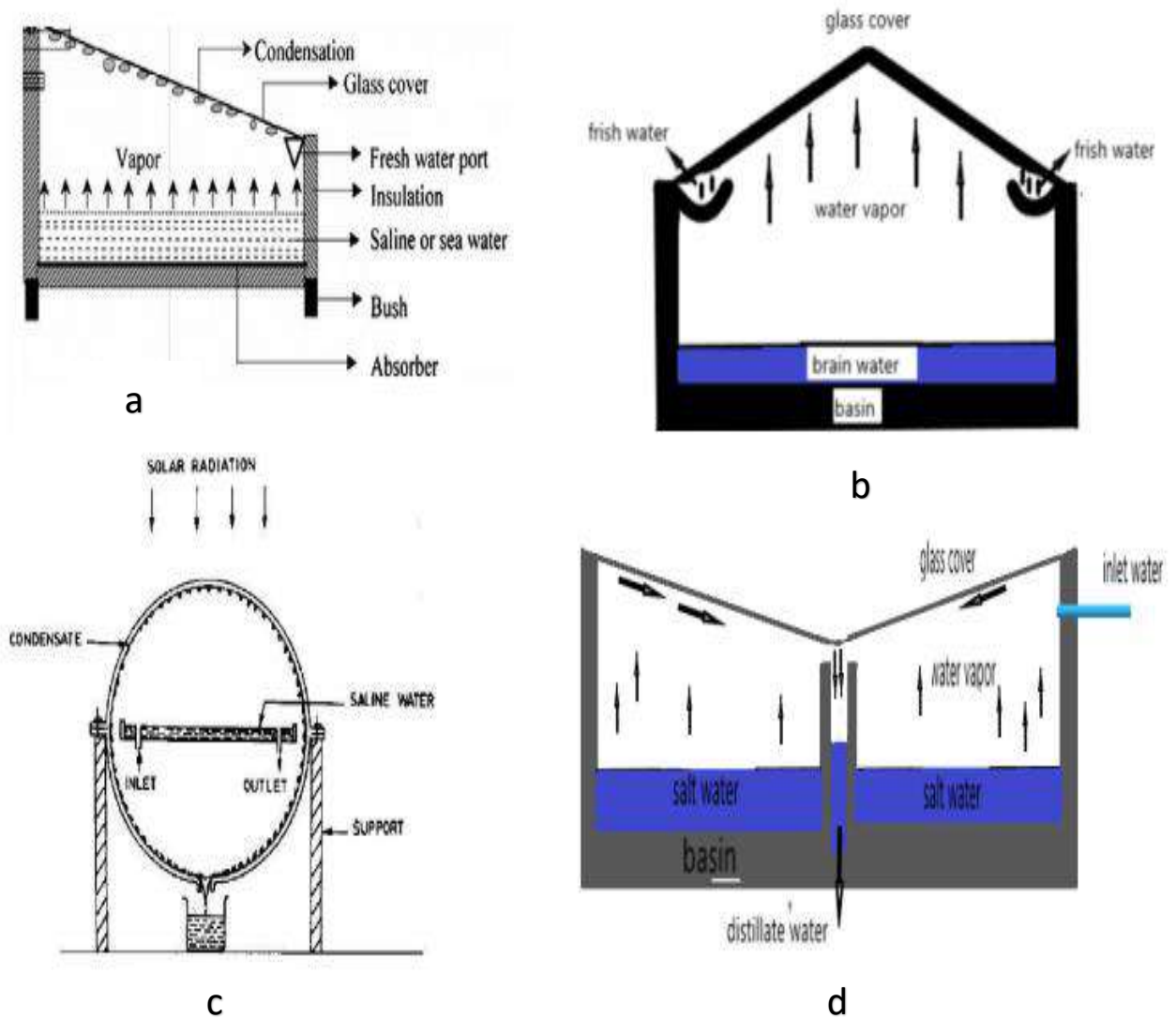
Figure (1.2): Solar still (a)Single slop, (b) Double slop, (c) Spherical. (d) V-type [7]

1.3 Solar Still

Distillation is a well-liked therapy approach all around the world. It is not surprising that numerous solar distillation systems have been created and enhanced during the past few years. The distillation process' primary drawback is its heavy reliance on traditional energy sources, which has a negative environmental impact. Solar stills, which a free and pure energy source that are can thermally drive, are a component of distillation systems. The basin-type solar still is a straightforward, easily constructed, low maintenance, and cost-effective

equipment. Despite these benefits, its low productivity prevents it from being widely used [7]. The solar still can be classified, as shown in Figure (1.3).
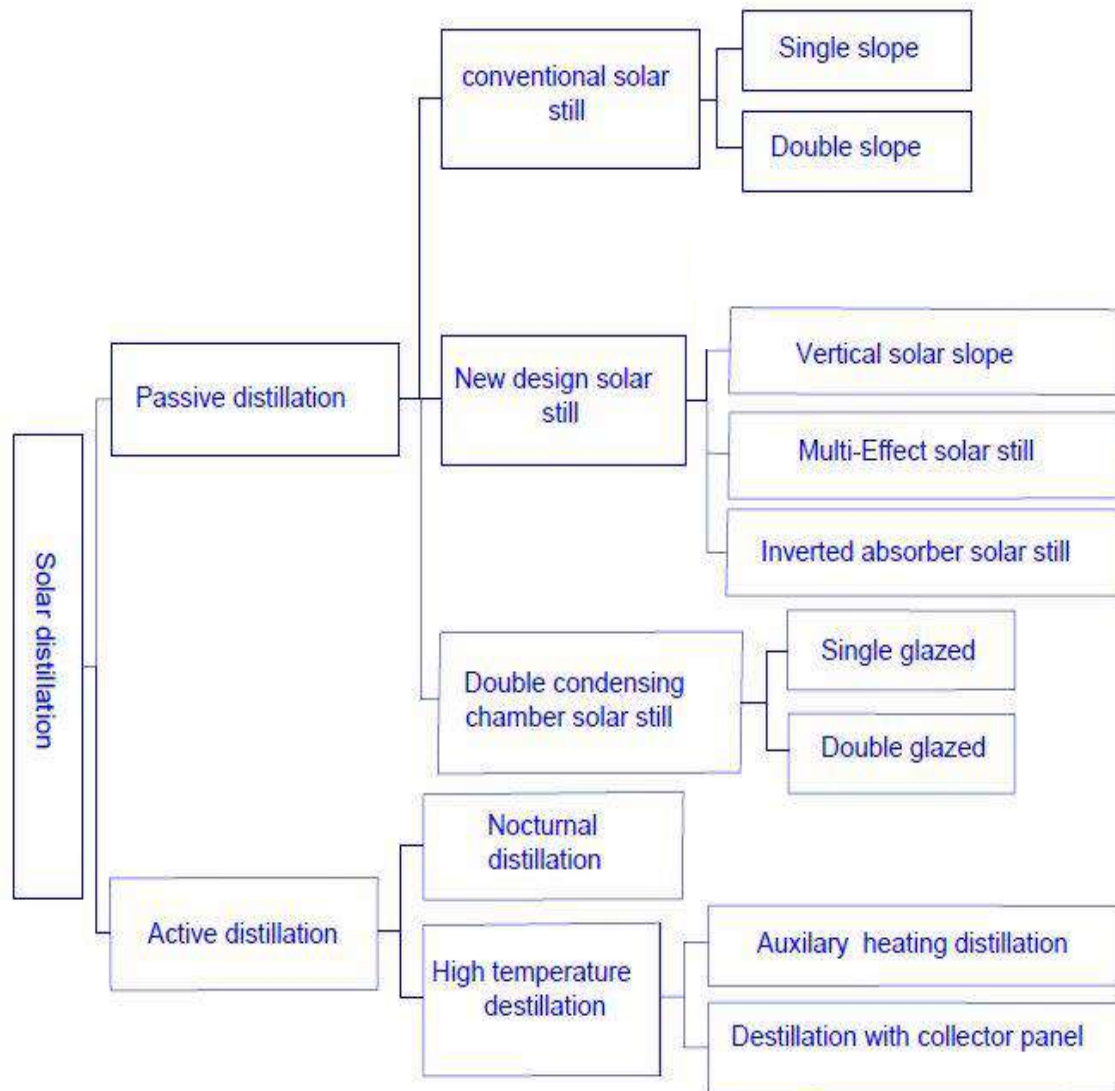
Figure (1.3) Solar still distillation classifications [7]

1.3.1 Types of Solar Stills

Two types of solar stills can be distinguished.

1.3.1.1 Passive Solar Still

Uses solar energy as its primary source of heat energy, while those that combine it with solar thermal energy are used to heat the water before distillation takes place directly. This development rate is explained by the low operating temperature and vapor pressure [8]. Passive solar stills can be categorized in various ways, such as by the size, form, number of basins, heat storage choices, and evaporator design and materials (such as wicks). Numerous basins or wicks

can provide multiple effects during distillation for a significantly larger output, as shown in Figure (1.4).
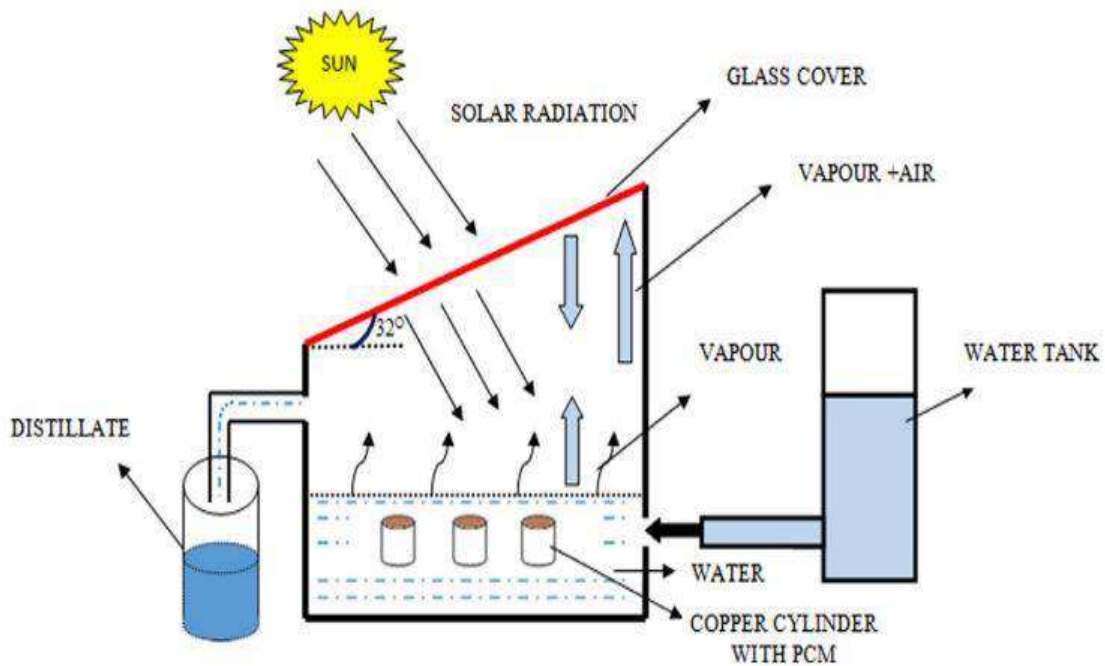
Figure (1.4) Passive solar still [8]

1.3.1.2 Active Solar Stills

These stills use extra thermal energy in the form of either a solar collector or any extra thermal energy produced by any industrial facility to combine with passive solar for faster evaporation. Factors affecting the production of basin-type solar stills [8].
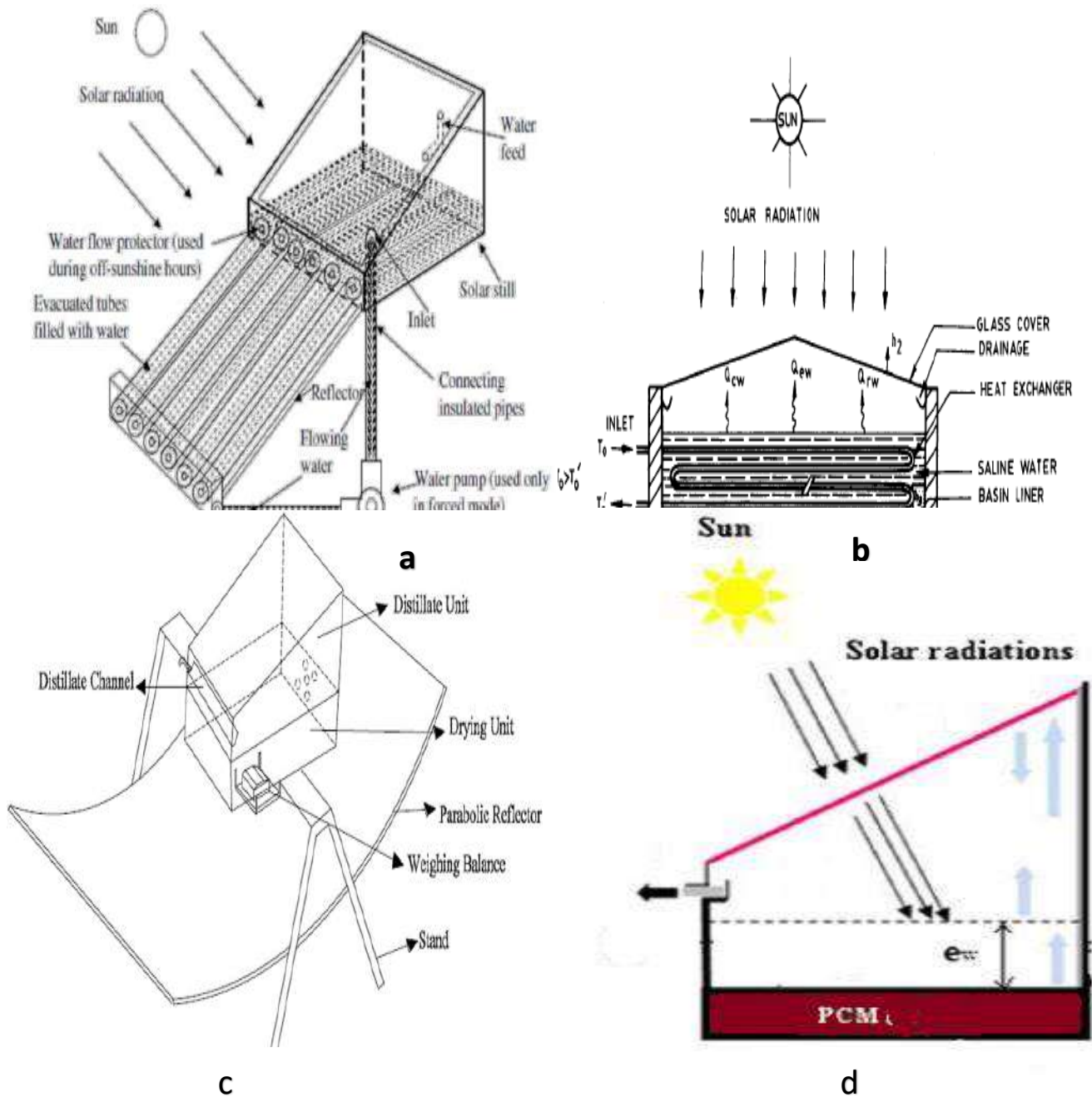
<center>Figure (1.5) Active Solar Still</center>

(a) Forced Mode with Evacuated Tube Collectors
(b) Heat exchanger
(c) cum drying unit with parabolic reflector
(d)The accumulated distillate [8]

1.3.1.3 Specially Designed Solar Still

Many changes have been made to grow the productivity of solar still by altering the design. The most important types of the new design (pyramid, spherical and tubular), as shown in Figure (1.6) [9].
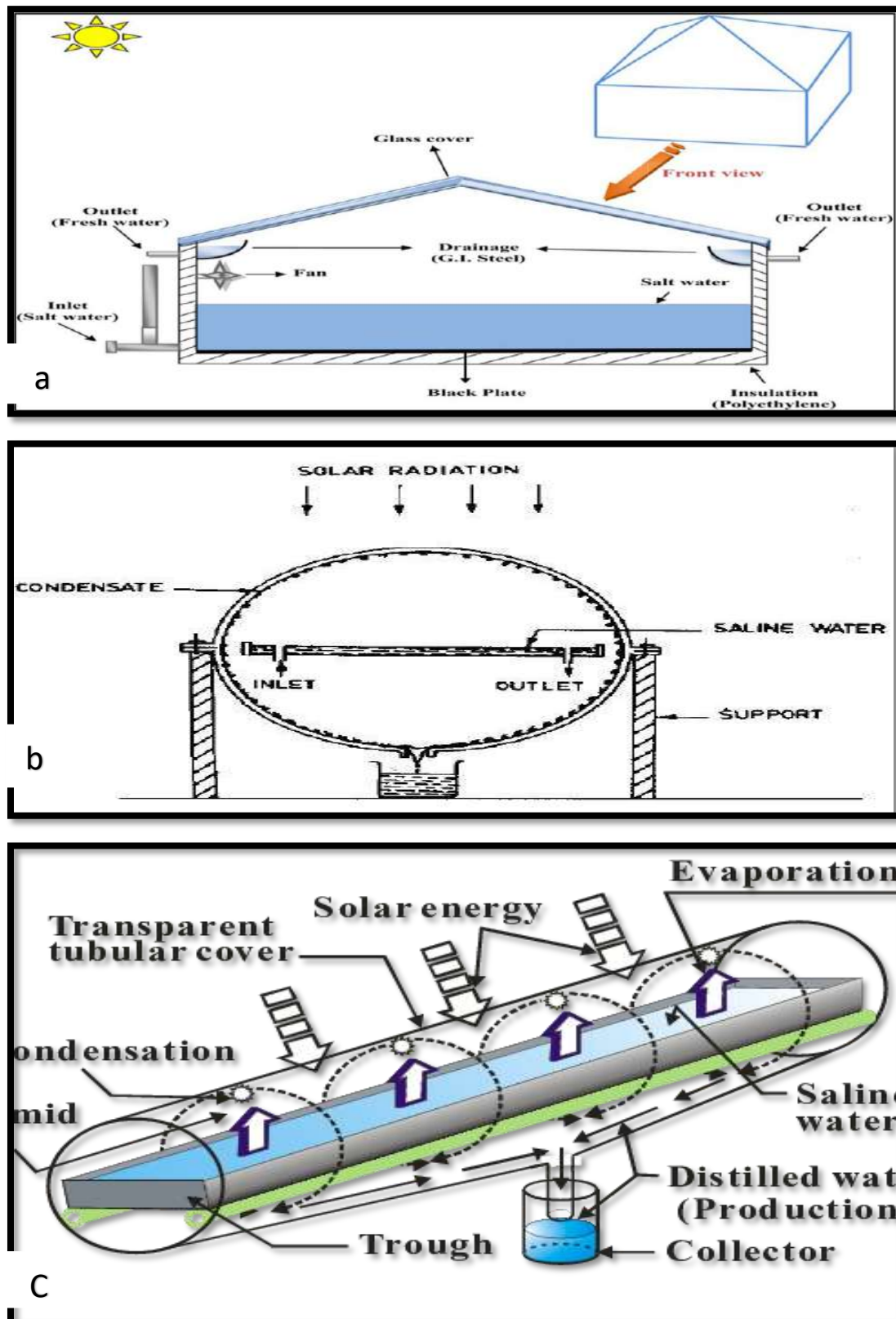
Figure (1.6) Specially Designed Solar Still

(a) Forced convective heat transfer using Fan

(b) Spherical, (C) Tubular [9]

1.4 Factors Affecting Solar Stills Productivity

The production rate and efficiency of solar desalination systems are affected by several factors. These factors include climatic, operational, and design conditions [10].

1.4.1 Climatic Factors

All climatic variables, taken collectively, impact solar still performance [11].

1.4.2 Solar Radiation

The most important component for still productivity is solar radiation. Numerous studies have looked into how solar radiation affects still productivity, and their findings show that solar productivity still rises as incident solar radiation increases [11].

1.4.3 Wind Speed

The coefficient of heat transfer from the condensing covers to the surroundings rises as wind speed rises. This widens the temperature gap between the water bulk and the cover, enhancing the natural convection [12].

1.4.4 Relative Humidity

Because of the low convection coefficient between the still and its surroundings and the lower saturation temperatures of the steam inside the still, the distilled water decreased as the relative humidity increased for a given ambient temperature, as can be seen from the effect of relative humidity at different ambient temperatures [13].

1.4.5 Temperature Difference

When considering the heat transport phenomena, brine temperature is important for all heat fluxes from basin water, including evaporation, free convection, and radiation. Higher water temperatures result in faster evaporation because the barrier between the liquid and gaseous states may be broken with less energy. Another way to look at it is that water will evaporate at saturation temperature at a particular pressure (atmospheric pressure), and the higher the brine temperatures, the closer they are to saturation temperature. As a result, it is not surprising that certain methods use excess heat to warm brine. Solar stills, in actuality, require only a few degrees Celsius to ten degrees Celsius above the environmental temperature to operate properly [14].

1.4.6 Dust and Cloud Cove

Dust buildup on the still's glass cover considerably reduces its transmittance, lowering the distillate's productivity. Cloud cover significantly lowers and significantly lessens the direct component of solar radiation [14].

1.5   Design parameters
1.5.1 Solar Reflectors

Internal reflectors are practical devices for focusing and rerouting solar radiation. They are advised when the sun is not very strong or the local temperature is not too high. To improve the flexibility of the absorber plate layout, such as the vertical solar absorber plate that is useful in recovering vapor latent heat of condensation, external reflectors are desired to be employed. When the sun is weak, or the local temperature is fairly low, external and/or interior reflectors are advised [15].

1.5.2 Angle of the glass cover's inclination

The current investigation results showed that solar production still could be quite sensitive to the choice of glass inclination angle. Under the same meteorological conditions, stills with inclination angles between 30 and 35 degrees are likely to yield less pure water than stills with different inclination angles. This might result from the still performance being more sensitive to temperature and wind at this angular range. Stills with inclination angles greater than 35 might expect output levels similar to those below 30. Due to the higher material and construction costs, employing stills with great inclination angles does not appear to provide any real advantages. [15].

1.5.3 The Inlet Water's Temperature

The temperature of the saline water regulates the evaporation rate since the latter rises as the temperature of the unpurified water does. The solar still is heated by combining parabolic concentrators, plate collectors, and a small solar pond. The entire solar still water may require a significant amount of energy to be heated. The temperature of the water-free surface area affects the evaporation rate in a direct proportion. We can utilize baffle-suspended absorber plates to improve the water-free surface area [16].

1.5.4 Thickness of Cover Plate

Two more elements that considerably impact the productivity of solar stills, Are the cover plate's thickness and the material used for the condensing cover. Highly transgressive missive content Due to their strong propensity to absorb radiation, materials like glass are frequently utilized as cover plate materials for solar stills. The highest solar still productivity is obtained with a 2-mm-thick cover plate and declines with an increase in cover plate thickness. As a result, stills with lower cover plate thickness are preferred for stills with better productivity. Cover

plates made of glass and plastic with lower densities can have productivity comparable to copper. To achieve optimum productivity, the material and thickness of the cover plate must be properly chosen [17].

1.5.5 Water Depth

The depth of the feed water influences any solar still system's production. A brief duration of operation (often 1-2 days) with shallow water depth increases production. Depth is proportional to the period of operation. Research on various water depths has revealed that depth and solar still productivity is inversely related. The solar still's productivity was still high at a small depth of 0.1 m, according to Singh and Tiwari's investigation into the effects of various water depths, including 0.05, 0.1, and 0.15 m. Even though more water is present in the solar, it still takes longer for the water to heat up [18].

1.5.6 The air gap between the water and the glass cover

The performance of the solar still can be improved by minimizing the distance between the evaporating surface and the condensing cover. The impact of reducing the gap distance is more significant than the effect of the cover slope. When the gap distance is reduced, the walls of the cover slope become shorter, reducing their shadowing effect. By decreasing the gap distance from 13.0 cm to 8 cm while maintaining the same cover slope, the output of the solar still increases by 11%. This increase is attributed to the saturated air taking less time to reach the condensing surface and promoting continuous and faster airflow within the still[19].

1.5.7 Systems for Tracking the Sun

Sun tracking is sensing and following the sun's solar radiation from sunrise to be dusk, which performed can manually or via an automated device. The explanation for sun tracking is not implausible. Since the basin-type solar still needs to heat the brine for evaporation and condensation to occur, a significant amount of the sun's irradiance must be delivered into the still basin. Higher sun intensity will result in faster evaporation and higher condensate, resulting in a larger distillate yield [20].

1.6 The effect of fin

The flat plate basin's fin-integrated solar still reduces the time needed to prepare the saline water before it evaporates. Fins speed up the heat transmission rate from the basin to the salt water, increasing the still's output [21], as shown in Figure (1.7).
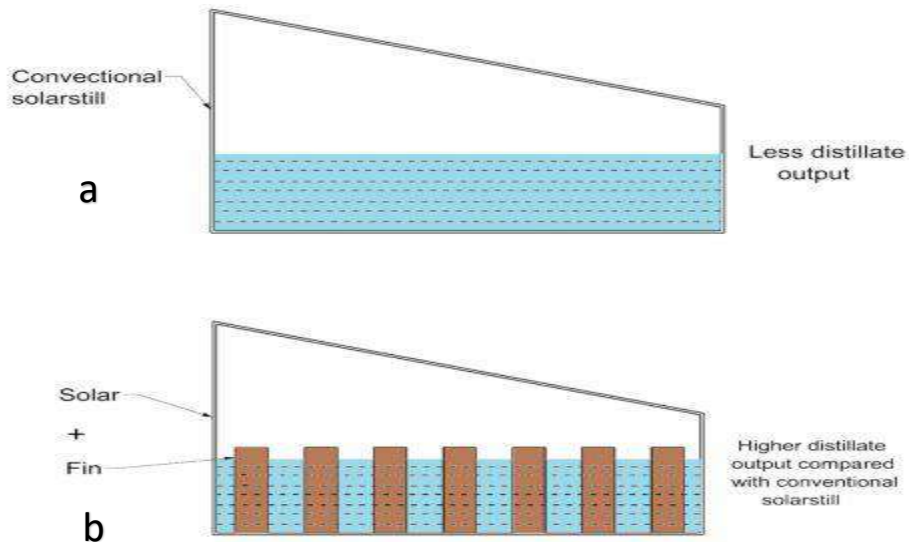
Figure (1.7) Effect of fins in solar still

(a) CSS, (b) Fins on the absorption plate [21]

1.7 Graphite

Natural graphite is a corrosion-resistant substance with a low density (2.1 g/cm³vs aluminum's 2.7 g/cm³), extremely high thermal conductivity (300-600 W/(m·K) in the in-plane direction), and a negligible coefficient of thermal expansion as shown in the table (1.1). Due to these characteristics, graphite is a great material for heat exchangers, HVAC systems, energy conversion systems, and automobile parts. The heat exchanger business has employed synthetic graphite in its products. Natural graphite thermal goods can be mass-produced affordably and with lower manufacturing and material costs thanks to the roll-embossing method. Due to their distinct characteristics, graphite heat exchangers (G-HEX) built from rolled graphite sheets could [22].

TABLE (1.1) The typical graphite laminate materials' properties [24]

PROPERTY	UNITS	DIRECTION	VALUE
Density	g/cm^3	------------	1.33
Thermal conductivity	w/m. k	In-plane	233
Thermal conductivity	w/m. k	thickness	4.5
Thermal Anisotropy	--------------	----------	52
CTE	10^{-6} m/m/^{o}c	In-plane	-0.77
Resistivity	Uohm.m	In-plane	4.9
Young Modulus	Gap	In-plane	13

Flexural Strength	Mpa	In-plane	11
Shear Strength	Mpa	In-plane	0.18

1.8 Magnetic Field

For more than 50 years, several aspects of the impact of magnetic fields (MF) on water treatment have been studied, and many researchers are still interested in this topic. The research first centered on safeguarding industrial facilities or domestic heating systems against the development of hard scales at high temperatures; more recently, the effects of MF in the liquid phase were examined in several fundamental features and potential practical applications [23]. Four different types of magnetized water (MW) were measured under the same conditions to determine the impact of magnetic field (MF) on the partial physical properties of water. It was discovered that after the MF treatment, the characteristics of TW had changed, as evidenced by an increase in evaporation rate, a drop in specific heat, and a rise in boiling point; the changes were dependent on the magnetization effect. Additionally, magnetic field strength (MFS) significantly affects the magnetization effect; the MFS of 300 mT was shown to be the ideal magnetizing condition [24].

1.8.1 The Influence of a Magnetic Field on Water Viscosity

A greater absolute viscosity was experimentally clarified based on stronger hydrogen bonding in the presence of an applied magnetic field compared with no area. The measurement is shown to rise at increasing temperatures slowly. Present these results in their experiment on the permanent magnet with a field strength of 7.5 kg and a recorded middle flow duration of water (336.27s) at (25.0 °C). The table below illustrates how a magnetic field affects water's viscosity [25], as shown in Table (1.2).

TABLE (1.2) Viscosities at varying temperatures with standard deviations and densities of water [25]

T (K)	ρ_0(kg dm^{-3})	$\eta_0 \pm$SD(mPa s)	$\eta \pm$SD(mPa s)	$\Delta\eta = \eta - \eta_0$
298	0.997 04 (0.997 07)	0.8904	$0.8915 \pm 3 \times 10^{-5}$	0.0011
303	0.995 65 (0.995 67)	$0.7972 \pm 2 \times 10^{-5}$ (0.7975)	$0.7986 \pm 2 \times 10^{-5}$	0.0014
308	0.994 03 (0.994 06)	$0.7192 \pm 3 \times 10^{-5}$ (0.7194)	$0.7209 \pm 6 \times 10^{-5}$	0.0017
313	0.992 21 (0.992 24)	$0.6533 \pm 5 \times 10^{-5}$ (0.6529)	$0.6551 \pm 6 \times 10^{-5}$	0.0018
318	0.990 21 (0.990 25)	$0.5965 \pm 5 \times 10^{-5}$ (0.5960)	$0.5984 \pm 5 \times 10^{-5}$	0.0019
323	0.988 04 (0.988 07)	$0.5470 \pm 2 \times 10^{-5}$ (0.5468)	$0.5490 \pm 4 \times 10^{-5}$	0.0020

1.8.2 The Influence of a Magnetic Field on Surface Tension

Subscript (0) refers to no magnetic field applied per unit interface area minus the entropy per unit area of the interface times the temperature. The abundance of hydrogen bonding gives water a high surface tension. The surface's internal energy will rise, the body's entropy will decrease, and there may be a significant net increase in Helmholtz's free interface energy due to hydrogen bond stabilization and an increase in the number of hydrogen bonds on the surface. Since hydrogen bonds enhance the actual volume relative to Helmholtz free energy due to their stability, Gibbs free energy does not rise with external effort (pressure-volume term). As a result, the difference in the surface level (4 cm at 10, the Tso-called Moses effect) [26] indicates that the net increase in the Gibbs free energy must be equal to the Gibbs free energy. In figure (1.8), the magnetic devices (m1 = 3300 gauss, m2 = 2900 gauss, m3 = 5000 gauss and electromagnetic m = 900 gausses) are mounted on the experimental system to obtain magnetized water. as shown in table (1.3) [27].

TABLE (1.3) Surface tension relation with magnetic fields [26]

B (T)	$\sigma \pm$ standard error (mN/m)
0	71.96 ± 0.14
2	72.12 ± 0.14
4	72.19 ± 0.14
6	72.45 ± 0.14
8	72.86 ± 0.14
9	72.99 ± 0.15
10	73.31 ± 0.16
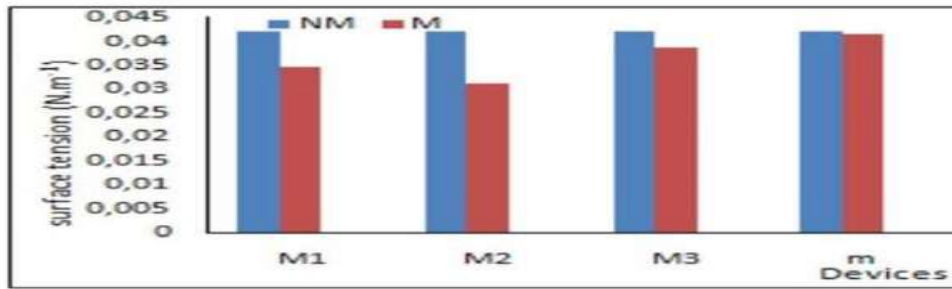
Figure (1.8) Effect of magnetic treatment of water on surface tension [27]

1.8.3 The Effects of the Evaporation Rate Under Magnetic Field

Temperature, moisture, and magnetic forces all impact evaporation, according to Yun-Zhu et al. [27]. A strong magnetic field causes evaporation rates to increase (8 Tesla). The strength of the hydrogen bonds and the shift of the Van der Waals forces at the liquid/gas boundary determine this parameter. The study above provides a motivation to research water's surface tension and its role in evaporation. As shown in Figure (1.9), they were mostly concerned with determining the significance and reproducibility of tests conducted under typical settings for a few days or weeks. If these results are confirmed, it might mean that water evaporates more quickly [28].
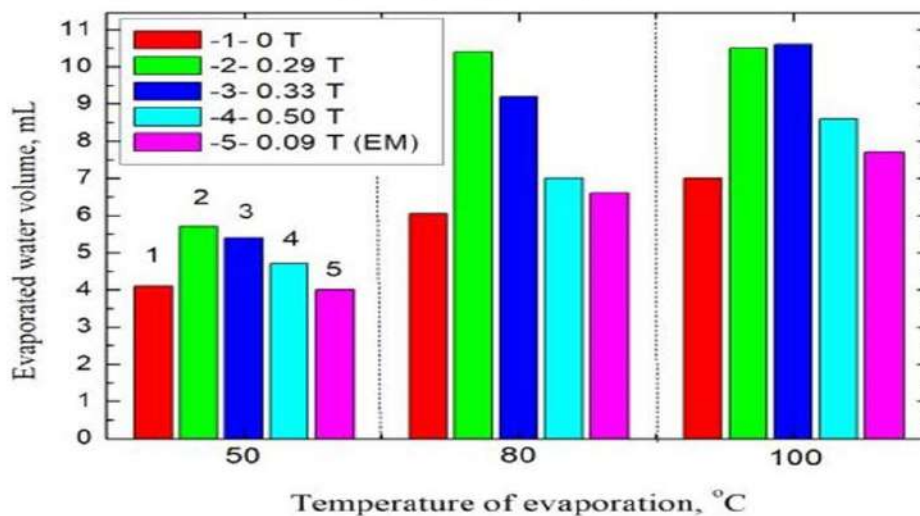
Figure (1.9) The Effects of the Magnetic field on Evaporation Rate [28]

1.9 The Aim of the Research

The aim of this research is to investigate the impact of employing fins and a magnetic field on the performance of a water solar still system with a solar collector in the outdoor conditions of Karbala, Iraq. A solar water heating system was designed and built following the engineering specifications. The study included two parts, experimental and numerical. To specify this aim, the following steps were considered:

1- Utilize Ansys-Fluent and MATLAB to model and simulate the impact of various factors on solar performance, including fin types, time, and magnetic field effects.

2- Construct a test rig to prevent total evaporation and condensation, ensuring accurate measurements and evaluation of the solar collector system.

3- Compare numerical and experimental results for different system configurations: without fins, with fins, with magnetic field, and without magnetic field.

4- Investigate the influence of fin height on system performance and identify the optimal height for maximizing system efficiency.

5- Analyze the effect of fin shape on solar system performance and determine the most suitable shape for optimal performance.

6- Evaluate the impact of fin thickness and material selection on solar system performance, identifying the optimal thickness and material for maximizing system efficiency.

2

LITRURE REVIEW

CHAPTER TWO

LITERATURE REVIEW

2.1 Introduction

This chapter reviews several studies and work on improving and rising the effectiveness of solar distillers and using creative designs and supplementary heat energy sources, like solar collectors or modified absorber plates, to warm the water inside the basin. Additionally, several researchers have conducted numerous investigations to leverage the properties of phase transition materials to store thermal energy that may be used in low solar radiation or after sunset.

2.2 Theoretical Studies

Kuan et al. [29] numerically analyzed the performance of a heat pump–assisted solar still with the concept of latent heat released during the condensation of water vapor regenerated using a compression heat pump for preheating the inlet saline water before entering into the solar still basin. The study improved the productivity by about 62% compared to CSS during summer climate.

Hansen et al. [30] researched inclined solar still with new wick elements and wire mesh. Various wick elements related to the wood pulp, coral fleece, and polystyrene sponge were recycled in flat and stepped absorbable plates. The maximum yield of 4.28 L/ day was reported when adopting coral fleece and wire mesh coated on the stepped-type absorbable plate.

Kabeel et al. [31] compared the productivity of a solar still using cement-coated red bricks with CSS and reported with 45% improved productivity. The results observed that the cement-coated red bricks have a higher heat absorption rate than normal red bricks.

Abu-Arabia et al. [32] studied theoretically a hybrid solar distillation system with a sun-heating collector. To increase the efficiency of distillation water, The study employed PCM. To boost water productivity at night, used sodium thiosulfate pentahydrate as a PCM used during the day to store thermal energy, also investigated how cooling the glass cover affected thermal performance. And created drinkable and hot water using a hybrid technique. According to the findings, the PCM well raised the basin's water temperature and productivity by 100%. Cooling of glass covers boosts output by 37%.

Medugu and Ndatuwong [33] made a theoretical study in which solar energy was used to distil water to calculate the results of some variables during the day. It was noted that the temperature of water and glass rises to a high level due to the heat flow transmitted through the glass (evaporation, radiation, and convection). The study favorably agreed between theoretical analysis and water produced by solar distillation.

Badran [34] studied theoretically the important factors related to improving the productivity of the solar still to verify the validity of the experimental results based on some factors such as (transmittance, solar radiation intensity, total heat loss coefficient, effective absorbance, the difference between external cover temperatures, water and wind speed, and change in insulation thickness 1, 1.5, 2 and 5 cm. The performance of the single-slope solar still and the effect of external conditions on the still, as it was found that by increasing the temperature of the basin water, the productivity increases, as well as the utilization of the latent heat to increase the distillation, as well as the productivity increases by increasing the difference between the temperature of surface condensation and evaporation.

Reddy [35] investigated the performance of combined solar desalination and hot water system. In his research, a solar device that can produce hot and drinking water was used, which was proposed and simulated using a mathematical model. It was proposed to use a tilted basin and a traditional basin. In this system, the solar distillate yields increased compared to the traditional system by 107%. The average temperature rate for hot water output of the solar distillation during the winter and summer was 45.09 ° C and 56.28 ° C, respectively. The water depth in the basin is 0.01 m, and the optimum thickness of the fluid film is 0.001 m. The perfect gap between condensing and evaporating surface is 0.1 m .The total efficiency of the unit through the winter and summer is about 59.61% and 67.018%, respectively.

Abd Elbar et al. [36] evaluated theoretically the performance of a single-slope solar still using energy assessment techniques. The study used a condenser with a tip fin as a heating element instead of the glass plate typically used in a standard solar still. The model's prediction of the distilled water rate in the solar still was very close to the experimental literature data. The suggested solar still had a better performance than a regular solar still. The solar still with a heating element as a condenser had a maximum productivity and efficiency of 0.88 kg/m^2 per hour and 61.72 percent, respectively, according to the results, compared to 0.43 kg/m^2 per hour and 30.35 percent for traditional solar stills under the same conditions. The solar still with the heating element condenser had an overall output of 5.25 kg/m^2 per day, compared to 2.77 kg/m^2 per day for a standard solar still. Using a heating element as a condenser improves the performance of the solar still.

Tiwari and Tiwari [37] studied annual performance analysis and thermal modelling for condensing cover inclinations. The conclusion reported that the optimum angle of 15° was the best in summer and rainy seasons for single-sloped solar, while the 45° was much better in winter. This study shows that the solar

angle must be positioned correctly for maximum performance. The depth of seawater in the still determines the evaporation rate of seawater.

2.3 Experimental Work

Dumka et al. [38] improved the solar still performance using sand-filled cotton bags as a sensible heat storage material for different quantities of basin saline water. The excess heat absorbed in the solar still basin was stored using sand during the peak sunshine hours. The result reported improved energy efficiency of about 31.3% for 40 kg and 28.9% for 50 kg compared to CSS.

Jani and Modi [39] studied the performance of the double slope solar stills using square and circular fins. The study has improved the efficiency of the solar still by 54.2% using circular fins and 26.8% using square cross-sectional fins. The results also showed maximum water depth productivity of 1- cm.

Design parameters for still using phase-changing materials were studied by **Khandagre et al. [40]** The experimental investigation was done on a double slope still. The basin was coated using a blackened absorbing surface, and the phase-changing material (PCM) (paraffin wax) was placed on the still basin, which was called an organic PCM. The comparison study was done between organic and inorganic PCM. Eutectics are used as an inorganic PCM. This yield still improved from 8.02 to 8.07 L/m^2 /day, which was more than the CSS, whose improvement was 4.01 to 4.34 L/m^2 /day.

Hidouri and Mohanraj [41] experimented with a heat pump–augmented solar still with different glass angle inclinations and improved the energy efficiency by 84.5%. The study also reported that the glass positions in solar still have a major role in performance enhancements.

Dumka Pankaj et al. [42] conducted a study to evaluate internal heat transfer coefficients, internal efficiency, exergy efficiency, and exergy destruction. The average partial pressure difference between basin water and inner condensing cover surface for MSS is 77.99% higher than CSS when experiments were carried out for 13 h. The maximum value of MSS's evaporative heat transfer coefficient leads over the CSS by 28.65% at 13:00 h. The distillate yield recorded during the experimentation for MSS is 49.22% higher than CSS. Water magnetization has enhanced MSS's overall internal and exergy efficiency over CSS by 49.17% and 110.26%, respectively.

Sharshir et al. [43] conducted experiments on solar still using graphite nanoparticles, film cooling, and phase change materials. Their results reported that solar productivity still improved by 73.8% compared to CSS.

Panchal and Shah [44] performed experimental work on three solar stills using nearby materials. The first solar is still of the traditional type, the second sun is made of aluminum plate, and the third solar is still made of galvanized iron.

Here, an experiment was conducted to increase distillate yield from the solar still. Experiments show that a solar still with aluminum plates inside produces 30% more energy than a regular solar still, while a solar still with galvanized iron plates inside produces 13% more energy than a typical solar still. Aluminum plates are, therefore, the finest to use with a solar still to increase distillate output.

Kaviti et al. [45] examined the state of many designs that employed now to increase the output of inclined solar stills. The most crucial design factors affecting productivity are glass inclination optimization, absorber plate area, the free surface area of water, and water depth. The biggest challenge with traditional stills is maintaining a shallow water depth and a broad water surface area. An inclined solar still can enhance water surface area while maintaining minimum depth.

The performance of a solar still enhanced with a pin-finned wick evaporating surface is the subject of an experimental examination in the work conducted by **Alaian et al. [46]** Two identical solar stills are used in the experimental setup, one conventional and the other featuring an evaporating pin-finned wick surface. The stills' productivity is tested experimentally to see how using a pin-finned wick affects it. Experimental data show that the growth in distillate changes depending on the surrounding environment. When the pin-finned wick is used in the still, it is demonstrated that the still's productivity increases. When the pin-finned wick is utilized, a system efficiency of roughly 55% is observed. During this series of studies, a rise in the still production of much more than 23% is noted.

Montazeri et al. [47] investigated the development of a step-type solar still with a sloping absorber plate. Under similar working conditions, the productivity index was experimentally evaluated in two different types of solar still. A review of the theoretical model revealed that the new absorber plate design absorbed 36% more solar radiation on a sunny day than the standard still. The modified still's overall productivity of 5.19 kg/m^2/day, or efficiency of 49.2% on a bright day, was determined in comparison to the ordinary still's daily efficiency of 42.3%, with the total productivity of 4.46 kg/m^2/day. The modified cascade solar still showed a 16% productivity boost on a sunny day. Still, on a chilly day, output was not an appreciable difference between the two stills under consideration.

Szcześ et al. [79] studied the magnetic field effect on thermal conductivity and evaporation of water; water was exposed to a weak static magnetic field (MF) produced by a stack of magnets (B = 15 mT) or a single permanent magnet (B = 0.27 mT) for various periods. Even after the water has been distilled, the MF decreases the water conductivity, which is inversely proportional to the flow rate, and increases the evaporated water. The hydrogen link network is strengthened, and the water's air Nanobubbles perturb the gas/liquid interface.

Amiri and Dadkhah [48] used magnetic field or physical water treatment as an attractive but controversial issue. According to their findings, the surface tension of water is too sensitive to trial conditions to be considered a safe and reliable indicator for testing the impact of magnetic fields on water. According to research, significant changes in the surface tension of a liquid sample after a day can be a useful indicator of physical or chemical changes in the sample.

Cai et al. [49] studied the effects of a magnetic field on the water experimentally. The physicochemical properties of water were altered as a result of this treatment, as evidenced by a decrease in surface tension and an increase in viscosity over time. The magnetic treatment makes the water even more stable, with lower molecular energy and higher activation energy than the calculation based on the results.

Chibowski et al. [50] carried out experiments on the magnetic field (MF) special effects on water evaporation rate and surface tension at room temperature (22–24 C) using neodymium ring magnets (0.5–0.65 T). The amount of water evaporated is partly influenced by which pole of the ring magnet was pointed up. The relatively strong MF (0.65 T) caused a small decrease in surface tension (2.11 mN/m) that lasted for more than 60 minutes, and the memory effect faded gradually. The MF action reduced the surface tension data. The study discovered that MF affects the hydrogen bonds between and within clusters of water molecules, possibly causing some of them to break. The Lorentz force is also taken into account.

Fujimuraa and Iino [26] investigated the surface tension of the water-air interface under magnetic field experimentally up to 10 T. It was discovered that as the square of the magnetic field increased, the surface tension increased linearly. At 10 T, the surface tension increased by 1.32 0.13 mN / m, or 1.83 0.18 percent. One explanation is that stabilizing hydrogen bonds raises the bulk Helmholtz free energy, raising surface tension. Another reason is that the Lorentz force dampens ripplons' surface excitation, lowers surface pressure at the surface, and thus raises surface tension.

Ghauri and Ansari [25] explained the effect of an applied magnetic field on water viscosity. In the presence of an applied magnetic field, absolute viscosity is higher than in the absence of a field, which stronger hydrogen bonds can explain. At higher temperatures, the measurement consistently increases. In a 7.5 kg. transverse magnetic field, the relative increase in viscosity is on the order of 103, where the viscosity changes compared to no-field viscosity at a given temperature.

Holysz et al. [51] looked into a weak static magnetic field (B = 15 mT), which was applied to water and electrolyte solutions for 5 minutes. The amount of evaporated water and its conductivity were then measured as a function of time.

These numbers were also obtained for magnetically untreated samples as reference systems simultaneously. A magnetic field regulates these two parameters, and their variations are affected by the thermodynamic functions of the hydration of these ions. A roughly linear conductivity variation was discovered compared to 'scaled' functions. According to this theory, the magnetic field induces changes in the hydration shells of the ions.

Pang and Deng [52] reported the properties of water and their changes under a magnetic field's action by the spectrum techniques of infrared, Raman, visible, ultraviolet and X-ray lights, giving insight into water's molecular and atomic structures. After applying the magnetic field, it was observed that some properties of water changed, as well as a change in the physical behavior of water. The magnetized effects of water are related to magnetized time, the intensity of an externally applied magnetic field, and the temperature of the water, although these relationships are not linear. Experiments revealed that the size of magnetized water contact angles on the surface of hydrophobic materials reduces, lowering the surface tension force of magnetized water compared to pure water.

Hamouda et al. [53] investigated the effects of magnetic treatment of irrigation water on surface tension and evaporation. The study employed four separate pieces of equipment, each with its characteristics. The introduction of a magnetic field changed the characteristics of the water, lowering the surface tension by up to 24% and increasing the volume evaporated in the raw water. Their experimental results are significant, according to statistical analysis.

2.4 Theoretical and Experimental Investigation

Gnanaraj and Velmurugan et al. [54] improved the performance of double slope solar still using fins, black granite, wick, reflector, and internal and external modifications by 58.4%, 69.8%, 42.3%, 93.3%, and 171.4% respectively when compared to CSS. Their results also showed that the internal and external modifications in the solar still could improve the overall thermal performance when compared to the usage of heat storage materials.

Nazari et al. [55] conducted experiments on a single-slope solar still coupled with a thermo-electric channel and nanofluid. The study improved the productivity, energy efficiency, and exergy efficiency of solar still using thermo-electric channels by 38.5%, 38.9%, and 31.2%, respectively. In addition, the solar still with thermoelectric channel and 0.08% nanofluid has enhanced the productivity, energy efficiency, and exergy efficiency by 82.4%, 81.5%, and 92.6%, respectively.

Yousef et al. [56] improved the energy and exergy efficiencies of the CSS using different absorbing materials by 25% and 5%, respectively. The productivity and carbon credit cost were reported as 0.0343 USD and 226.6 USD,

respectively. Their results also proved that the heat-absorbing materials have significantly reduced the exergy losses in the solar still basin.

Dhivagar et al. [57] made a 4E analysis of gravel coarse aggregate sensible heat storage material–assisted solar still. It was reported that the energy and exergy efficiencies were improved by 32% and 4.7%, respectively. The productivity cost was estimated as 0.0618 USD per liter, and the payback period was estimated as 4.3 months. The coarse aggregate solar still has 8.27 tons of CO_2 emissions for 10 years.

Dhivagar and Murugesan [58] conducted a study where they demonstrated the improved productivity, energy efficiency, and exergy efficiency of GPF-MSS compared to CSS. The GPF-MSS system showed a 19.6% increase in productivity, a 21.4% improvement in energy efficiency, and an 18.1% enhancement in exergy efficiency when compared to conventional solar stills (CSS). These findings highlight the significant advantages and superior performance of the (GPF-MSS) system over traditional solar stills, indicating its potential for more efficient and sustainable water desalination processes. The results of this study provide valuable insights into the potential of GPF-MSS as a promising technology in the field of solar desalination.

Samuel et al. [59] conducted a theoretical and experimental study of single-slope solar still using salt balls and sponges to store energy. The results showed that the use of salt balls gives the highest product comparison with the presence or absence of the sponge; water production was 3.7 L/m^2, 2.7 L/m^2, and 2.2 L/m^2, respectively. Finally, the use of materials and low cost of solar distillation produces water at the expense of less.

El-Agouz. [60] suggested a practical and theoretical investigation to develop the performance of solar distillation using a stepped still basin with the possibility of water circulation at the same conditions. Two types of water were used seawater with total dissolved solids (TDS) entering 57100 mg/L and salty water, with (TDS) reaching 2370 mg / L before desalination. The effect of using each black and cotton was studied with the stepped still basin. The results showed an improved water production when using saltwater and seawater with black absorption compared with conventional still about 48% and 43%, respectively. While the creation of water using saltwater and seawater with cotton was 47% and 53%, the efficiency increased to about 20% higher than the conventional still.

2.5 The Scope of Present Work

The above review of the previous studies can be divided into two main categories:

1-The analysis of theoretical studies and practical experiments aims to improve the performance of solar stills by using innovative techniques such as heat pumps, new wick elements, cement-coated red bricks, and phase change materials (PCM).

The impact of magnetic fields on the performance of solar stills and the use of advanced materials such as advanced solar coatings and nanomaterials are also explored.

2- Furthermore, these studies involve modeling and simulation of performance using computer programs and engineering modeling tools to analyze the behavior of solar stills and understand the factors that affect their performance.

Overall, these studies aim to increase energy productivity and improve desalination efficiency by developing new designs and using advanced materials and innovative techniques in solar stills.

2.6 Review Design Conditions Single Slope Solar Still with Graphite Fins and Magnets

Reference	Studied Parameter	Year	Results
Tarawneh et al. [61]	Effect of water depth	2007	Lowest possible depth
Kabeel et al. [62]	Effect of water depth	2019	Lowest possible depth
Aljubouri et al. [63]	Effect of water depth	2017	Lowest possible depth
Hitesh et al. [64]	Effect of Performance on variations of the glass cover thickness	2016	The best thickness was 4mm
Panchal et al. [65]	Effect of Performance on variations of the glass cover thickness	2012	The best thickness was 4mm
Edeoja et al. [66]	Effect of Performance on variations of the glass cover thickness	2015	The best thickness was 4mm
Nafey et al. [67]	Effect of the Thickness of Galvanized Cover Sheets on Productivity	2001	The best thickness was 2mm

Reference	Studied Parameter	Year	Results
Rashid et al. [68]	Effect of the Thickness of Galvanized Cover Sheets on Productivity	2020	The best thickness was 1.1mm
Tigrine et al. [69]	Effect of the Thickness of Galvanized Cover Sheets on Productivity	2021	The best thickness was 2mm
Hitesh and Shah [70]	Effect of Coating material to the bottom surface on efficiency	2011	Found the best productivity was when black painted
Moustafa et al. [71]	Effect of Coating material to the bottom surface on efficiency	2022	Found the best productivity was when black painted
Mevada et al. [72]	Effect of Coating material to the bottom surface on efficiency	2022	Found the best productivity was when black painted
Taqi et al. [73]	Effect of material Insulation to Galvanized Cover Sheets on Productivity	2021	Used Cork sheets 6cm & plywood panels 1.1cm
El-Agouz et al. [60]	Effect of material Insulation to Galvanized Cover Sheets on Productivity	2014	Used 30mm glass wool with a layer of aluminum thickness (0.5mm)
Abdullah et al. [74]	Effect of material Insulation to Galvanized Cover Sheets on Productivity	2013	Used Fiberglass 5cm thick

Velmurugan et al. [75]	The effect of the shape and dimensions of the fins on performance	2008	Found the best productivity was when they used five solid rectangular fins of 35mm height, 900mm length, and 1mm breadth welded at the bottom of the basin
Modi et al. [76]	The effect of the shape and dimensions of the fins on performance	2022	Found the best productivity was when they used 16 wick-fins with outer diameter of 0.0254m and height of 0.02m
Bataineh and Mohammad Abu Abbas [77]	The effect of the shape and dimensions of the fins on performance	2020	Found the best productivity was when they used flat plate thickness of 0.001mm, pitch length
Dumka et al. [42]	The effect of Magnetic, quantity, and distribution method on water evaporation	2019	The best amount of evaporated water was achieved when they used a magnetic field of 90mT with a pitch of 0.2m
Seyfi et al. [78]	The effect of Magnetic, quantity, and distribution method on water evaporation	2017	The best amount of evaporated water was achieved when they used a perpendicular magnetic field at the interface with the N pole being upward
Szcześ et al. [79]	The effect of Magnetic, quantity, and distribution method on water evaporation	2011	The best amount of evaporated water was achieved when they used B = 0.27
Wang et al. [23]	The effect of Magnetic, quantity, and distribution method on water evaporation	2018	The best amount of evaporated water was achieved when they used B = 0.3 mT

Mathematical Model
& Numerical Analysis

Chapter THREE

Mathematical Model and Numerical Simulation

3.1 Introduction

This chapter is divided into two main sections: the first section includes the mathematical equations, which govern the heat transfer inside the solar water distillation system while the second section devotes to the details of the construction of the numerical software (computational program) used in the current research. The purpose of this study is to conduct numerical investigations on the temperature profiles of the water and steam within the distiller, as well as the temperature distribution across various components of the solar water distillation system, including the base and glass cover of the distiller.

3.2 Mathematical Model

This section shows the partial differential equations governing Two phase flow's thermal properties inside the solar distillation system. These equations are the continuity, momentum and energy equations in addition to some assumptions.

3.2.1 Assumptions

The following assumptions would be applied to obtain the energy balance equations [26], [80].

1- The water inside the basin of the solar distillation device is maintained at one level.
2- The heat capacities of the absorbed materials, insulation materials and glass cover are neglected.
3- The vapor leakage from the distiller is neglected.
4-The temperature gradients in the water depth and the glass cover are neglected. 5-The heat transfers solar distiller basin liner is done by the one-dimensional and quasi-steady state heat conduction,
6-Laminar, incompressible flow,
7-The tests are carried out at the atmospheric pressure conditions,
8-The variation in the temperature of insulating materials is neglected.
9-The inclination angle of the glass cover is negligible.
10-The basin of a solar still is insulated to reduce conductive heat loss.
11-The thermophysical properties of glass and saline water are assumed constant.
12- Solar irradiation is directly striking the basin of the solar still.
13-Steady state.
14-Newtonian Fluid.

3.2.2 Governing Equations

The behavior of fluids flow is governed by the following laws: -

1- Continuity equation,
2- Newton's second law and
3- The first law of thermodynamics.

Accordingly, the mathematical model of computational fluid dynamics (CFD) includes solving the equation of mass conservation, Newton's second law and the thermodynamics first law as follow [81]

The equation of mass conservation is: -

$$\frac{\partial \rho}{\partial t} = \nabla \cdot (\rho \cdot \vec{v}) = S_m \tag{1}$$

Newton's second law is: -

$$\frac{\partial}{\partial t}(\rho . \vec{v}) + \nabla \cdot (\rho \cdot \vec{v} \cdot \vec{v}) = -\nabla p + \nabla \cdot \bar{\bar{\tau}} + \rho \cdot \vec{g} + \vec{F} \tag{2}$$

$$\frac{\partial}{\partial t}(\rho \cdot E) + \nabla \cdot [\vec{v}(\rho E + p)] = \nabla \cdot \left[k_{eff.} \nabla T - \sum_j h_j \cdot \vec{J_j} + (\bar{\bar{\tau}}_{eff.} \cdot \vec{v}) \right] + S_h \tag{3}$$

Thermodynamic analysis:

The equations used for thermodynamic analysis are presented in this section.
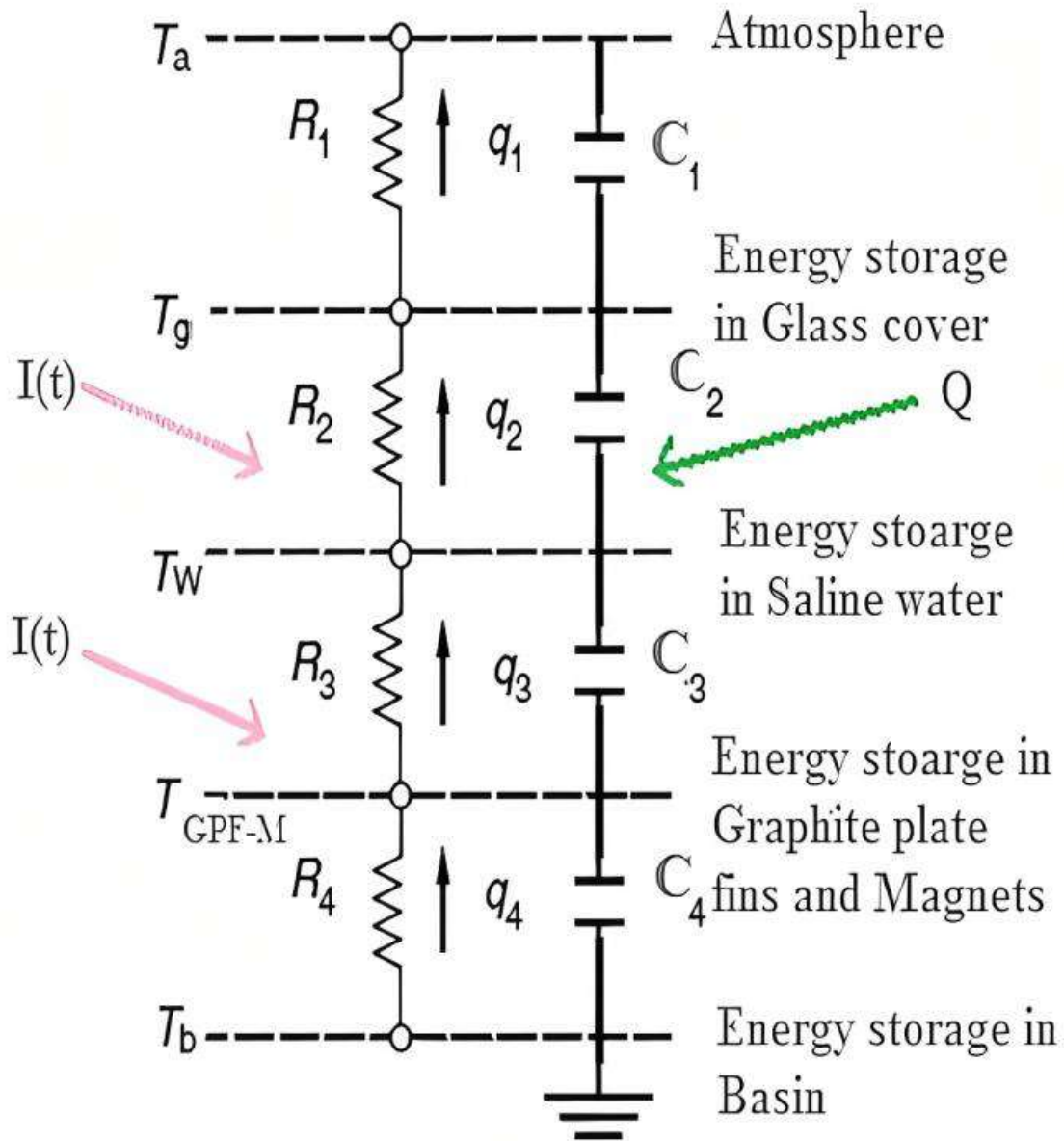

Figure (3.1) Electrical analogy network of GPF-MSS

Energy analysis

The energy balance equation based on the first law of thermodynamics is given by Eq. (4) to (28) (Dhivagar et al. 2021) [58]:

$$E_{\text{in}} + E_{\text{ge}} = E_{\text{out}} + E_{st} \tag{4}$$

Basin:

$$\alpha_b \tau_g \tau_w I(t) A_b = m_b c_{pb} \frac{dT_b}{dt} + h_c b - w + U_o b - a(T_b - T_w)$$

(5)

Graphite plate fins:

$$\left(\frac{k_{gp}}{x_{gp}}\right)(T_b - T_{gp}) = \left(\frac{k_{ins}}{x_{ins}}\right)(T_{gp} - T_a) + m_{gp} C_P, gp \frac{dT_{gp}}{dt}$$

(6)

Magnets:

$$\left(\frac{k_{mg}}{x_{mg}}\right)(T_b - T_{mg}) = \left(\frac{k_{ins}}{x_{ins}}\right)(T_{mg} - T_a) + m_{mg} C_{P,mg} \frac{dT_{mg}}{dt}$$

(7)

Basin with graphite plate fins and magnet:

$$\alpha_b \tau_g \tau_w I(t) A_b = m_b c_{pb} \frac{dT_b}{dt} + h_c b - w + \left(\frac{k_{gp}}{x_{gp}}\right)(T_b - T_w)$$

$$+ \left(\frac{k_{mg}}{x_{mg}}\right)(T_b - T_{mg})$$

(8)

Saline water:

$$\alpha_w \tau_g I(t) A_w + h_c b - w(T_b - T_w) = m_w c_{pw} \frac{dT_w}{dt} + U_{ow-g}\left(T_w - T_g\right)$$

(9)

Glass cover:

$$\alpha_g I(t) A_g + U_{ow-g}\left(T_w - T_g\right)$$
$$= m_g c_{pg} \frac{dT_g}{dt} + (h_c g - sky + h_r g - sky)\left(T_g - T_{sky}\right)$$

(10)

The electrical analogy network of GPF-MSS is given in Figure (3.1), the heat transfer between the glass cover to the atmosphere is given by:

$q_1 = h_{g-a}(T_g - T_a)$

(11)

The heat transfer between the saline water to the glass cover is followed by:

$$q_2 = (h_c w - g + h_{eva} w - g + h_r w - g)(T_w - T_g) \qquad (12)$$

The heat transfer between the basin to saline water is given by:

$$q_3 = (A_b - A_{gp.mg})h_w(T_b - T_w) \qquad (13)$$

The heat transfer between the basin to the atmosphere is given by:

$$q_4 = h_b (T_a - T_b) \qquad (14)$$

The useful heat energy stored in the solar still is given by:

$$Q = m_w C_{p,w}(T_w - T_b) \qquad (15)$$

The overall heat transfer coefficient of saline water and glass cover is given by:

$$U_{ow-g} = (h_c w - g + h_{eva} w - g + h_r w - g) \qquad (16)$$

The convective heat transfer coefficient is given by:

$$h_{c,w-g} = 0.884\left[T_w - T_g + \frac{(P_w - P_g)T_w + 273}{268,900 - P_w}\right]^{1/3} \qquad (17)$$

Here, P_g and P_w are:

$$P_g = \exp\left[25.317 - \frac{5,144}{T_g + 273}\right]$$
$$P_w = \exp\left[25.317 - \frac{5,144}{T_w + 273}\right] \qquad (18)$$

The following equation estimates the evaporative heat transfer coefficient:

$$h_{eva} w - g = 0.016 h_c w - g \frac{(P_w - P_g)}{(T_w - T_g)} \qquad (19)$$

The radiative heat transfer coefficient between saline water and glass cover is given by:

$$h_{r,w-g} = \sigma \varepsilon_{eff} \left[(T_w + 273)^2 - (T_g + 273)^2 \right] (T_w + T_g + 546)$$

(20)

Here,

$$\varepsilon_{eff} = \frac{1}{\left[\frac{1}{\varepsilon_w} + \frac{1}{\varepsilon_g} - 1 \right]}$$

(21)

The convective heat transfer coefficient between glass and sky is given by:

$$h_{c,g-sky} = 2.8 + 3.0V$$

(22)

The radiative heat transfer coefficient between glass and sky is given by:\vskip1pc

$$h_{r,g-sky} = \frac{\varepsilon_{eff} \sigma (T_g^4 + T_{sky}{}^{\wedge 4})}{T_g - T_{sky}}$$

(23)

The sky temperature is given by:

$$T\_sky = 0.0552 * T\_a^{\wedge} (1/5)$$

(24)

The convective heat transfer between two surfaces can be calculated using the following relation:

$$h_c = \frac{k \times 0.15 \times (Gr \cdot Pr)^{0.333}}{L}$$
$$Gr = \frac{gv \times \beta \times \Delta T \times L^3}{\gamma^2}$$
$$(\beta) = \frac{1}{T_f + 273.16}$$
$$(T_f) = \frac{T_1 + T_2}{2}$$

(25)

The latent heat of saline water during vaporization is given by:

$$L = 2.4935 \times 10^6 \times \left[\begin{array}{c} 1 - 9.4779 \times 10^{-4} T_w + 1.3132 \times 10^{-7} \\ \times T^{\wedge 2} - 4.794 \times 10^{-9} \times T_w{}^{\wedge 3} \end{array} \right]$$

(26)

The hourly solar still productivity is given by:

$$m_w = \frac{h_{\text{eva } w-g}(T_w - T_g) \times 3600}{L} \tag{27}$$

The solar still energy efficiency is given by:

$$\eta_{E,ss} = \frac{m_w \times L}{A_{ss} \times \sum(I_{ss}) \times 3600} \tag{28}$$

3.3 Numerical Simulation

This section describes the software that simulates heat transfer (by solving the governing differential equations) from and into the solar water heating and distillation system. Building the software (its structure or sections) is also shown. The software used in the current work is Fluent, One of Ansys's branches (version 2021 R1 of Workbench). It was used to obtain the numerical solutions of water temperatures inside the solar system and the daily productivity of water distillate. This software was selected in the current work because it gives more precise results and is nearer to the experimental results. In addition, it can solve the conservation equations of mass, momentum and energy. This is for conditions such as two or three-dimensional fluid flow, steady or unsteady state (transient), compressible or incompressible fluid, and others. Furthermore, it has been used in many research fields as the heat transfer field (the present work field). The steps of construction of this software are: constructing the geometry, generating the mesh, constructing the setup, and finally displaying the results.

3.3.1 Geometry of Test Section

SOLIDWORKS was used to design a three-dimensional test model of the solar water distillation system. This is for all the simple and complex geometric shapes. Firstly, the x-y plane was chosen to design the test model. After that, an extrude order was applied to obtain the test model's three-dimensional structure. All the walls of the test model were made as adiabatic walls. The top surface represents the glass cover of the test model. The bottom surface of the test model was designed to be the vapor entrance to the test section. The geometric dimensions of the test model are the same as the dimensions of the experimental rig. Figure (3.2) shows the geometry of the solar distillation system.
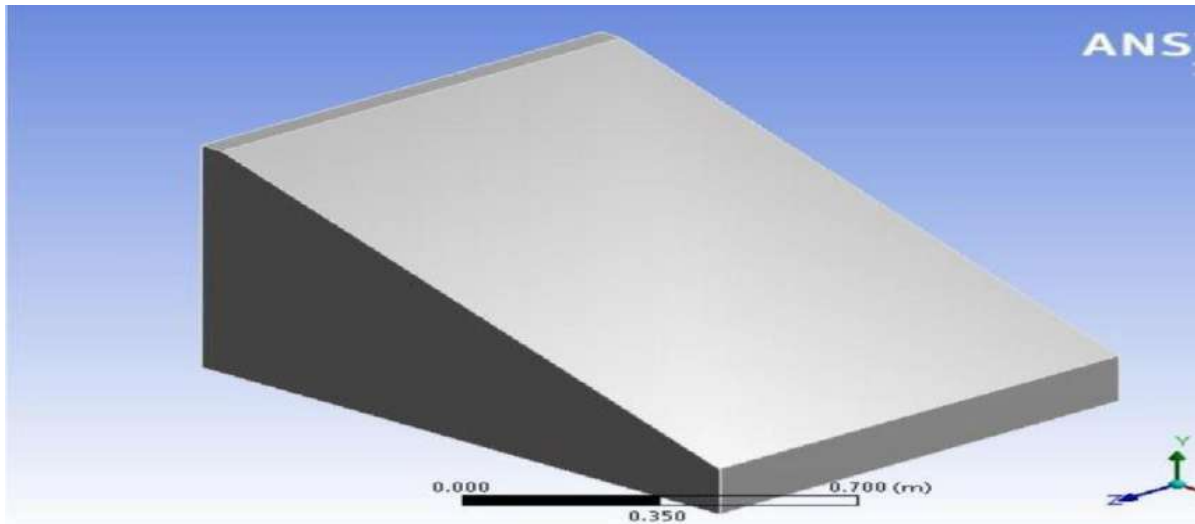
Figure (3.2) Three-dimensional geometry of test model

3.3.2 Mesh Generation

The second stage of constructing a computational fluent program is mesh or grid generation. After constructing the test model's geometry design, the domain mesh (the test section) is generated. In other words, the test section is divided into very small elements. There are several types of grids, and applying the appropriate type is related to some limitations, such as the type of research work, the geometry, the field of flow, etc. The choice of grid size and type has major importance on the CPU (central processing unit) time requirements, the convergence rate, and the accuracy of the results [82]. The mesh type chosen in the current work is quadrilateral, and the size of the elements is (1 * 1 * 1) mm. The computational grid's structure is tetrahedral. This was obtained after several tests with different sizes and grid types at the same boundary conditions. The quadrilateral mesh with the size of (1 * 1 * 1) mm produces the best results compared to the other types and sizes of mesh. Table (3.1) includes the properties of the mesh. Figure (3.3) show the grid in the test section in three dimensions, respectively.

Table (3.1) The properties of mesh

Setup	Specifications
Preference of Physics	CFD
Preference of Solver	Fluent Ansys CFX 2021 R1
Rate of Growth	Default (1.2)
Sizing	Fine
Minimum Size	0.1 mm

Maximum Size	1 mm
Nodes	310778
Elements	1210326
Transition	Slow
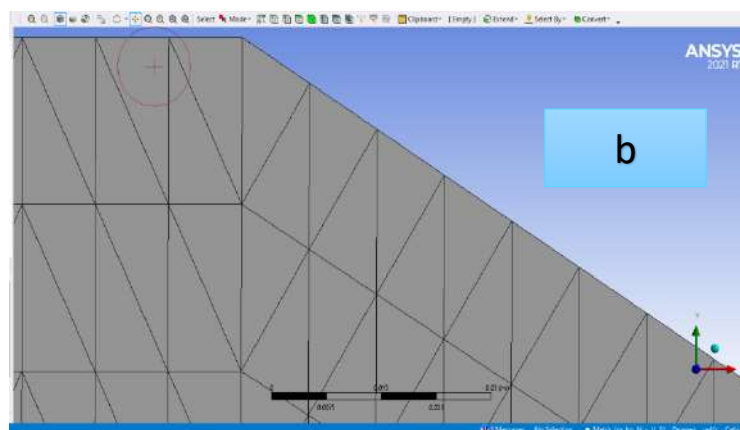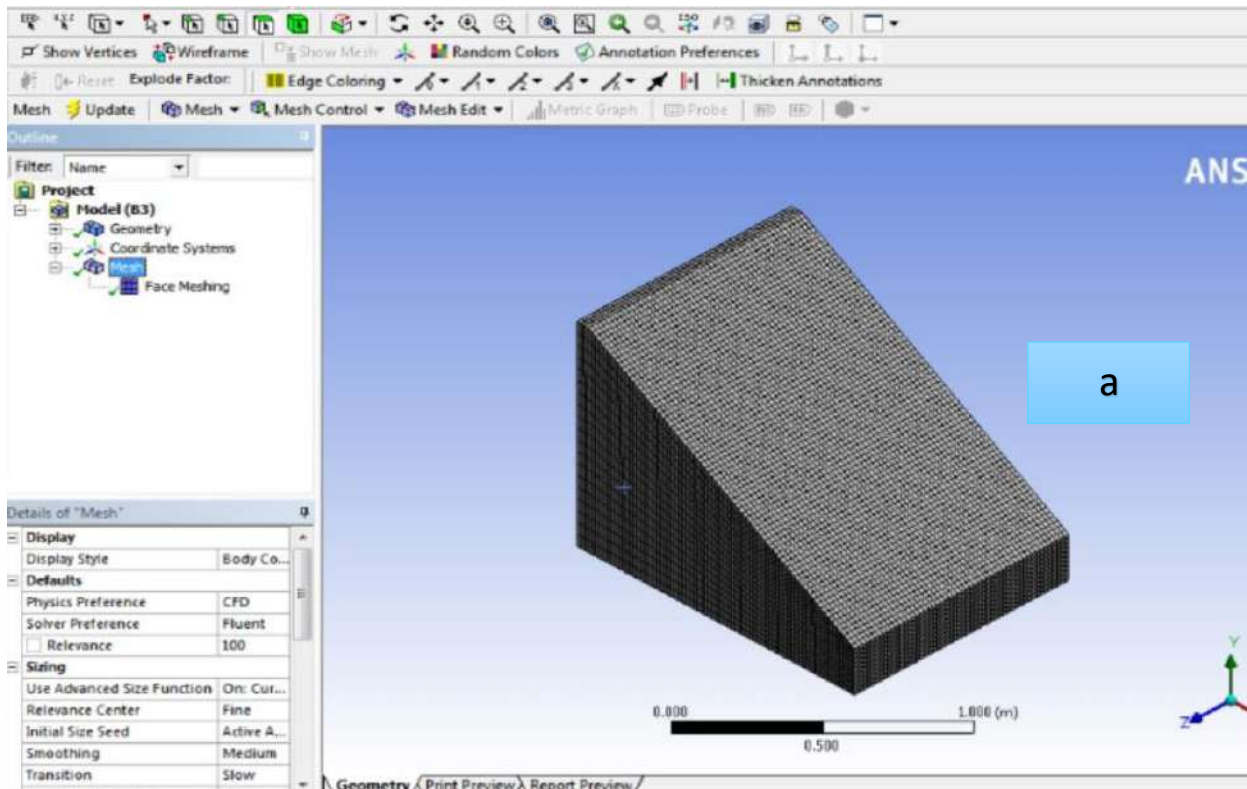
Figures (3.3) The mesh of test section

(a)3D, (B) Edge

3.3.3 Setup and Solution

3.3.3.1 Boundary Conditions

In the present study, the water is considered a primary phase, and the water vapor is considered a secondary phase. For the mathematical model used in the present work, the boundary conditions were divided into three groups: inside and outside the solar distiller and at the distiller walls.

Inside the **solar distiller,** the following boundary conditions were applied**.**

o The mixture of water and vapor at the beginning (t = 0) is the specific initialization of the working fluid,
o The water temperature entered into the test section is 32 °C,
o The volume fraction of vapor and water is 0.999, 0.001 respectively,
o The reference pressure is 1 atm.
o The reference density is 1.225 kg/m^3.

Outside **the solar distiller,** the boundary conditions were set at the ambient pressure and temperature.

For the boundary conditions at the **solar distiller walls,** all the sides of the distiller wall were set as thermal conductor walls.

3.3.3.2 Solution Method

Fluent solver has four numerical solution methods [SIMPLE]. The suitable solution method can also be selected depending on previous studies in the same field or by carrying out four tests (one test for each solution method). This is after the selection of the turbulence model. To determine the appropriate method, the results of the above methods are compared separately with the experimental results of the same study or other studies under the same test conditions.

3.4 Types of Errors in the numerical solution

The total error consists of the following:

1) Error in the model due to a mismatch between the physical position and the mathematical model.

2) Error in data due to measurements of questionable accuracy.

3) Human error due to human errors.

4) Common error: The error in the following process steps is due to a previous error.

5) Truncation error: Truncation error usually refers to errors introduced when a more complex mathematical expression is "replaced" with an initial formula. This same formula can only be approximated to the real values. Therefore, it will not produce accurate answers.

Therefore, it is possible to include a small difference in some practical results from the theoretical results as a truncation error. In all cases, the results showed that the theoretical and practical results are congruent by less than 10%.

4

EXPERIMENTAL

Part

CHAPTER FOUR

# EXPERIMENTAL PART

4.1 Introduction

The solar desiccant collector manufacturing process is described in this chapter, along with a calibration chart for each device used to take the measurements. Then, a new model was devised that includes graphite fins and
magnetite provides the best performance of the solar collector through the pilot effort.

4.2 Process of manufacturing the solar still collector

The following steps show the manufacture of a solar–desiccant collector device, as shown in Figure (4.1). The first step was to manufacture the device's internal structure from galvanized iron sheets with a thickness of (1 mm). With a net area (of 1 m^2) from the inside, with a height of (0.75 m) from the back and the front a height of (0.1 m) to achieve a fixed tilt angle from the top by (32°) throughout the year for the city of Karbala, the sides of the device are from the same structure Galvanized steel, either from the top used a movable glass cover with a thickness of 6 mm and a total area of 1 * 1.13 m^2. This glass cover relies on an iron flange, which increases the cohesion of the device's internal structure in addition to a campaign for the glass cover. A flexible and tight rubber gasket surrounds the glass cover to prevent the leakage of steam produced from the absorbent material and to prevent damage to the glass cover during day and night lifting and closing. The device is isolated from all sides by Arm Flexi insulation type with a thickness of 30 mm. The lower part was insulated using glass wool with a thickness of 30 mm with a layer of galvanized iron and fixed by welding to increase thermal insulation and reduce energy losses.

Figure (4.1) The solar still collector components
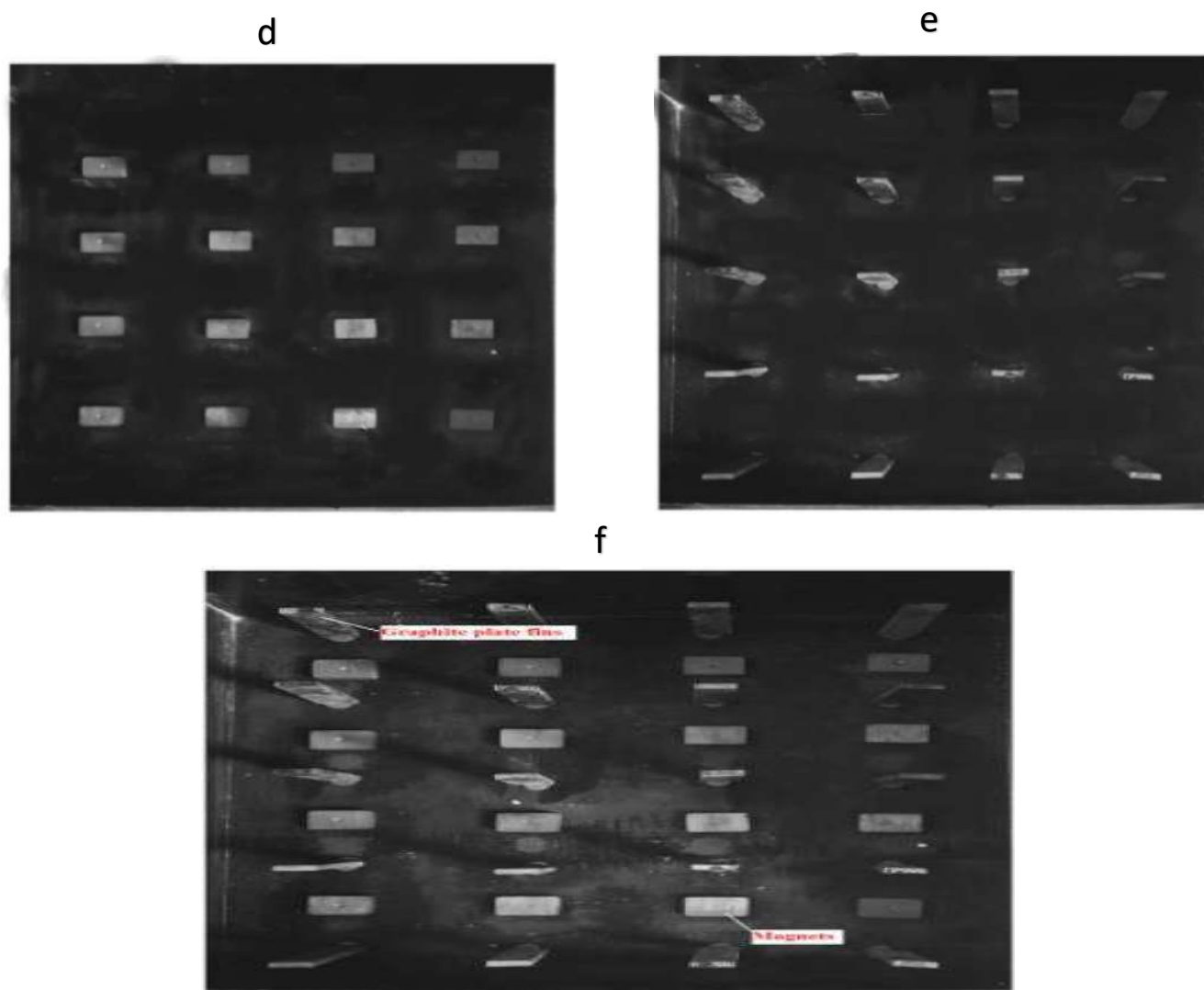(a)Manufacturing a solar still
(b)Installing the device on the rooftop

a

b

c

d

e

f
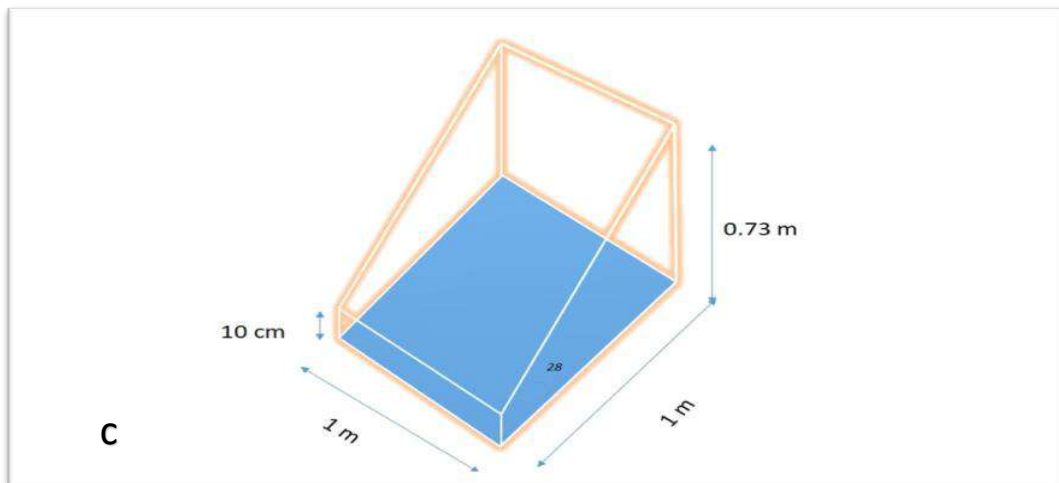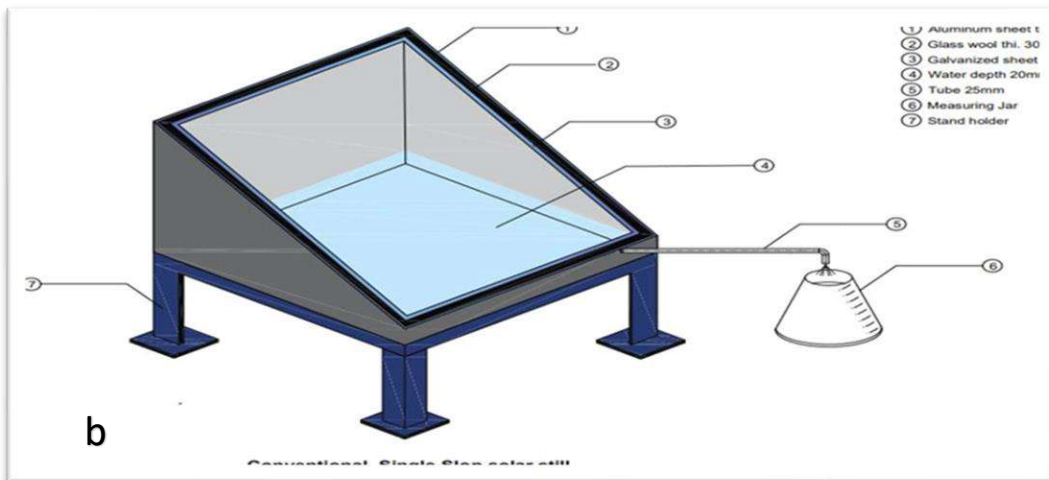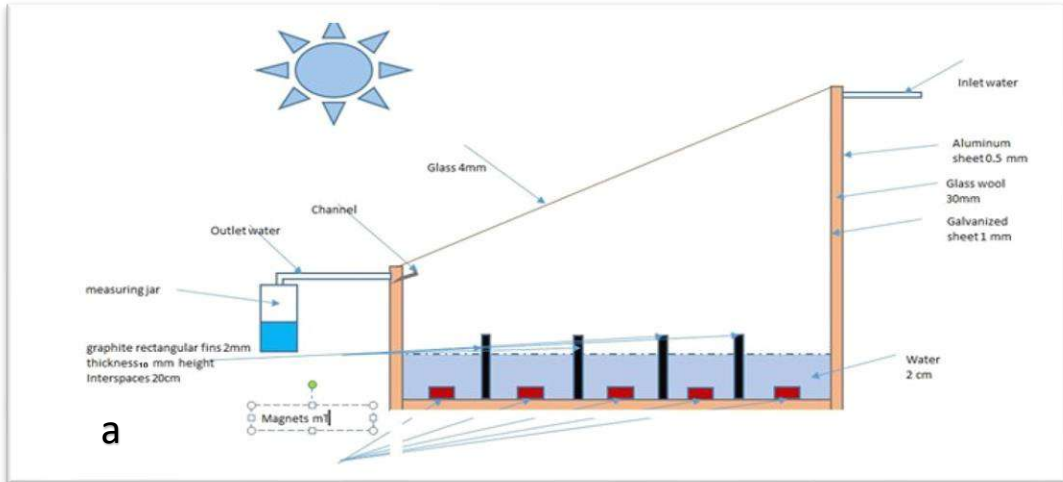
Figure (4.2)
(a) Schematic diagram of GPF-MSS
(b) Schematic diagram of CSS
(c) Photograph of graphite only and magnets only
(d) Locations of magnets
(e) Locations of graphite plate fins
(f) Locations of graphite plate fins and magnets

Table (4.1) The specifications of the solar still collector components

Component	Dimensions	Remarks
Iron structure	A net area (of 1 m^2), with a height of (0.75 m^2) from the back and front a height of (0.1 m^2)	Material: galvanized iron sheets with a thickness of (1.1 mm)
Side thermal insulator	The thickness of 30 mm	Material: Arm flexi type
Bottom insulator	The thickness of 30 mm	Material: glass wool type
Movable top cover	total area of 1 * 1.13 m^2 with a thickness of 6 mm	Material: glass
Iron flange	length 1.19 m, width 1.06 m	Material: iron
Gasket	_	Material: Rubber
Channel for collecting water	length 1 m, width 0.05 m	Material: galvanized iron sheets
Tube	quarter inch diameter	Material: Copper
Bottle	_	Material: Plastic

Table (4.2) The components of the system

No.	The Description
1	Solar still collector
2	Thermocouples
3	Temperature recorder
4	Digital solar power meter

4.3 Measurement Devices

Several measurement tools were employed during the experiment, including a solar meter, thermometer and thermocouples, and a relative humidity sensor.

4.3.1 Solar power meter

The total solar radiation is measured using a digital solar power meter of type TES-132 with an accuracy of ($\pm5\%$), a reading range of (1 to 2000) W/ m^2. The correction factor was computed after the calibration with a different calibrated device (a standard device) and simultaneous reading recording.

Figure (4.3) Digital solar power meter

4.3.2 Temperature Recorder

Temperature recorder model (BTM-420SD) with 12 channels, as shown in Figure (4.4). It has an SD card to save the temperature, read data with time, and information into an SD memory card and can load it to the Excel software. It uses for different sensor types of thermocouples such as J/K/T/R and S. It works as an auto data logger or manual data logger sampling time range of 1 to 3600 seconds. The SD card capacity is 1 GB to 16 GB, has Rs 232/USB computer interface, and the microcomputer circuit provides intelligent function and high accuracy. In the present experiment, the temperature is measured at 12 positions. Figure (4.8) shows the location of 9 thermocouples in the collector, and still. These thermocouples are fixed in different positions, which are selected to measure the temperature in most systems. Thermocouple's wire is conducted with a temperature recorder, which works to catch signal response and transform it to digital reading.

Figure (4.4) Photograph of temperature recorder device

4.3.3 Thermometer Device

The thermometer device is calibrated at (the University of Karbala at the Laboratory of Mechanical Engineering Department) using the standard thermometer. The thermocouples, type - K, are made by the same company. This thermocouple is put inside the insulation oven, and the range temperature (20C to 220C) takes the reading every minute from this calibration. The equation of calibrating and R-Square is 0.99, as shown in Figure (4.5), and the maximum and minimum error of temperature between standard and measured is (+4.24C, - 3.2C), as shown in Figure (4.6) that mean in percentage (+1.94%, -1.55%). Also, the thermometer device had the certificate of calibration from (the Ministry of Science and Technology)
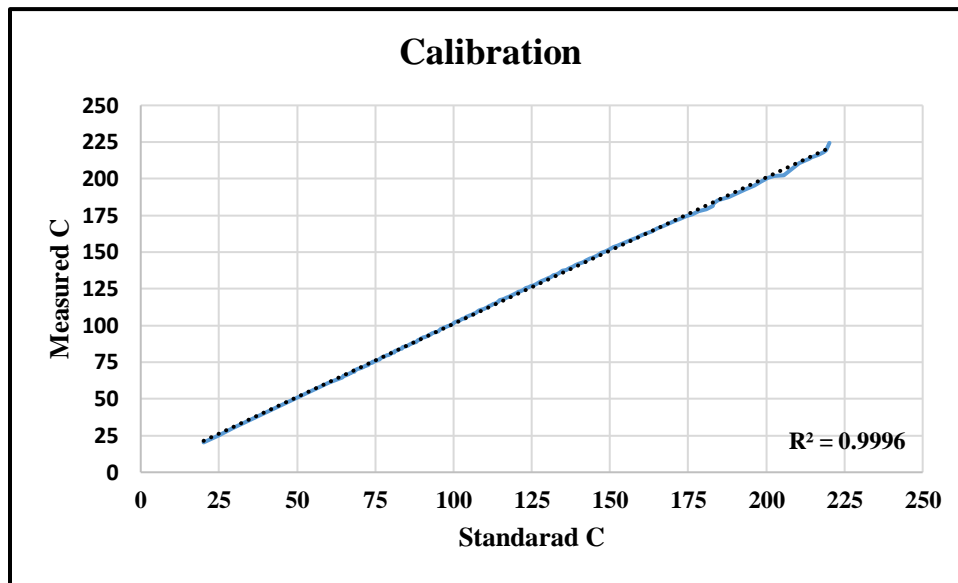
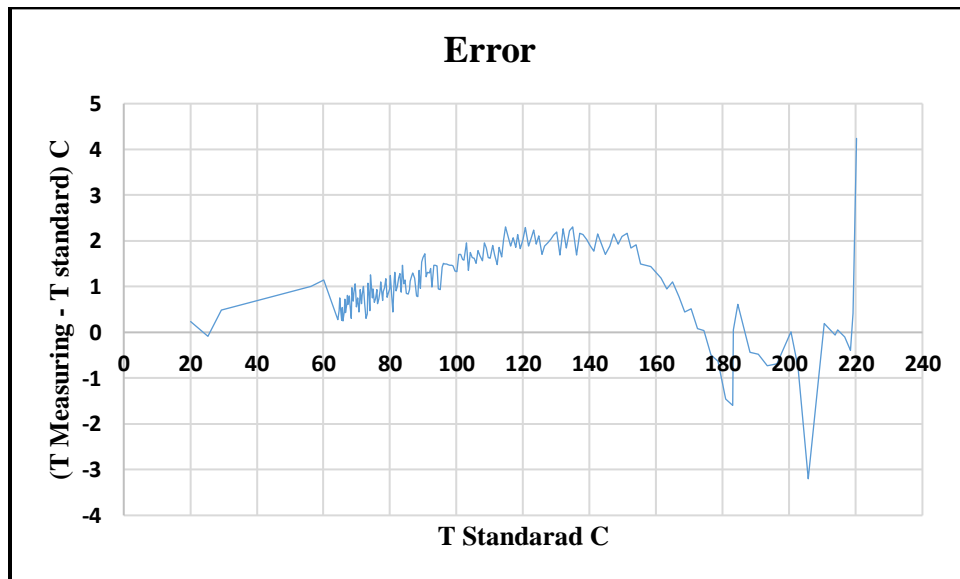Figure (4.5) The reading between standard and measuring calibration temperature

Figure (4.6) The measuring error to standard

Thermocouples are attached to the solar collector by putting the ball-welded end of the thermocouple wire in direct contact with the surface to estimate its temperature and covering this end with a heat sink compound to ensure the end insulated from the environment and outside effects. This heat sink compound is a kind of thermally conductive adhesive highly effective in eliminating air gaps or spaces (which act as a thermal insulator) from the interface area; then, the

thermocouples were taped with rubber splicing tape that can be used on cables whose emergency overload temperature can reach 130 C⁰, as shown in figure (4.8).

Figure (4.7) Thermocouples covered with heat sink compound and taped with rubber splicing tape
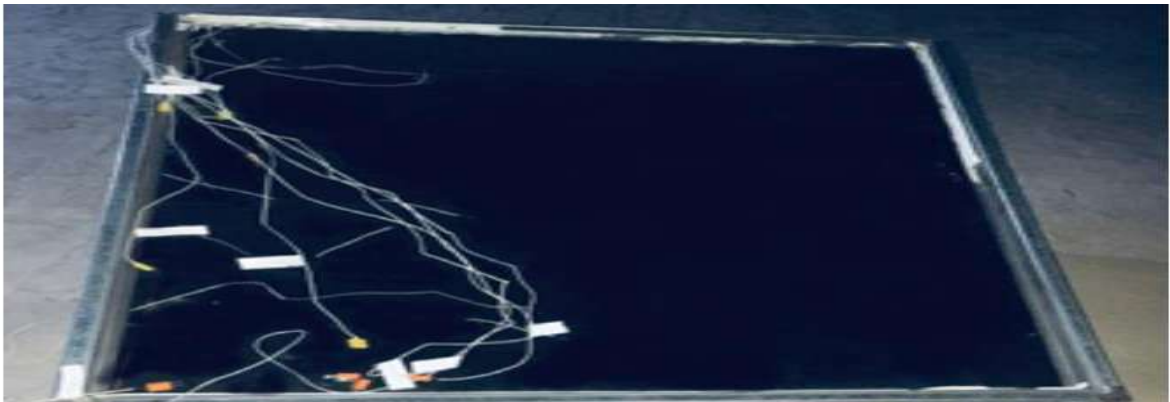

Figure (4.8) Temperature logger and thermocouples

Table (4.3) Network thermocouples distribution of the solar desiccant collector

No.	location
1	External glass cover temperature
2	Inner glass cover temperature
3	Gap temperature
4	Fins temperature
5	Magnet's temperature
6	Bottom plate temperature
7	Saline water temperature
8	Collector base temperature
9	Ambient temperature

4.4 Experimental Procedure

The experimental work involved the use of a solar still. The system was positioned in a sun-exposed area without any obstructions or buildings that could block solar radiation and airflow. To ensure accurate results, the system was properly covered to prevent external heat interference before the start of the experiment. The experiment commenced at 8:00 AM, with the system being uncovered, the surface cleaned, and readings recorded.

The experimental study can be divided into four groups, each with specific conditions:

The first group involved testing without the presence of magnets or fins.

The second group included testing with magnets but without fins.

The third group focused on testing with fins but without magnets.

The fourth group encompassed testing with both fins and magnets.

The following steps describe the experimental procedure for all cases:

A. The solar still was oriented towards the south to maximize solar radiation exposure for distillation.

B. Temperature measurements were monitored, recorded, and taken every 10 minutes.

C. Water was opened and filled to achieve the desired water depth.

D. The system was operated from 8:00 AM to 5:00 PM.

E. Solar radiation intensity readings were taken every 60 minutes using a radiometer device with a lens parallel to the glass cover surfaces of the distillation unit.

F. Temperature data was transferred to a computer, and the water was replaced with fresh water for the subsequent test.

By following these steps, the experimental process and workflow were carefully executed to ensure accurate and reliable results.

4.5 Fins

The length of time needed to prepare the salt water before it evaporates is decreased by the fin-integrated solar still in the flat plate basin. The output of the still rises due to faster heat transfer from the basin to the salt water due to the fins. as shown in table (4.4).

Table (4.4) The properties of fins

Fin type	Thickness/ dia	Hight	Width
rectangular	2 mm	10 cm	10 cm
cylindrical	5 mm	10 cm	
Flat plate	2mm	10 cm	80 cm

4.6 Magnetic Treatment Unit

The magnetic treatment unit was connected before the distillation unit, as shown in Figure (4.8). Using magnetic water produces low surface tension, which increases evaporation and the productivity of water distillation. The magnet used in this experiment was Neodymium N52 magnets with dimensions 6 * 2 * 1 cm, as shown in Figure (4.9). DC Gauss meter Model GM1-HS is used to measure moderate-strength static magnetic fields up to 800 G with a resolution of 0.01G. It measures the magnetization of ferrous metals, solenoids and the far field of strong magnets, as shown in Figure (4.10) the magnetic has 1191.4 G magnetic strength.

Figure (4.9) Neodymium N52 magnets
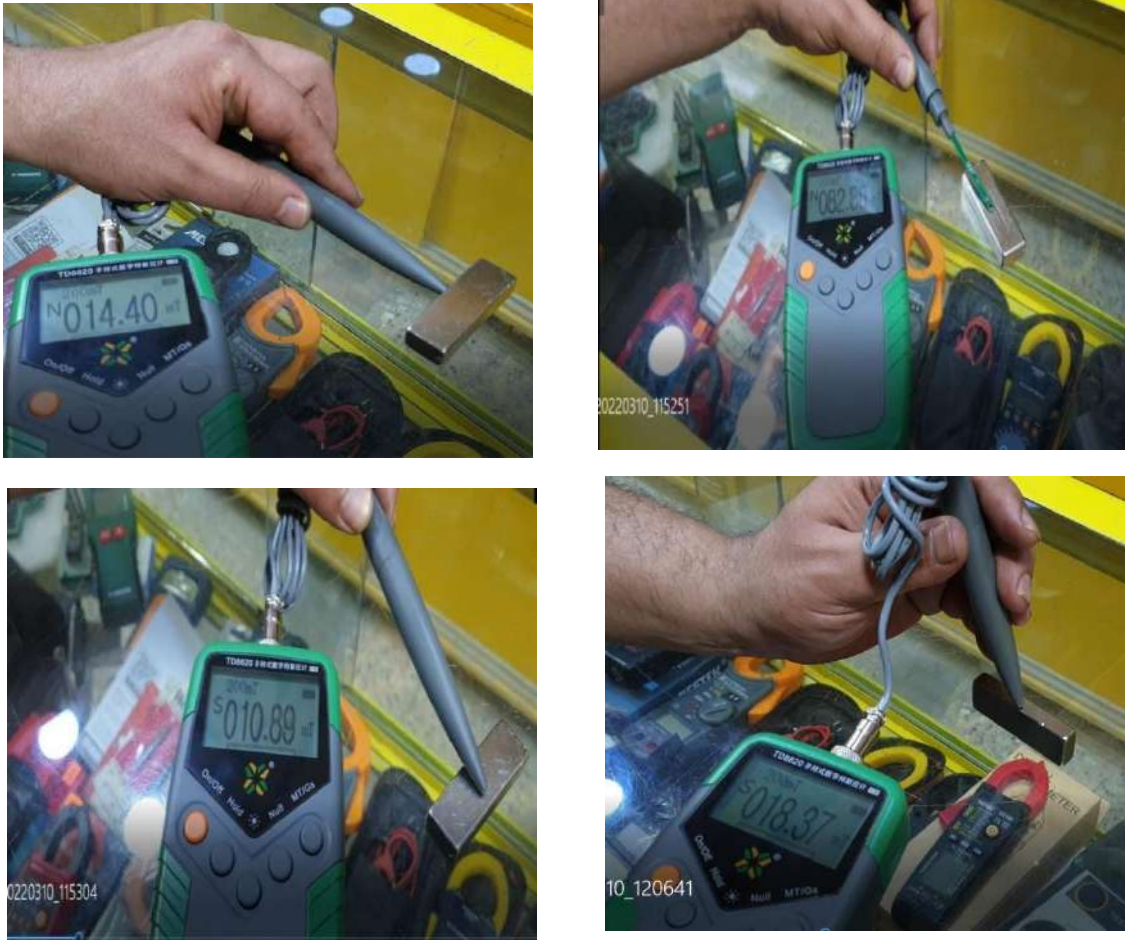
Figure (4.10) DC gauss meter model GM1-HS

4.7 Instrumentation

Nine calibrated K-type thermocouples with an accuracy of ± 0.2 °C were strategically placed within the solar still to measure temperatures at various locations, including the ambient air, basin, graphite plates, magnets, glass, and saline water. These thermocouples were connected to a digital temperature indicator with a resolution of 0.1 °C. Additionally, a solar intensity meter with an accuracy of ± 5 W/m² was utilized to measure the solar radiation, while a cup-type anemometer with an accuracy of ± 0.1 m/s was used to measure wind speed. The strength of the magnetic field was recorded using a digital Gaussmeter with an accuracy of ± 1 mT. Hourly productivity was quantified using a calibrated jar, and the depth of the saline water was measured using a scale attached to the walls of the solar still basin. Detailed information about the instrumentation can be found in Table (4.5), and the properties of the graphite plate fins and magnets are provided in Table (4.6).

Table (4.5) Details of measuring devices

Instrument	Accuracy	Range	Uncertainty (%)
Thermometer	$\pm$ 0.2 °C	0–100°C	$\pm$ 0.492
K-type thermocouple	$\pm$ 0.1 °C	0–200°C	$\pm$ 0.487
Digital temperature indicator	$\pm$ 0.1 °C	0–200°C	$\pm$ 1.195
Solar intensity meter	$\pm$ 5 W/m^2	0–1000 W/m^2	$\pm$ 1.491
Cup-type anemometer	$\pm$ 0.1 m/s	0–15 m/s	$\pm$ 9.712
Gaussmeter	$\pm$ 1 mT	0.1–2400 mT	$\pm$ 1.198
Measuring jar	$\pm$ 10 ml	0–1000 ml	$\pm$ 9.814

Table (4.6) Properties of graphite plate fins and magnets

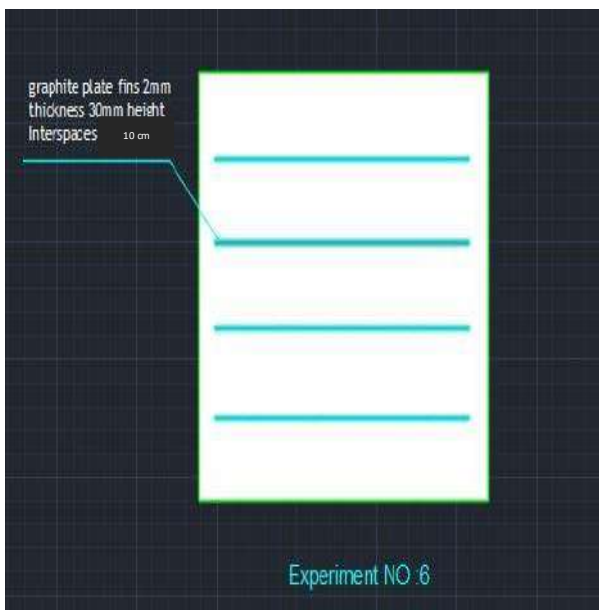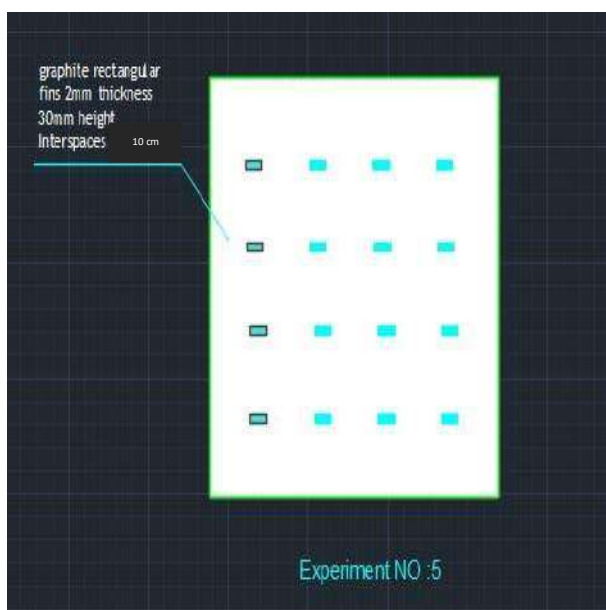| 1	Thermal conductivity of graphite (W/mK)	6
2	Graphite thermal expansion coefficient (μm/mK)	3.2
3	Graphite density (g/m³)	1.7
4	Graphite porosity (%)	13
5	Magnet thermal conductivity (W/mK)	7.7
6	Linear thermal expansion of magnetic(μm/mK)	3.4
7	Magnet density (g/m³)	7.5
8	Magnetic field strength (mT)	0.3,0.6,0.9

4.8 Experimental Cases

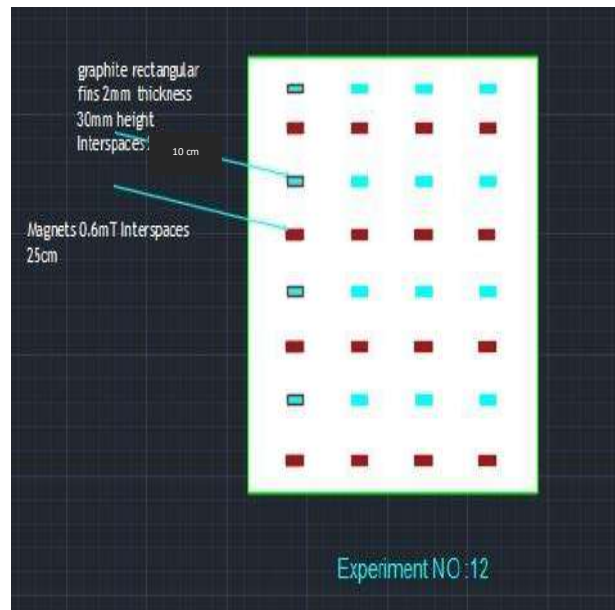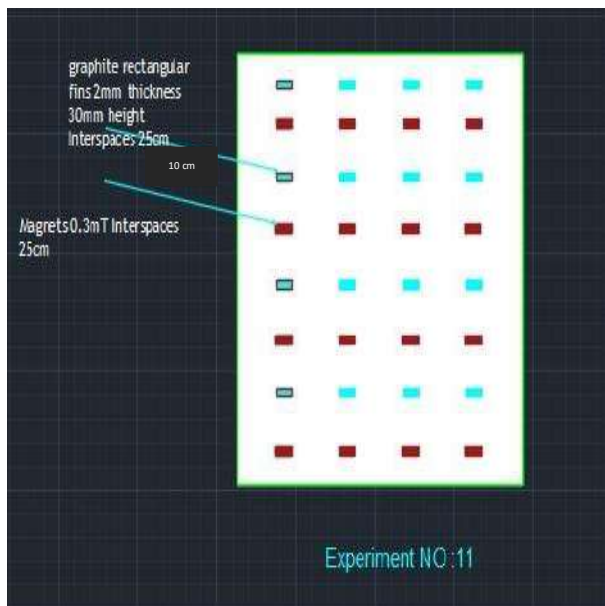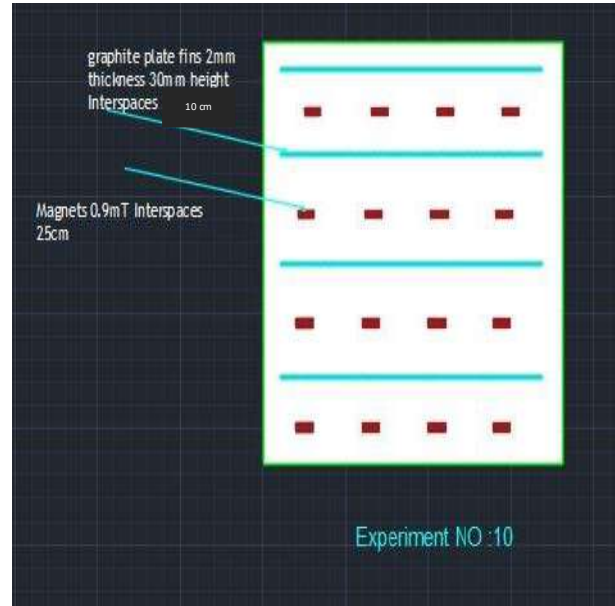In the table below are the cases that were tested during the theoretical and practical part of the research.
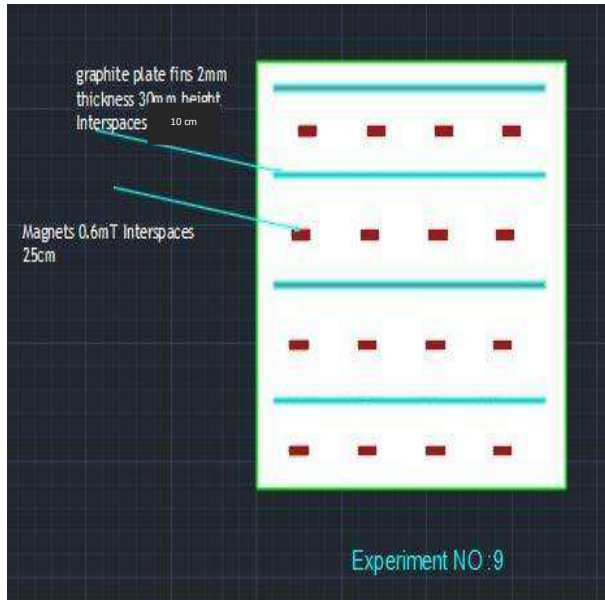
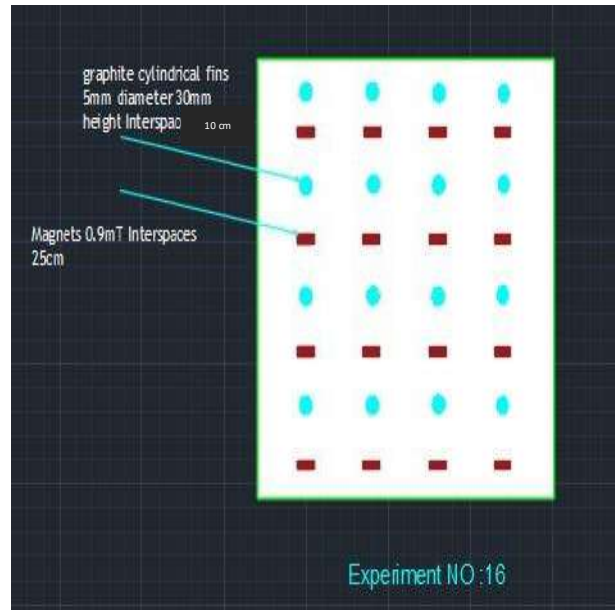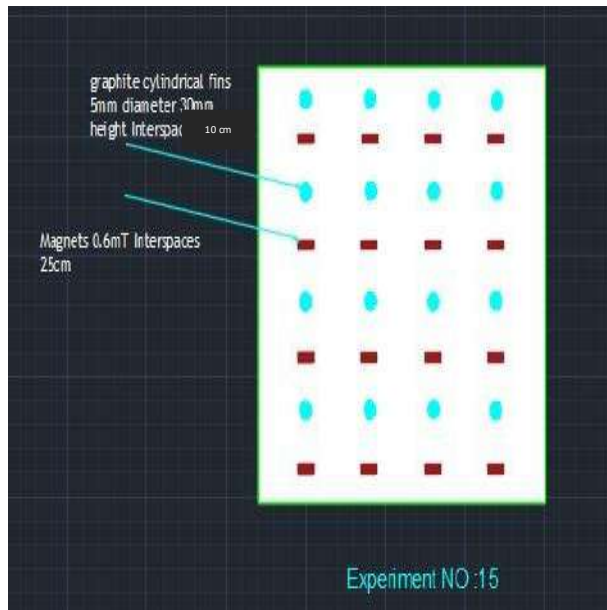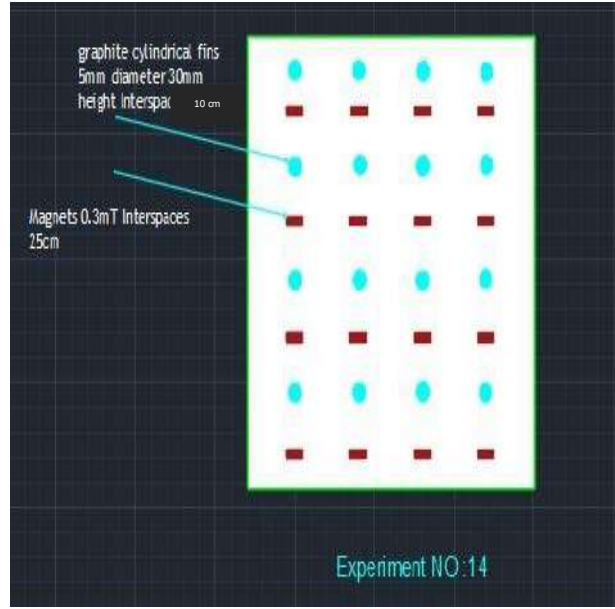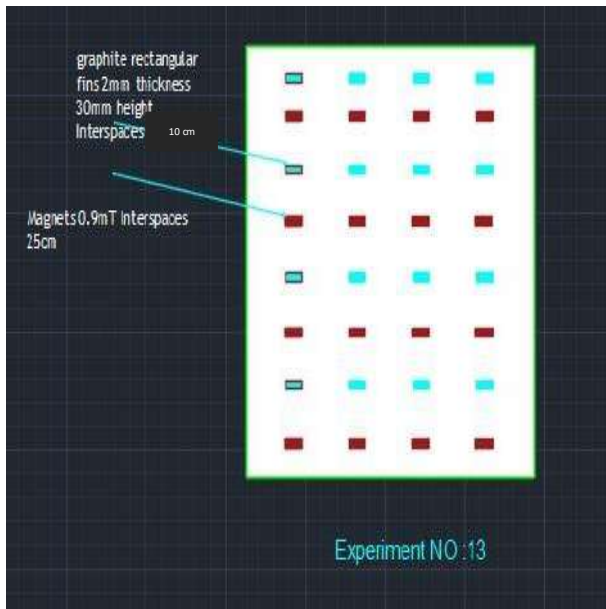Table (4.7) The cases tested during the research's theoretical and practical parts

Test number	Existing practical part	Number parts	spaces between parts (cm)
1	conventional	-	-
2	Magnates .3mT	16	20
3	Magnates .6mT	16	20
4	Magnates .9mT	16	20
5	Graphite rectangular fins	16	20
6	Graphite plate fins	4	20
7	Graphite Cylindrical fins	16	20
8	Graphite plate fins & Magnates .3mT	4&16	10
9	Graphite plate fins & Magnates .6mT	4&16	10
10	Graphite plate fins & Magnates .9mT	4&16	10

11	Graphite rectangular fins & Magnates .3mT	16&16	10
12	Graphite rectangular fins & Magnates .6mT	16&16	10
13	Graphite rectangular fins & Magnates .9mT	16&16	10
14	Graphite Cylindrical fins & Magnates .3mT	16&16	10
15	Graphite Cylindrical fins & Magnates .6mT	16&16	10
16	Graphite Cylindrical fins & Magnates .9mT	16&16	10

conventional

Experiment NO : 1

Magnets 0.3mT
Interspaces   10 cm

Experiment NO :2

Magnets 0.6mT
Interspaces   10 cm

Experiment NO :3

Magnets 0.9mT
Interspaces   10 cm

Experiment NO :4

graphite rectangular fins 2mm thickness 30mm height Interspaces 10 cm

Experiment NO :5

graphite plate fins 2mm thickness 30mm height Interspaces 10 cm

Experiment NO :6

graphite cylindrical fins 5mm diameter 30mm height Interspaces 10

Experiment NO :7

graphite plate fins 2mm thickness 30mm height Interspaces 10 cm

Magnets 0.3mT Interspaces 25cm

Experiment NO :8

graphite plate fins 2mm thickness 30mm height Interspaces 10 cm

Magnets 0.6mT Interspaces 25cm

Experiment NO :9

graphite plate fins 2mm thickness 30mm height Interspaces 10 cm

Magnets 0.9mT Interspaces 25cm

Experiment NO :10

graphite rectangular fins 2mm thickness 30mm height Interspaces 25cm

10 cm

Magnets 0.3mT Interspaces 25cm

Experiment NO :11

graphite rectangular fins 2mm thickness 30mm height Interspaces

10 cm

Magnets 0.6mT Interspaces 25cm

Experiment NO :12

Figures (4.11) The schematic cases tested during the research's theoretical and practical parts

5

RESULTS AND DISCUSSION

Chapter Five

Results and Discussion

5.1 Introduction

The numerical and experimental results retrieved from the distilled solar system will be discussed in this chapter. A comparison of experimental and computational fluid dynamics data was then used to examine and investigate the behavior and properties of the solar distillate. The experimental part includes using solar distillation coupled with the magnetic field. After determining the optimum, the magnitude of the magnetic field was introduced to the system in three different fins, plate fin, cylinder fin and rectangular fin (to enable sustained productivity of the distillate after sunset). Water temperature, solar distilled basin temperature, inner glazier lid temperature, outside glazier lid temperature, and vapor temperature within solar still are evaluated numerically. Validation was performed to verify the numerical model by comparing it to experimental data.

5.2 The Numerical Solution

The program employed a numerical solution of the input temperatures and sun radiation intensity. The use of boundary conditions for the aim of CFD to know and analyze the temperature distribution was evaluated and implemented, as well as the use of ANSYS Networks (mesh). The analysis was performed at various inlet temperatures and solar radiation for solar still. This was done using SOLIDWORKS software. The objective of the numerical CFD is to examine solar still prototypes for temperature distribution.

5.2.1 The Velocity Vector

The velocity vectors in the Figures from (5.1) to (5.13) show the speed through this issue at 11 a.m., 1 p.m., and 3 p.m. under various scenarios, including the use of distilled alone and distilled with magnets and fin. The warm steam rises due to the buoyant force acting on it when the upper layer of the water basin evaporates, resulting in swirling streams of steam. When the vapor reaches the top, water droplets begin to condense, and vortices grow in number and size, signaling that the convection heat transfer mechanism has become more intense.

5.2.2 The volume fraction

Figures (5.1) to (5.13) at a time show the volume fraction contours obtained during a solar still test (11 am, 1 p.m., and 3 p.m.). It is for the solar still only, and the solar still is connected with fins and magmatic. The figures show that the volume

fraction is higher at one o'clock because of the significant temperature differential between the ambient and steam temperatures, which increases condensation. The volume fraction acceptable for condensing water droplets is obtained by setting the contour between the zeros on the (1*10^-3) graph—the systems underneath and in the side, view corresponding to the contours of the water volume fraction. The surface contact is clear, and the liquid and vapor phases may be separated. It appears as a liquid phase on the internal face of the glass lid and at the bottom of the model's shape.

5.2.3 Temperature contour

Figures (5.14) to (5.48) illustrate the temperature distribution contours for two-phase flow through a solar still testing (11 am, 1, 3 pm). The solar still alone and solar still linked with fins and magmatic have different temperature distributions. In these graphs, a descending temperature gradient through a solar still is used to show the contour of the temperature distribution. It was determined that rising sun intensities were the cause of the temperature gradient's upward trend. As the flow velocity reduces as the pressure rises, we also note the stream lines' distribution and how they relate to the pressure lines.
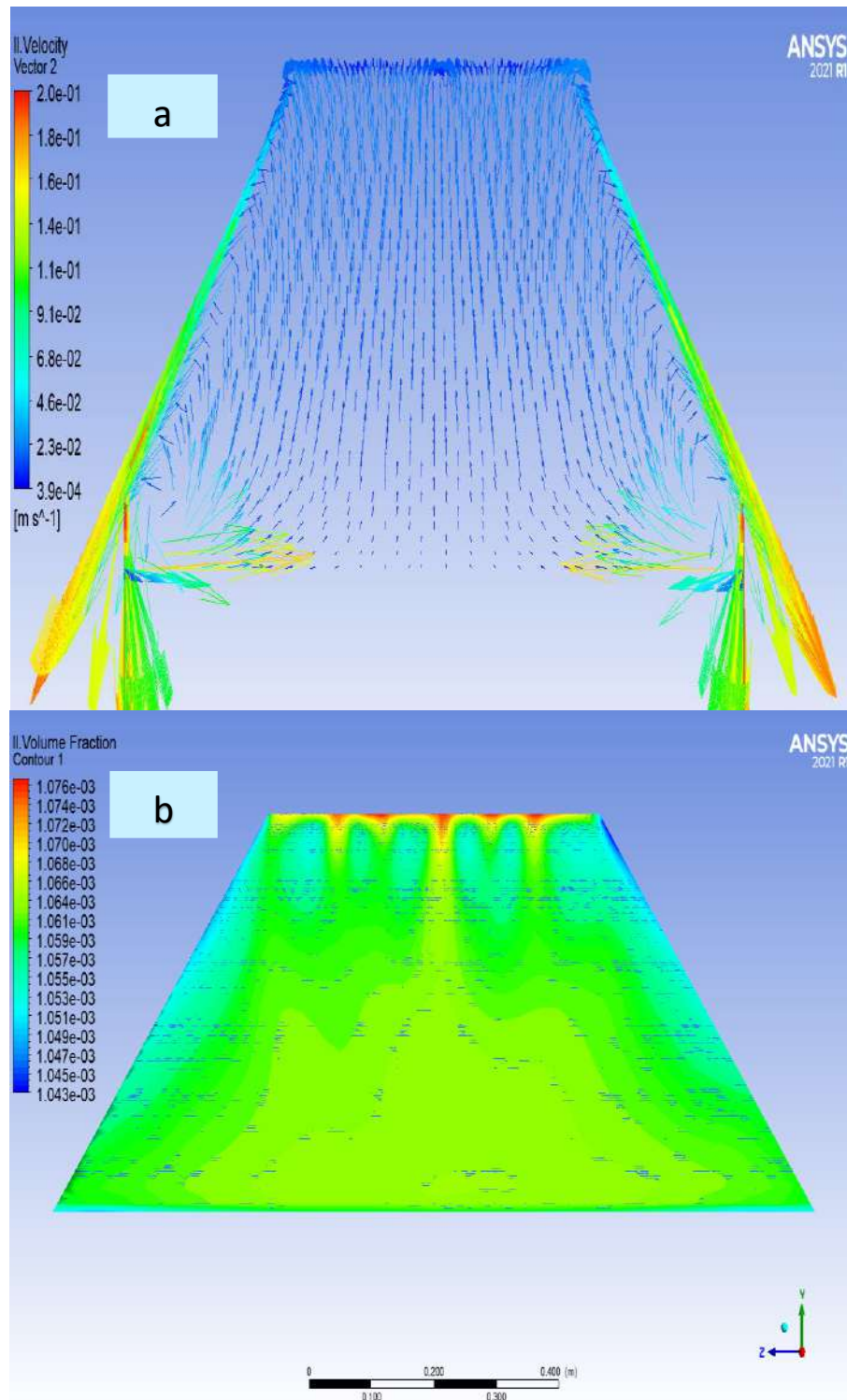
Figure (5.1) Solar still (CSS) at 11 am (a)Velocity vector, (b)Volume fraction
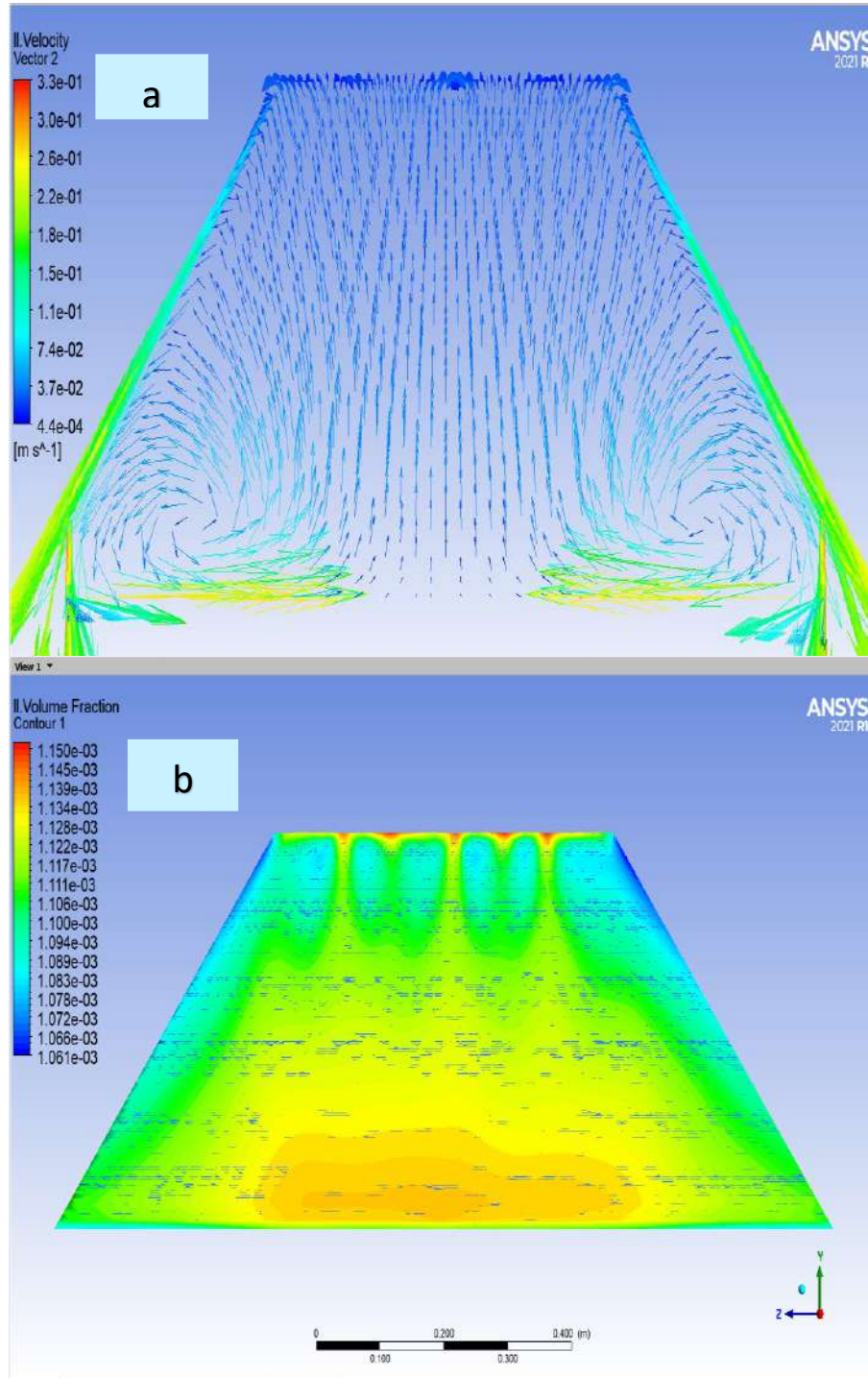
Figure (5.2) Solar still (CSS) at 1 pm (a)Velocity vector, (b)Volume fraction
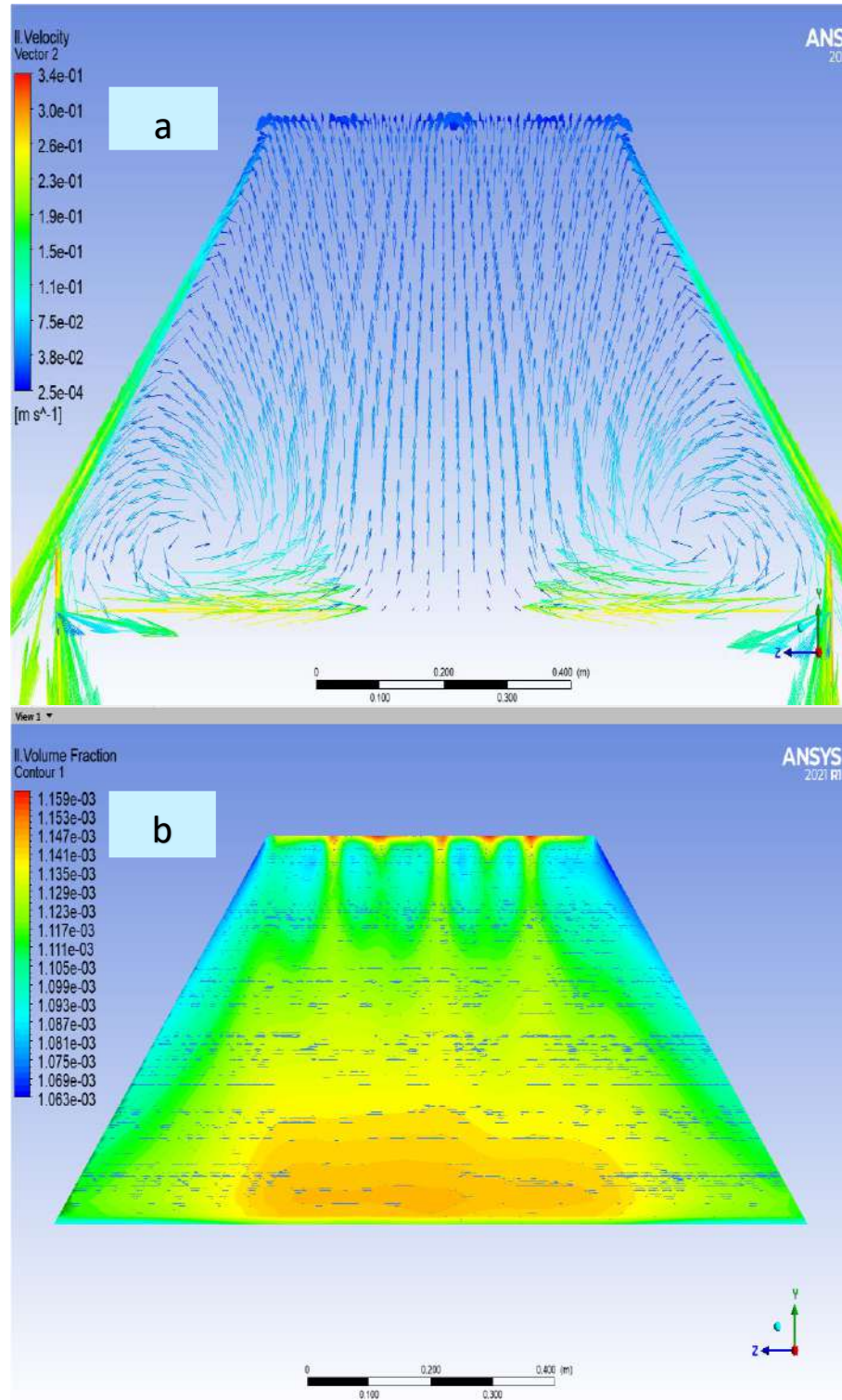
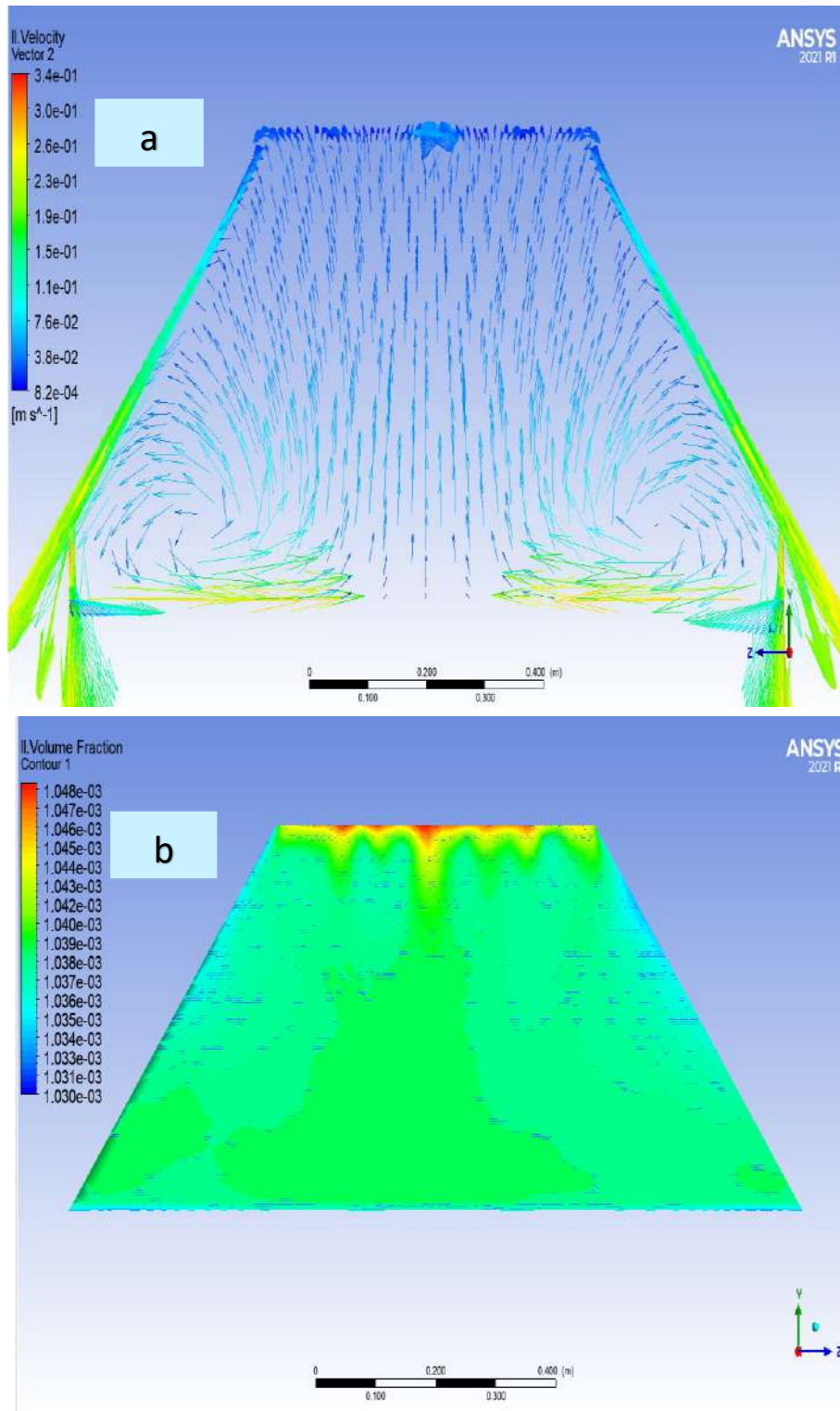Figure (5.3) Solar still (CSS) at 3 pm (a)Velocity vector, (b)Volume fraction

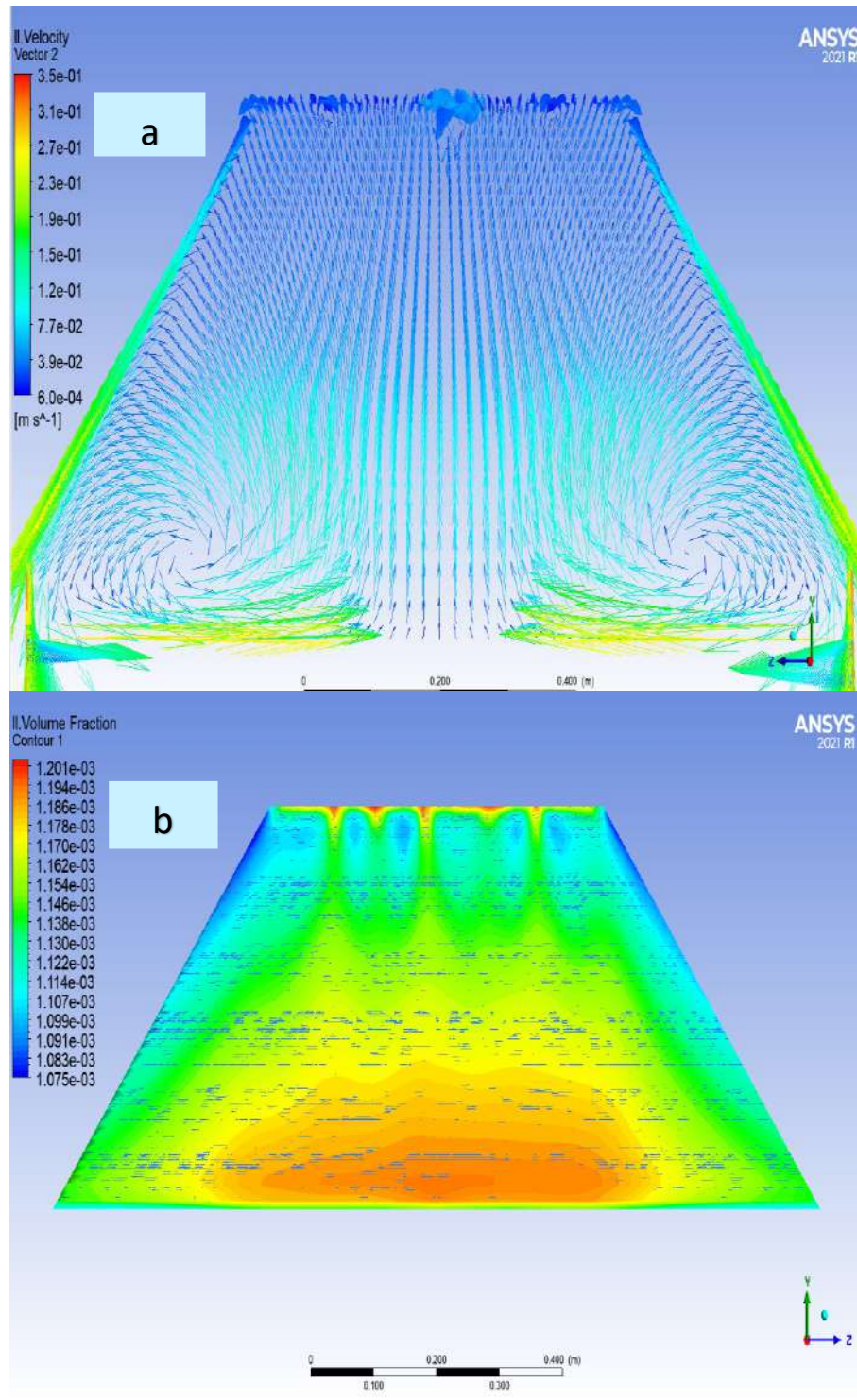Figure. (5.4) Solar still and (MSST3) at 11 am (a)Velocity vector, (b)Volume fraction

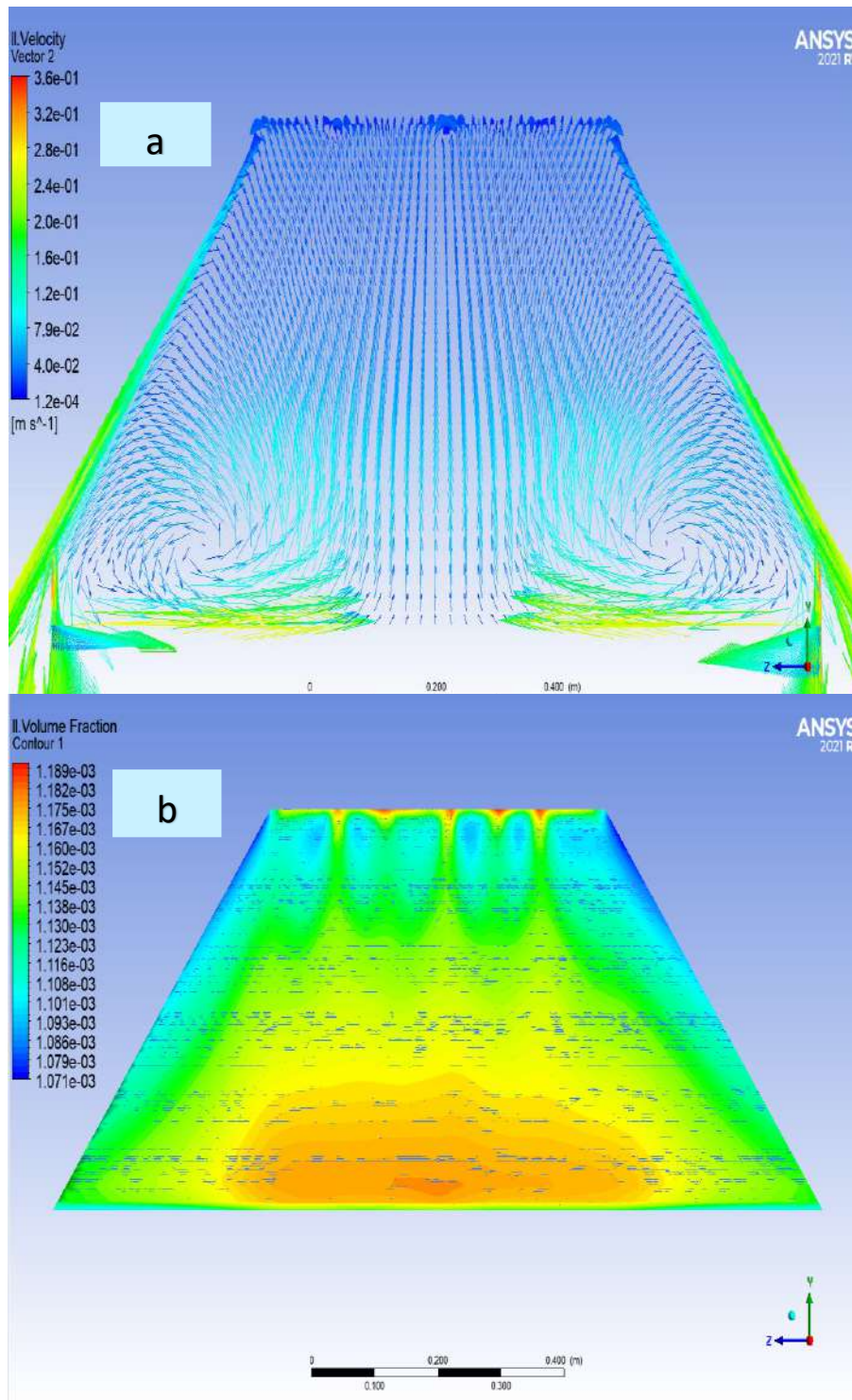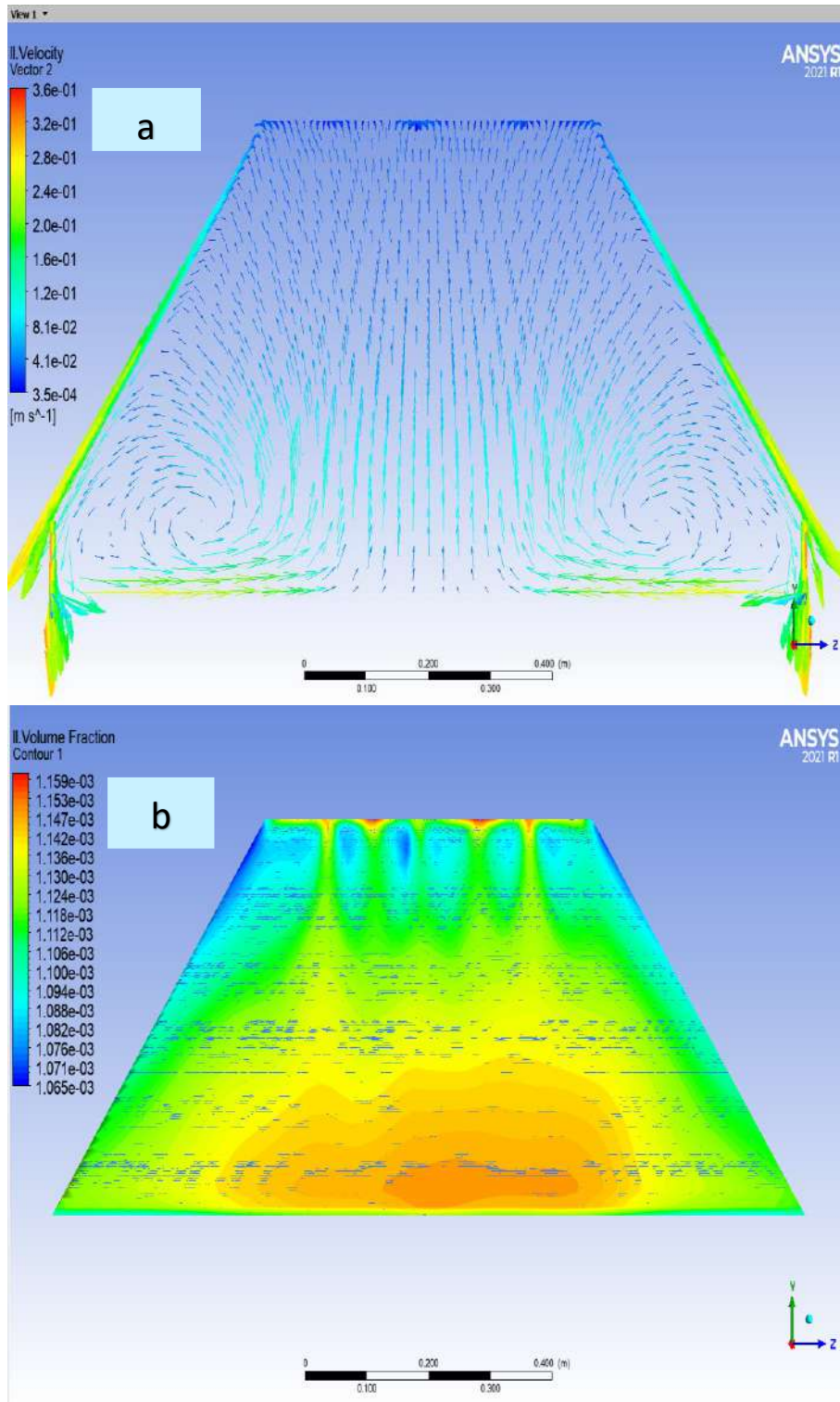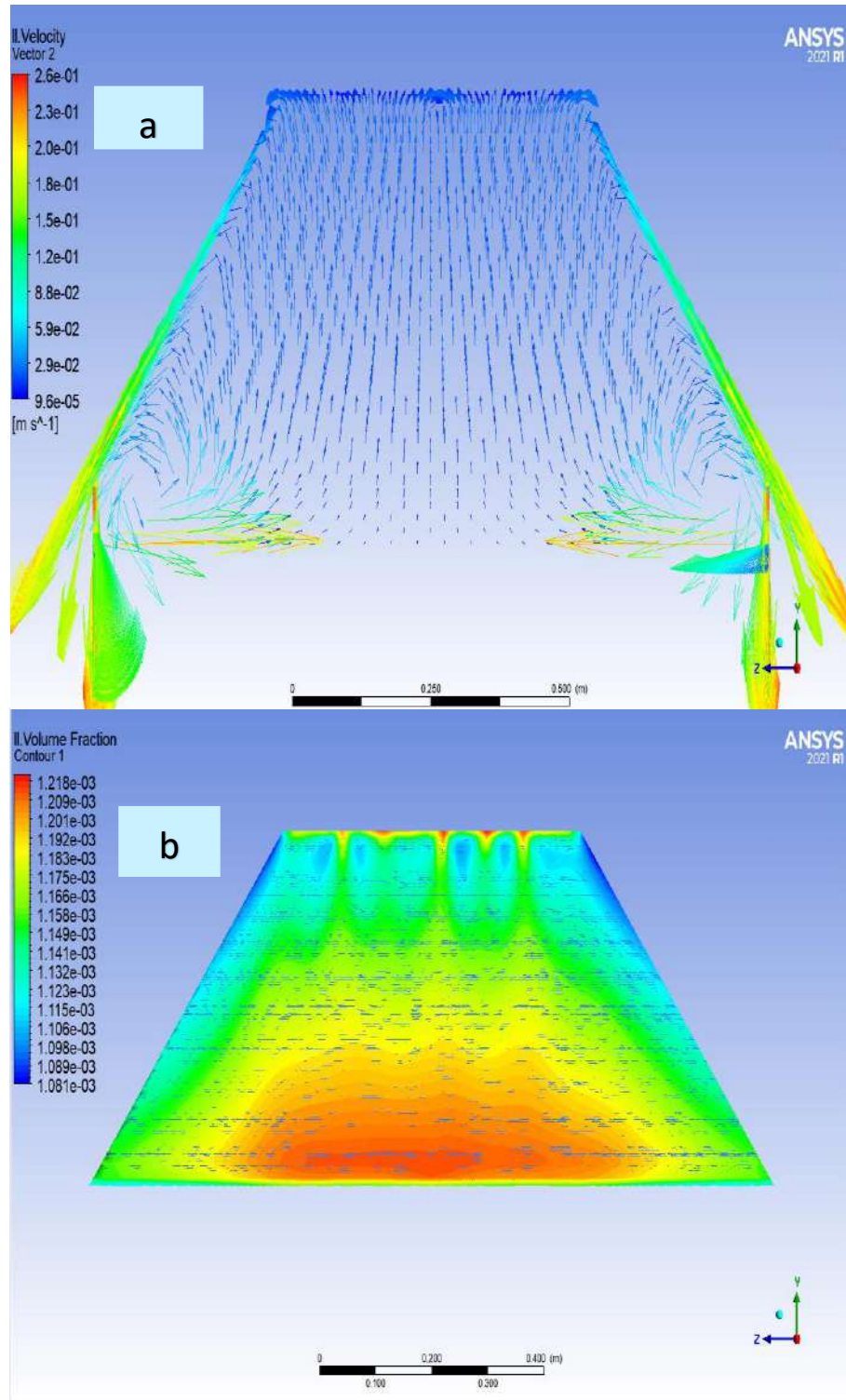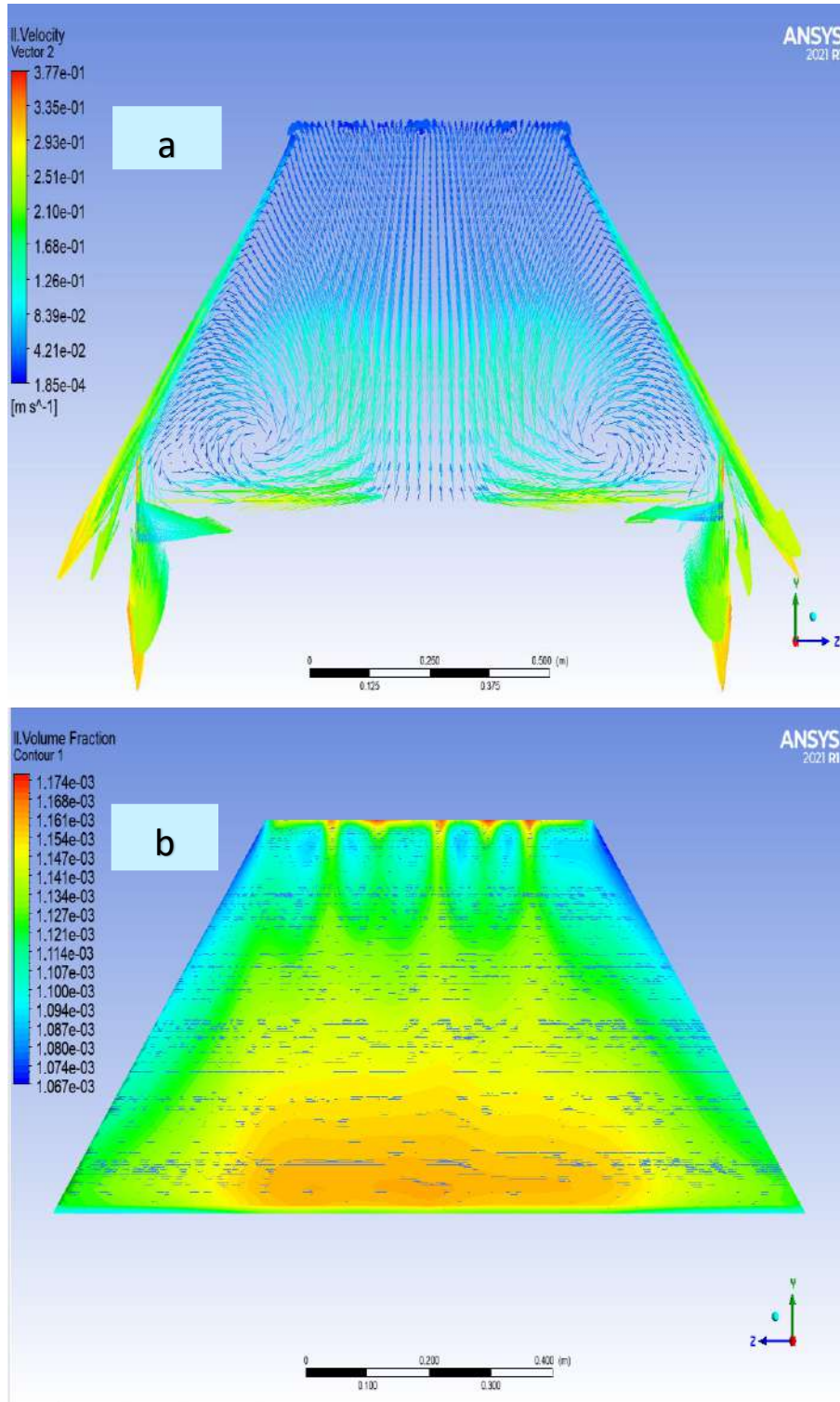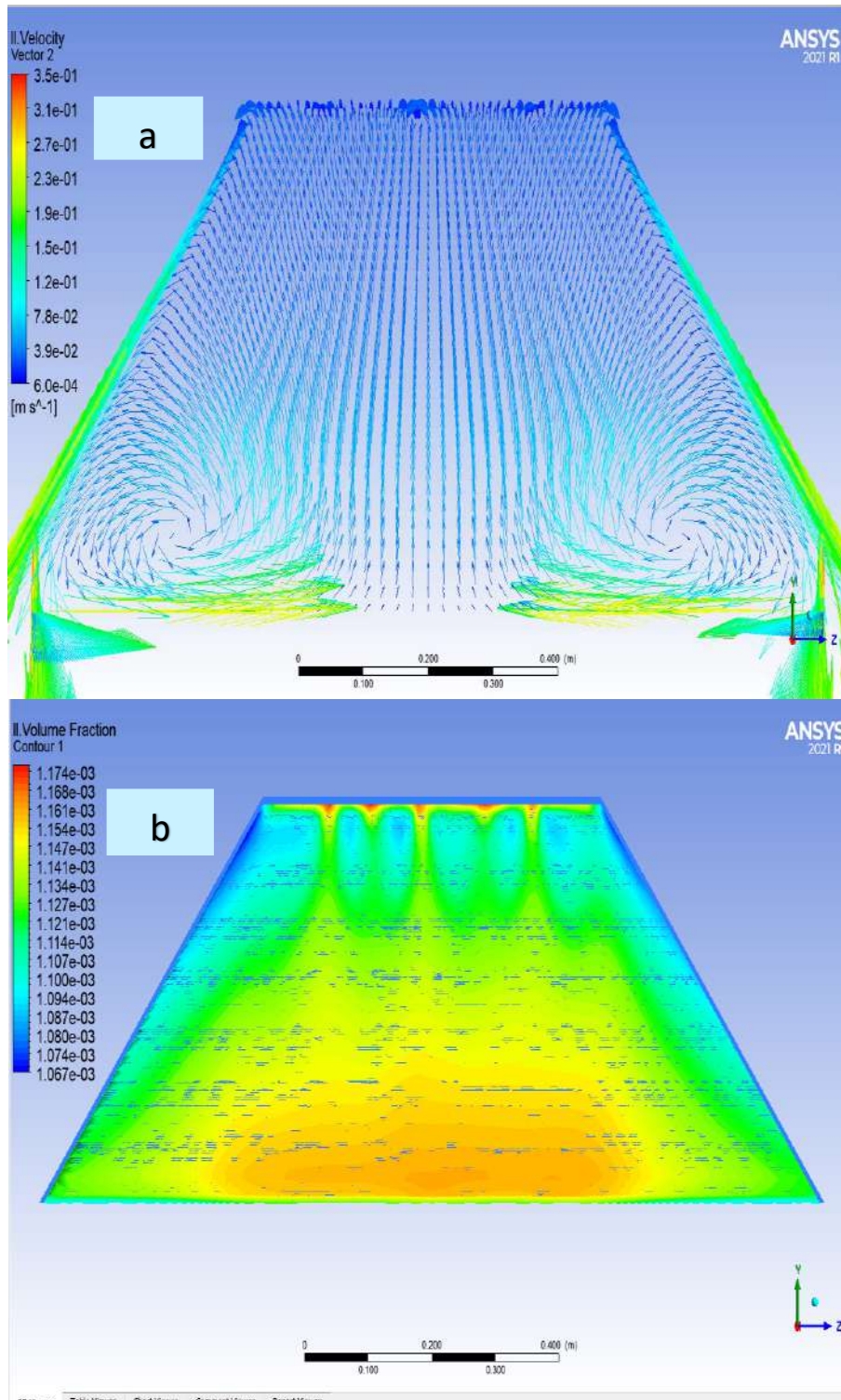Figure (5.5) Solar still (MSST3) at 1 pm (a)Velocity vector, (b)Volume fraction

Figure (5.6) Solar still (MSST3) at 3 pm (a)Velocity vector, (b)Volume fraction

Figure (5.7) Solar still (GPLF) at 11 am (a)Velocity vector, (b)Volume fraction

Figure (5.8) Solar still (GPLF) at 1:00 pm (a)Velocity vector, (b)Volume fraction

Figure (5.9) Solar still (GPLF) at 3:00 pm (a)Velocity vector, (b)Volume fraction

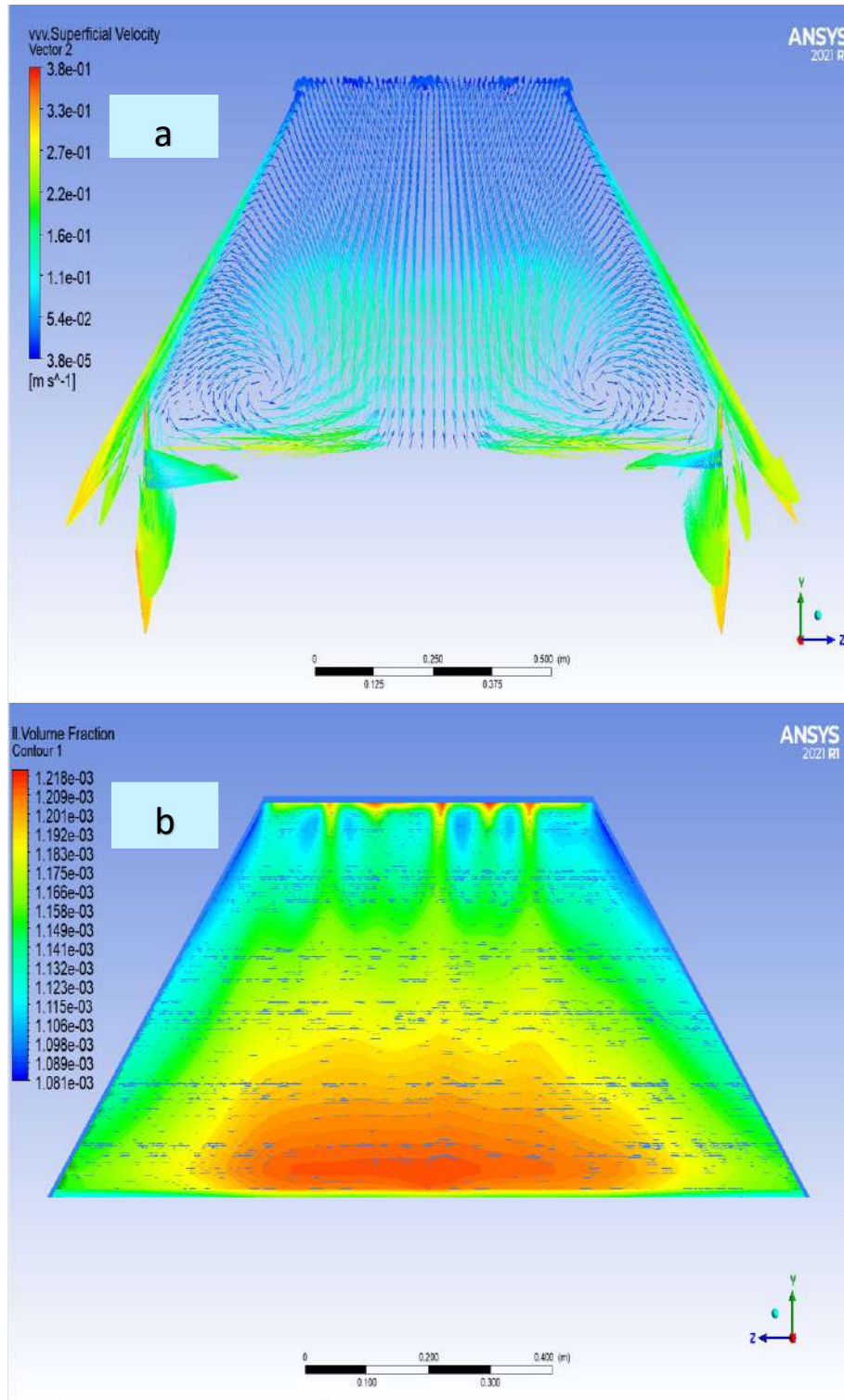Figure (5.10) Solar still (GPLF and MSST3) at 11 am (a)Velocity vector,

(b)Volume fraction

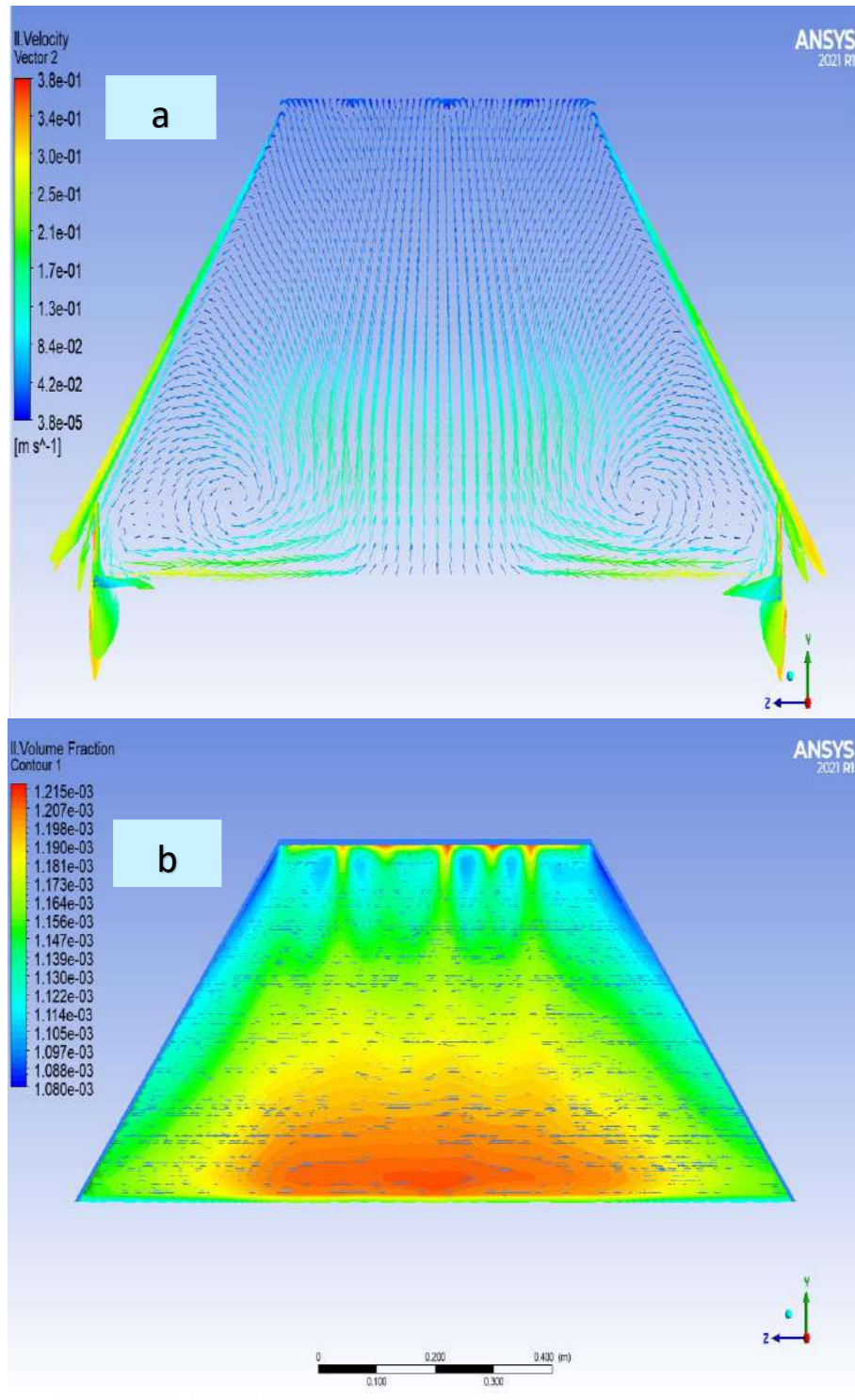Figure (5.11) Solar still (GPLF and MSST3) at 1 pm (a)Velocity vector,

(b)Volume fraction

Figure (5.12) Solar still (GPLF and MSST3) at 3 pm (a)Velocity vector,
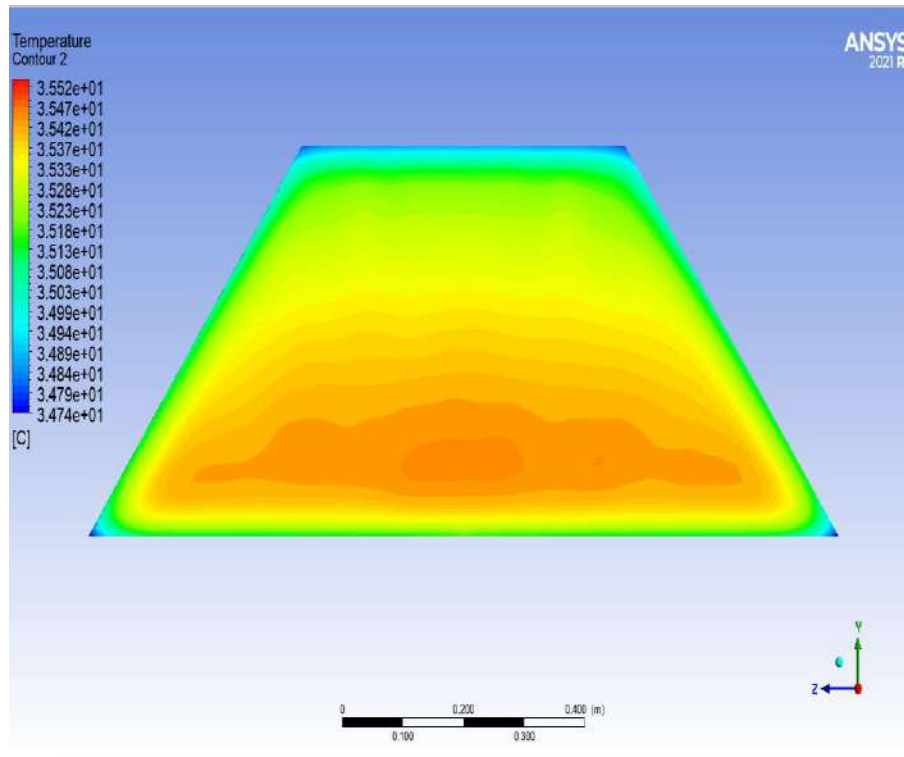
(b)Volume fraction

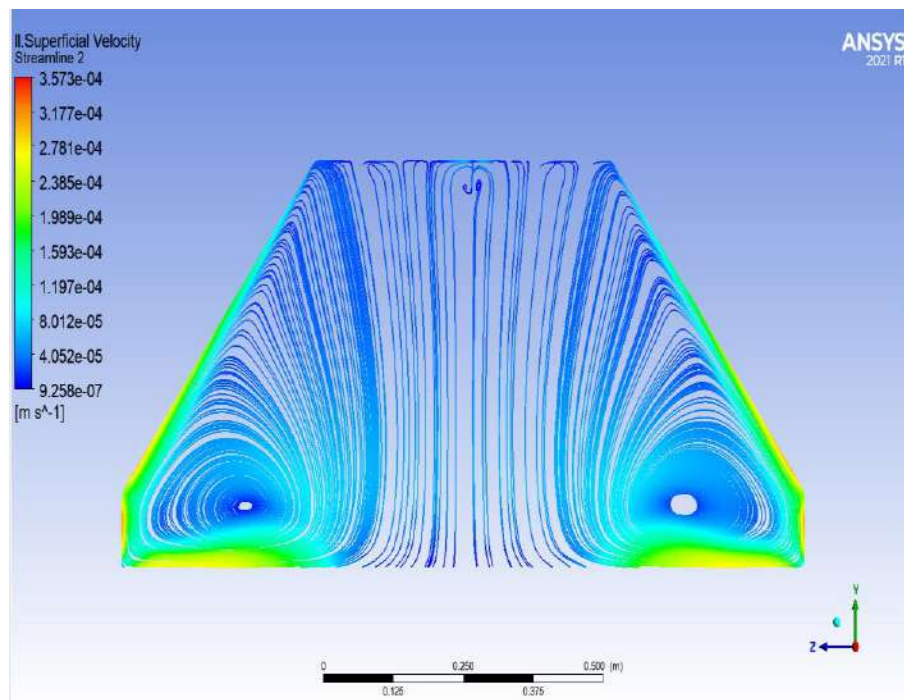Figure (5.13) Temperature distribution when using (CSS) only at 11 am

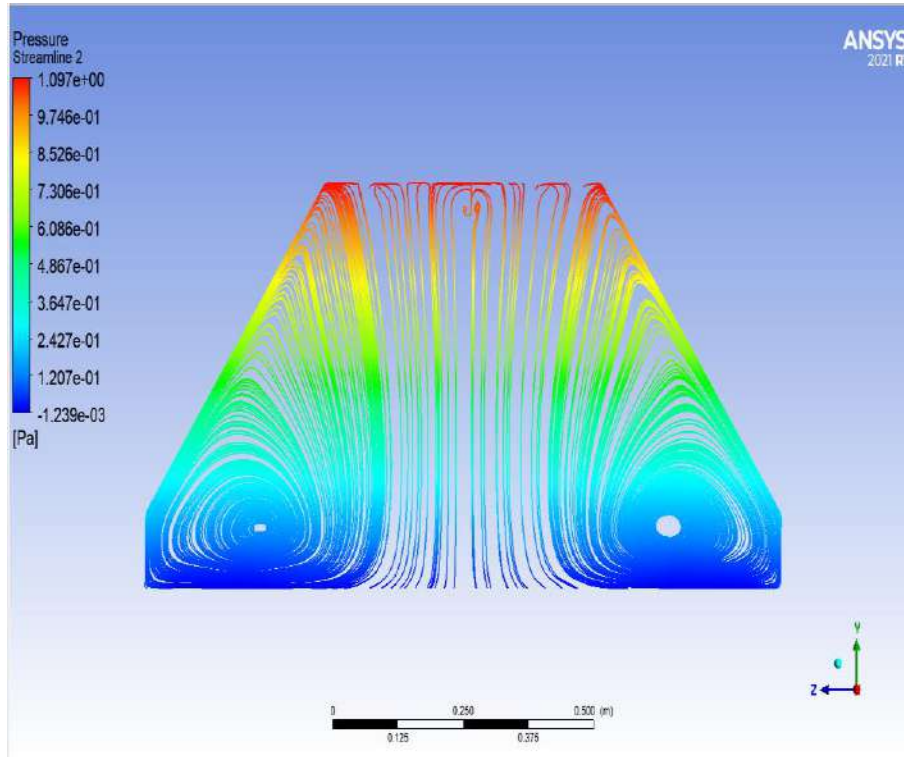Figure (5.14) Streamline distribution when using (CSS) only at 11 am

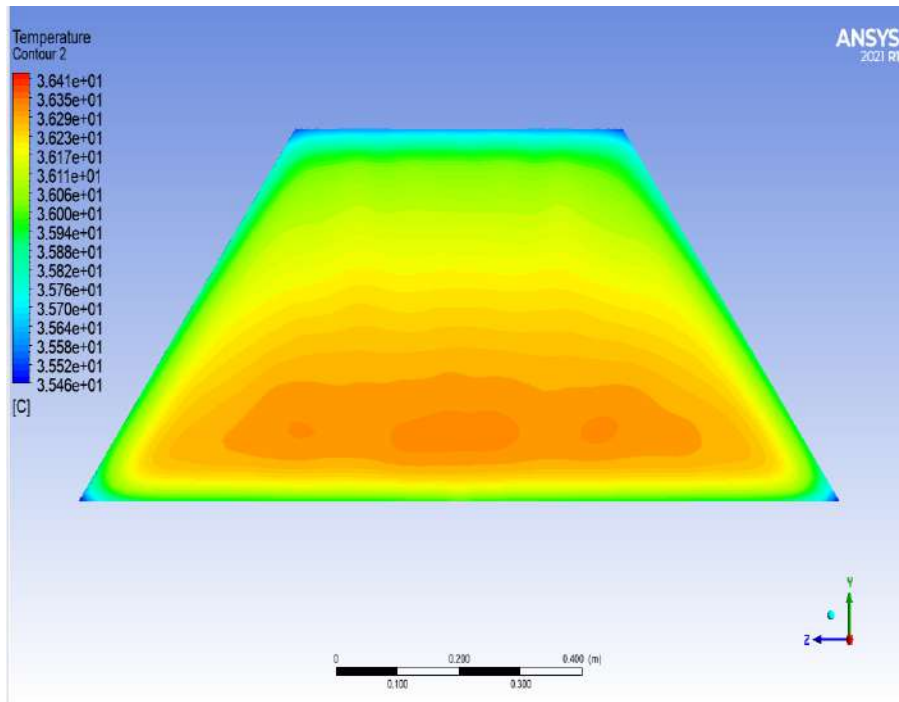Figure (5.15) Pressure streamline distribution when using (CSS) only at 11 am

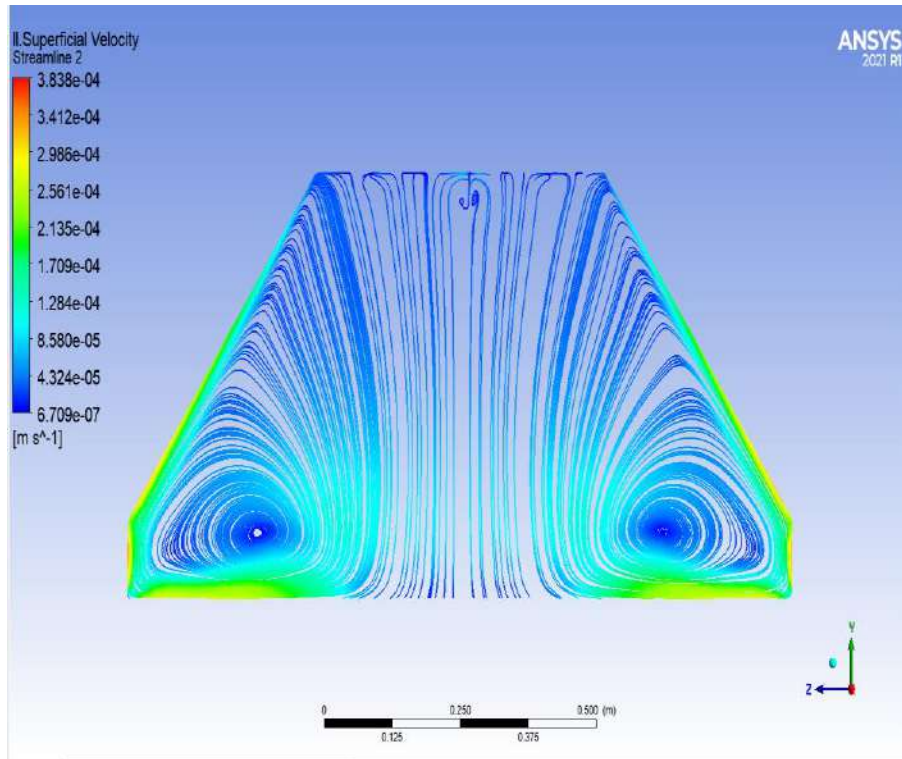Figure (5.16) Temperature distribution when using (CSS) only at 1 pm

Figure (5.17) Streamline distribution when using (CSS) only at 1 pm
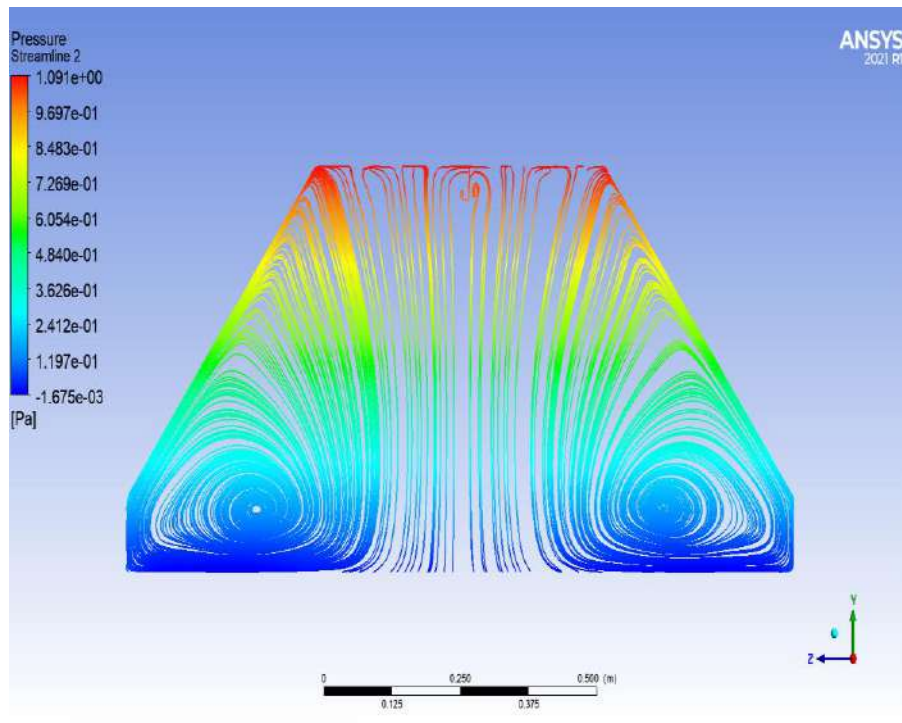

Figure (5.18) Pressure streamline distribution when using (CSS) only at 1 pm

Figure (5.19) Temperature distribution when using (CSS) only at 3 pm
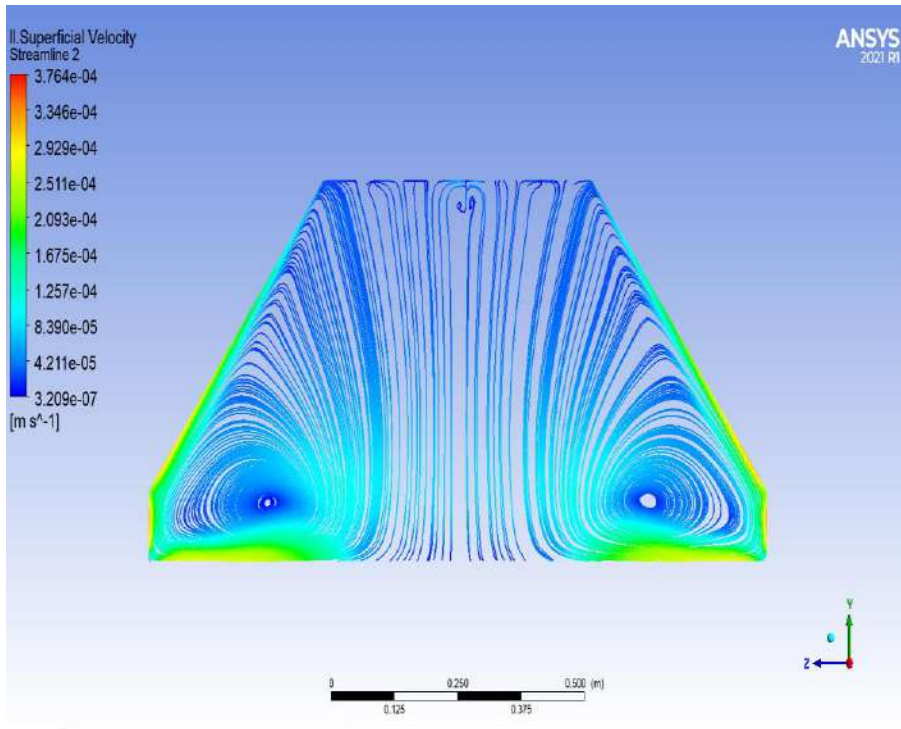
Figure (5.20) Streamline distribution when using (CSS) only at 3 pm
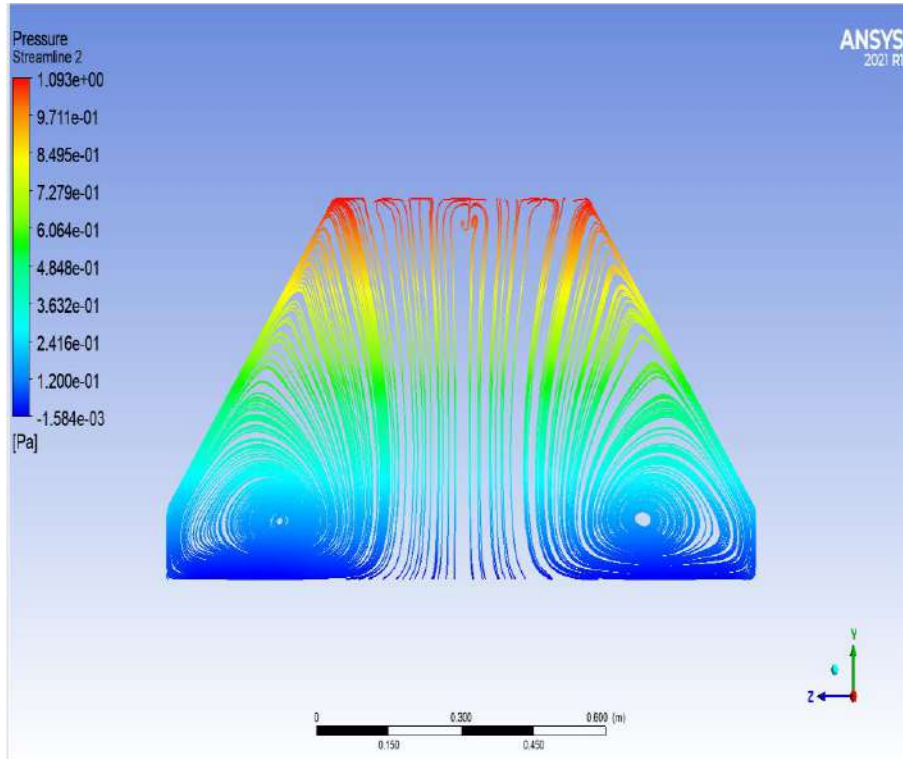
Figure (5.21) Pressure streamline distribution when using CSS only at 3pm

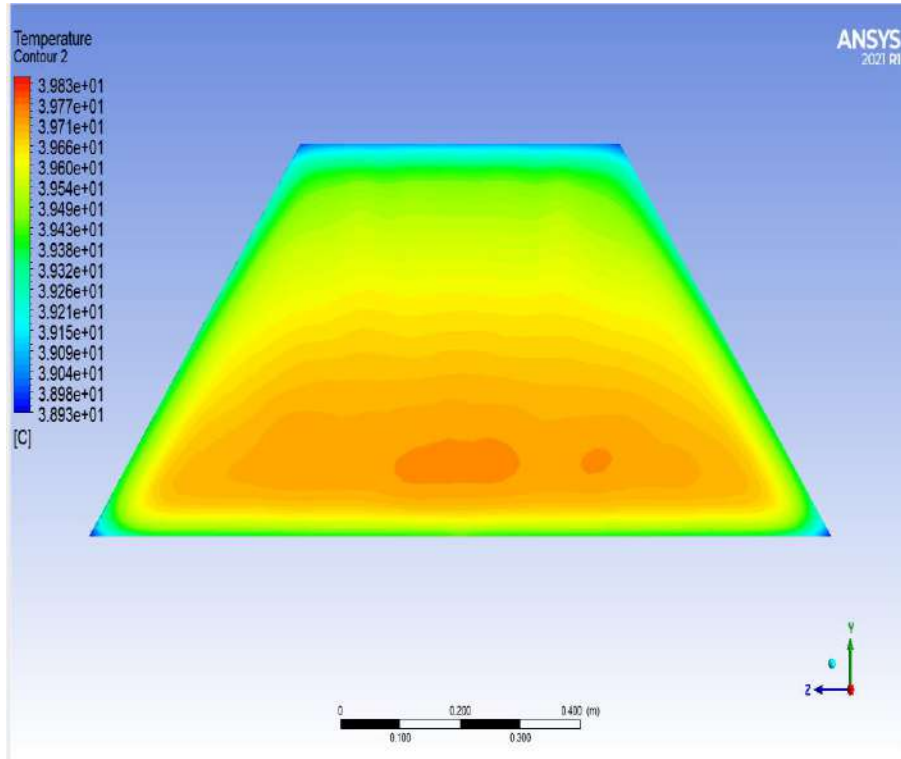Figure (5.22) Temperature distribution when using solar still (MSS$_{T3}$) at 11 am

Figure (5.23) Streamline distribution when using solar still (MSS**T3**) at 11 am

Figure (5.24) Pressure streamline distribution when using solar still (MSS**T3**) at 11 am

Figure (5.25) Temperature distribution when using solar still (MSS_{T3}) at 1 pm

Figure (5.26) Streamline distribution when using solar still (MSS_{T3}) at 1 pm

Figure (5.27) Pressure streamline distribution when using solar still (MSS$_{T3}$) at 1pm

Figure (5.28) Temperature distribution when using solar still (MSS$_{T3}$) at 3 pm

Figure (5.29) Streamline distribution when using solar still (MSS_{T3}) at 3 pm

Figure (5.30) Pressure streamline distribution when using solar still (MSS_{T3}) at 3pm
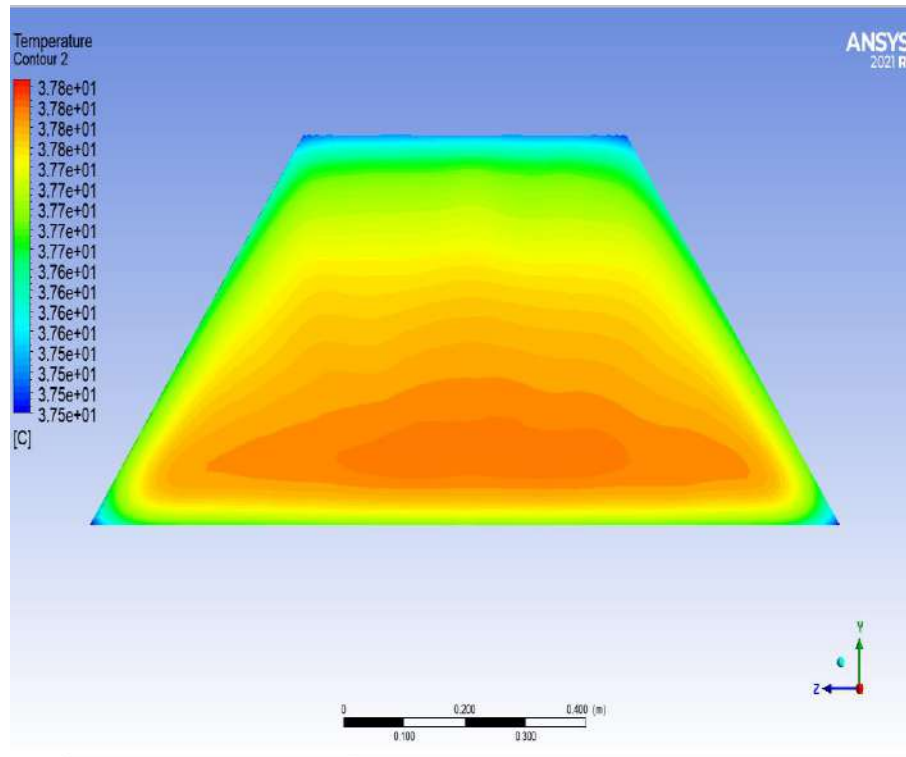
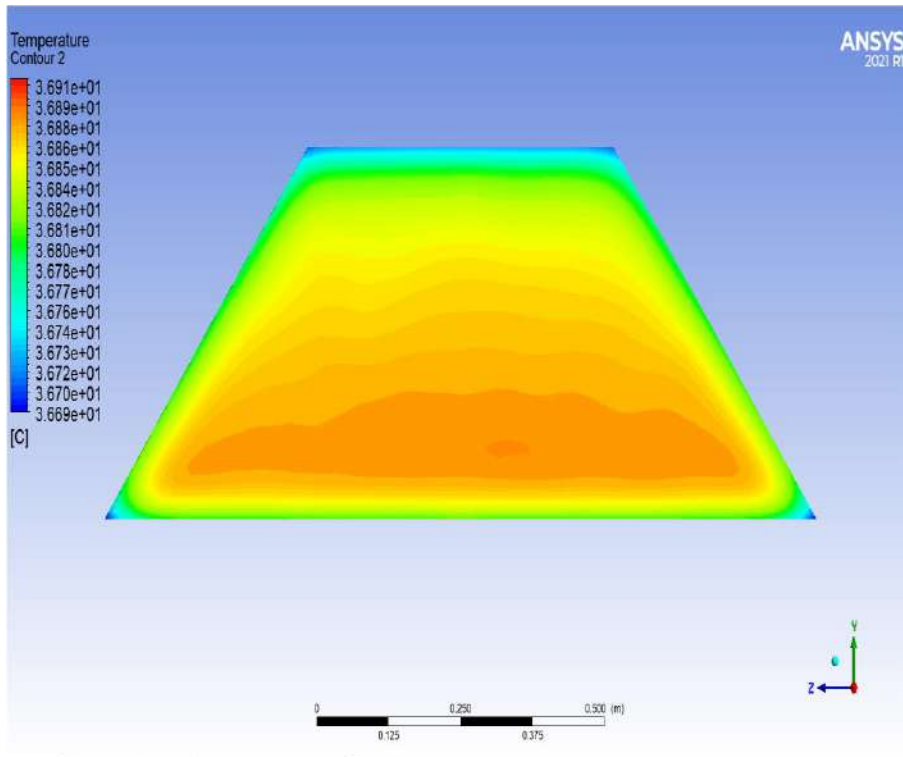Figure (5.31) Temperature distribution when using solar still (GPLF) at 11 am
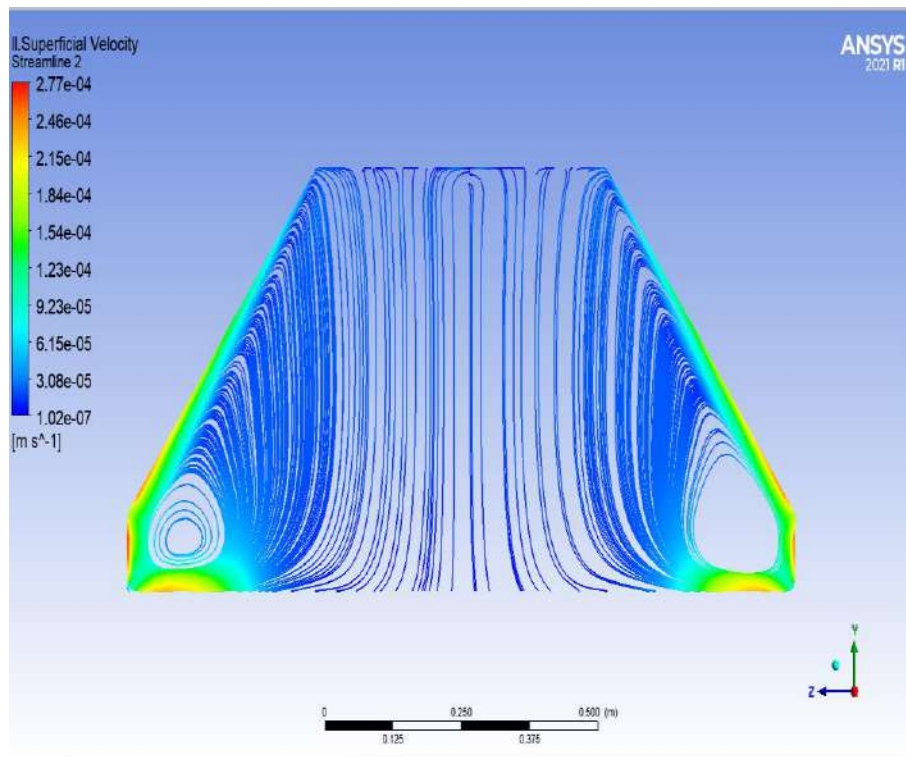
Figure (5.32) Streamline distribution when using solar still (GPLF) at 11 am
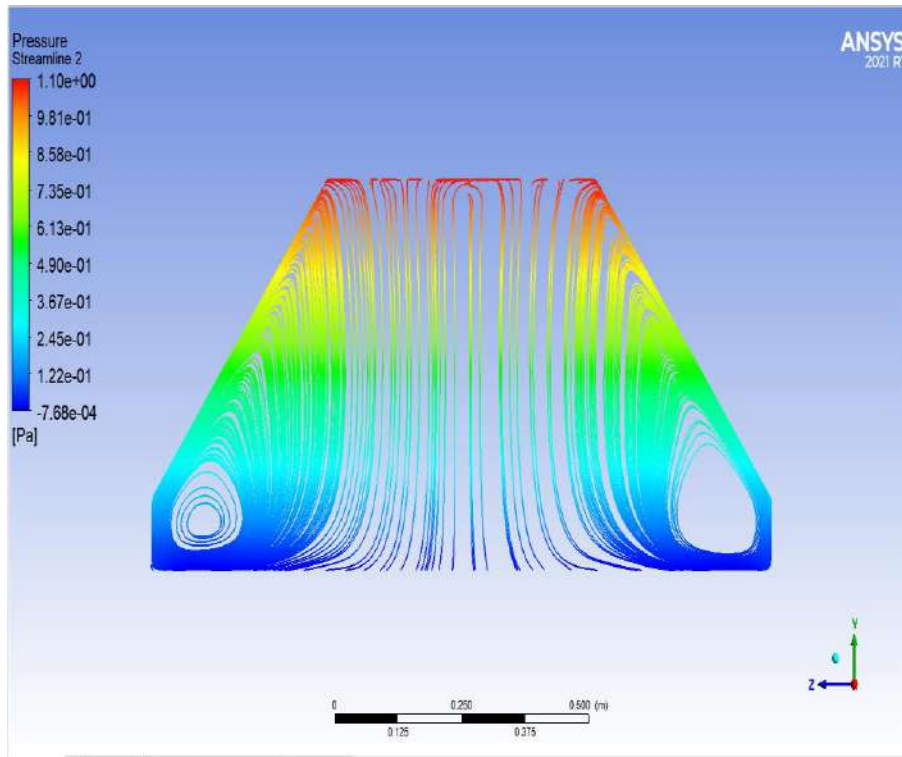
Figure (5.33) Pressure Streamline distribution when using solar still (GPLF) at 11 am
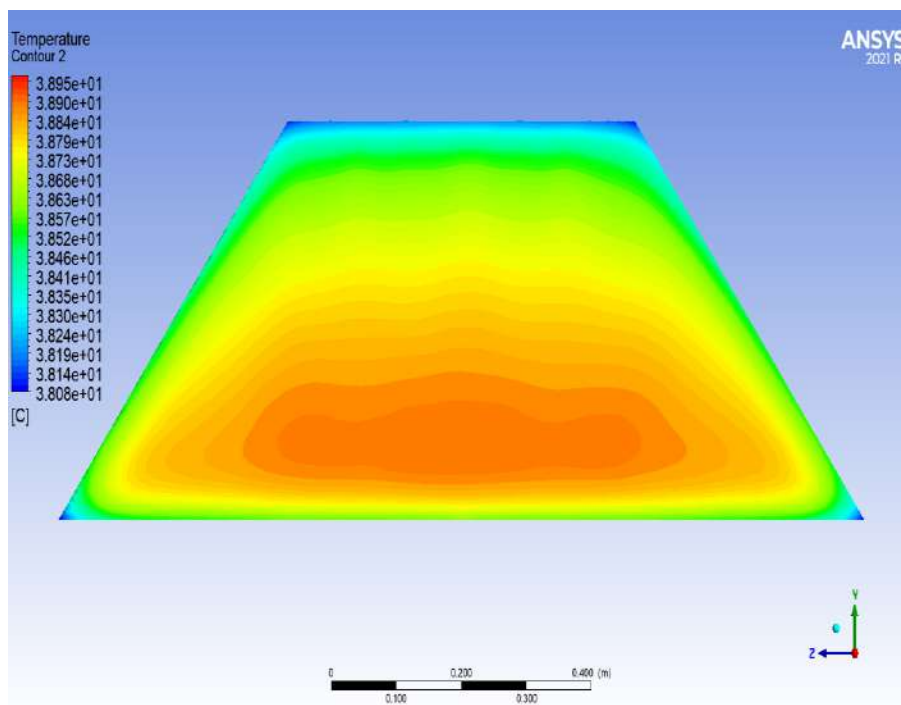
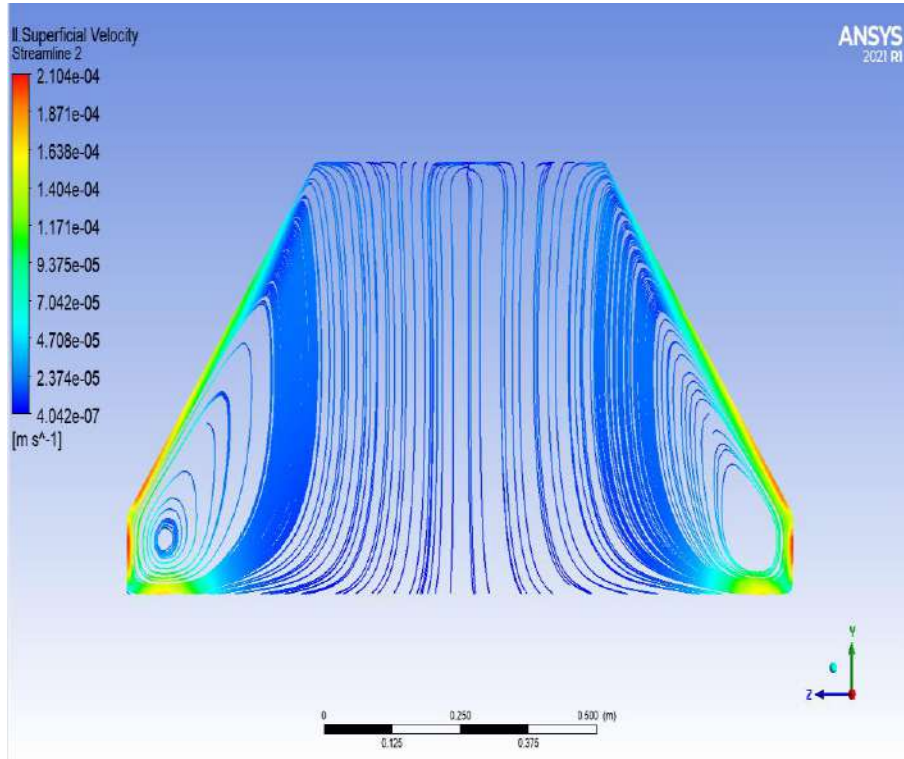Figure (5.34) Temperature distribution when using solar still (GPLF) at 1pm
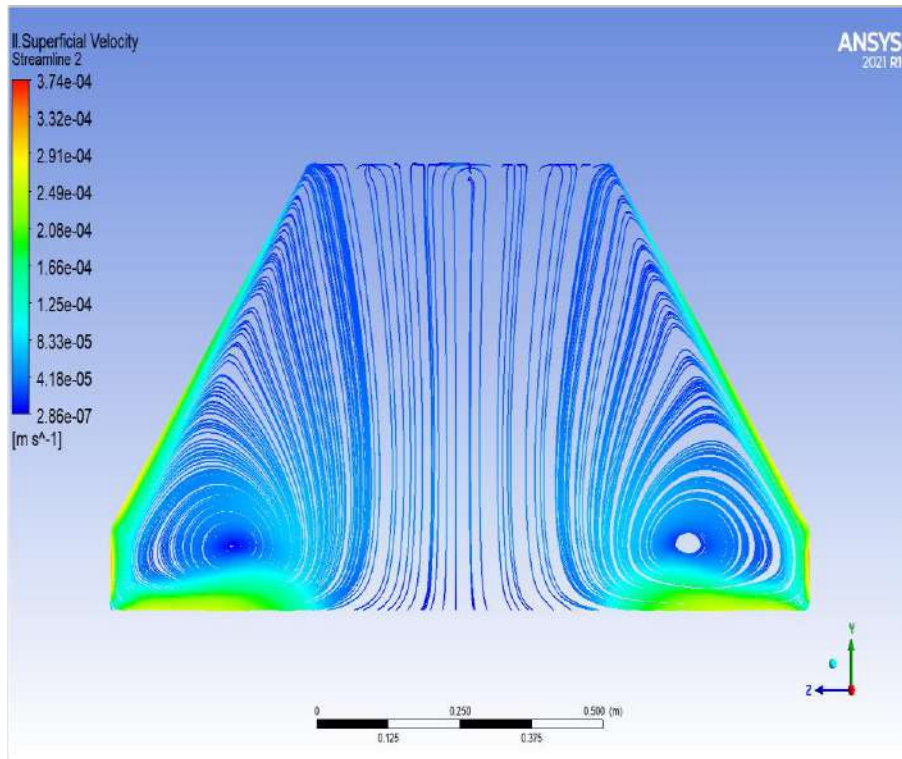
Figure (5.35) Streamline distribution when using solar still (GPLF) at 1 pm
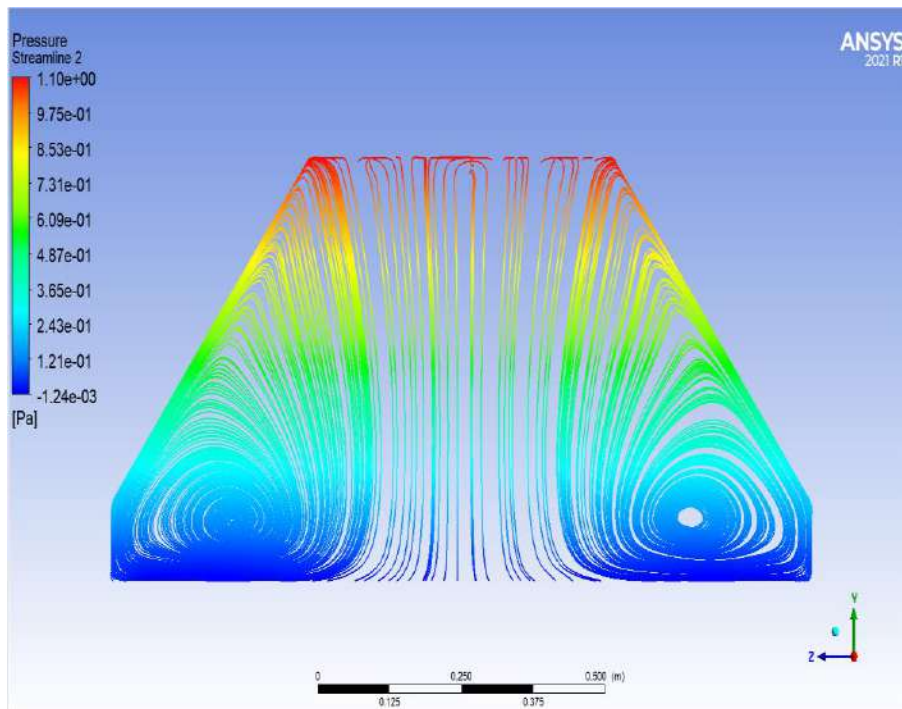
Figure (5.36) Pressure Streamline distribution when using solar still (GPLF) at 1 pm
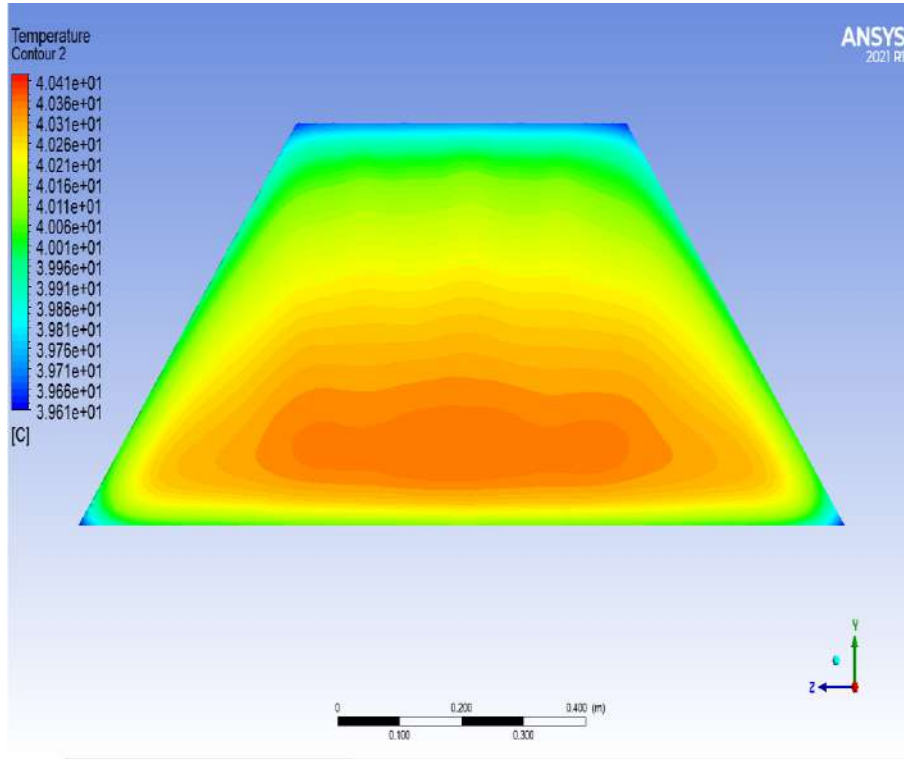
Figure (5.37) Temperature distribution when using solar still (GPLF) at 3pm
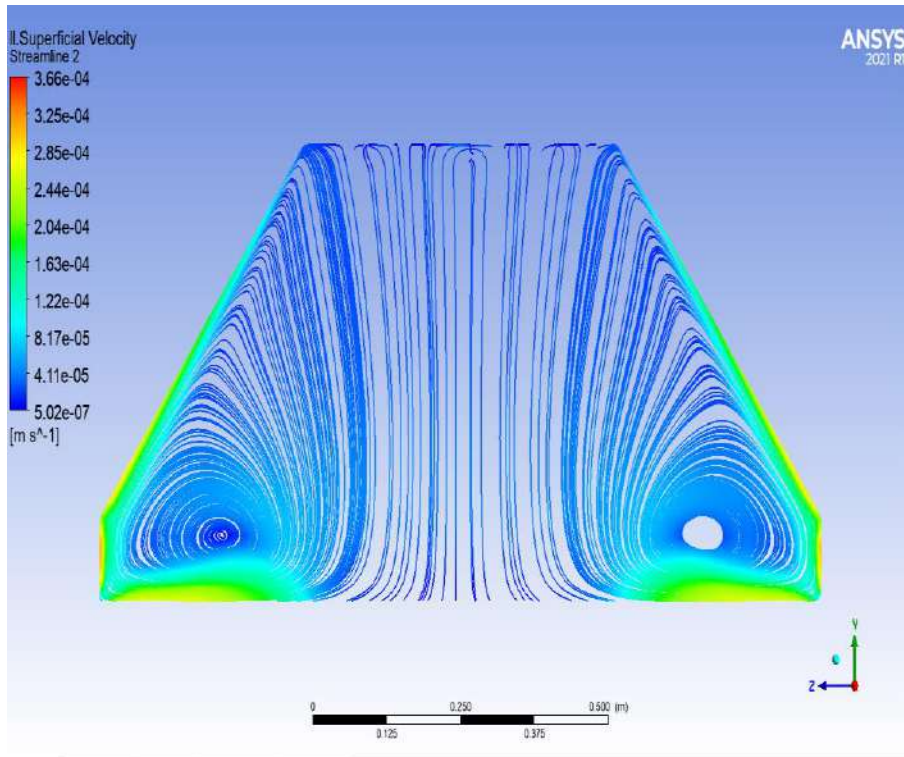
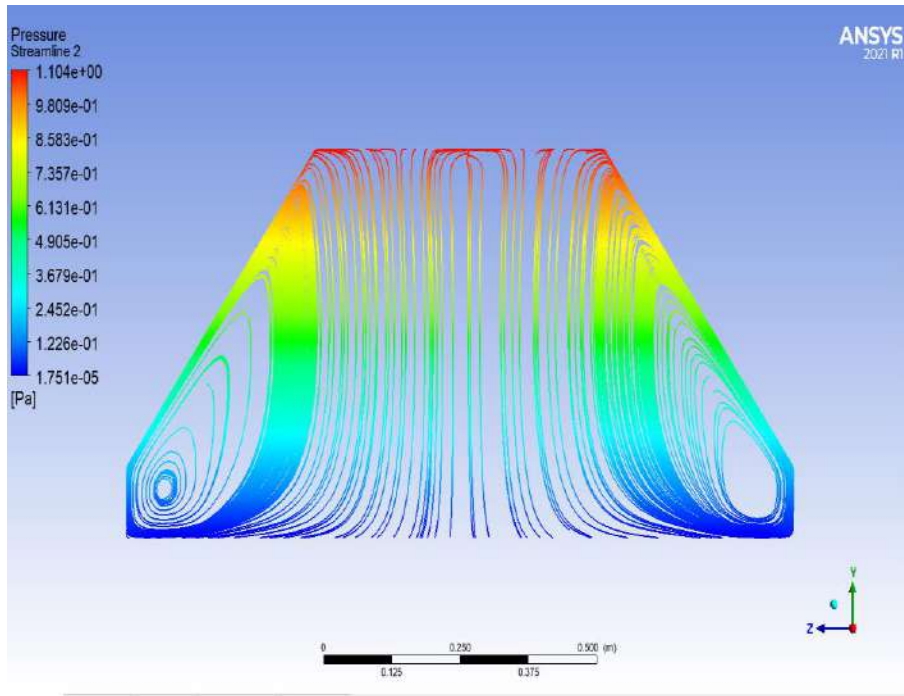Figure (5.38) Streamline distribution when using solar still (GPLF) at 3pm
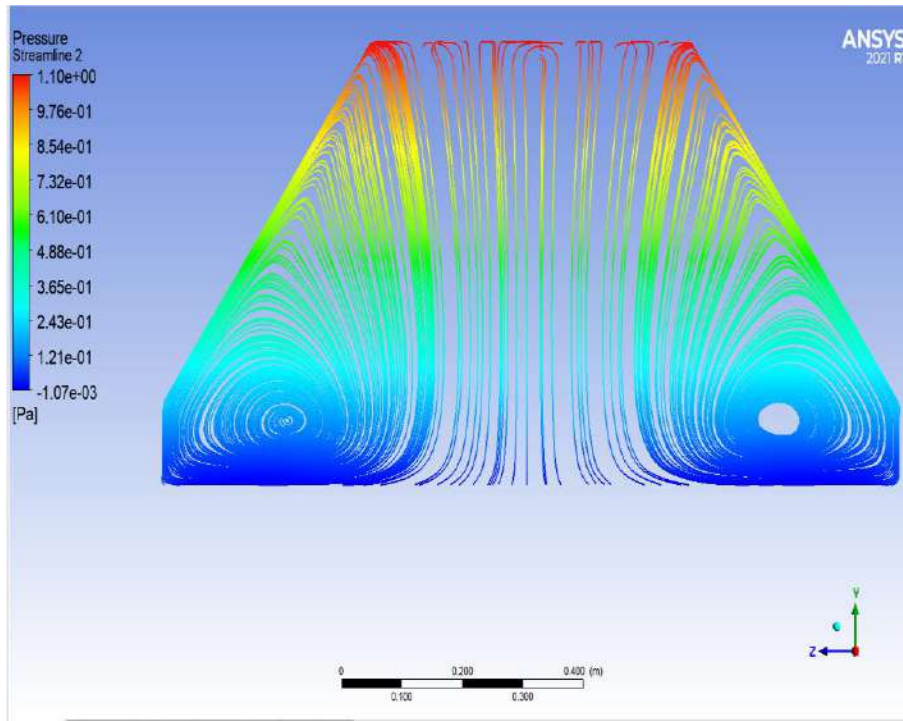
Figure (5.39) Pressure streamline distribution when using solar still (GPLF) at 3 pm
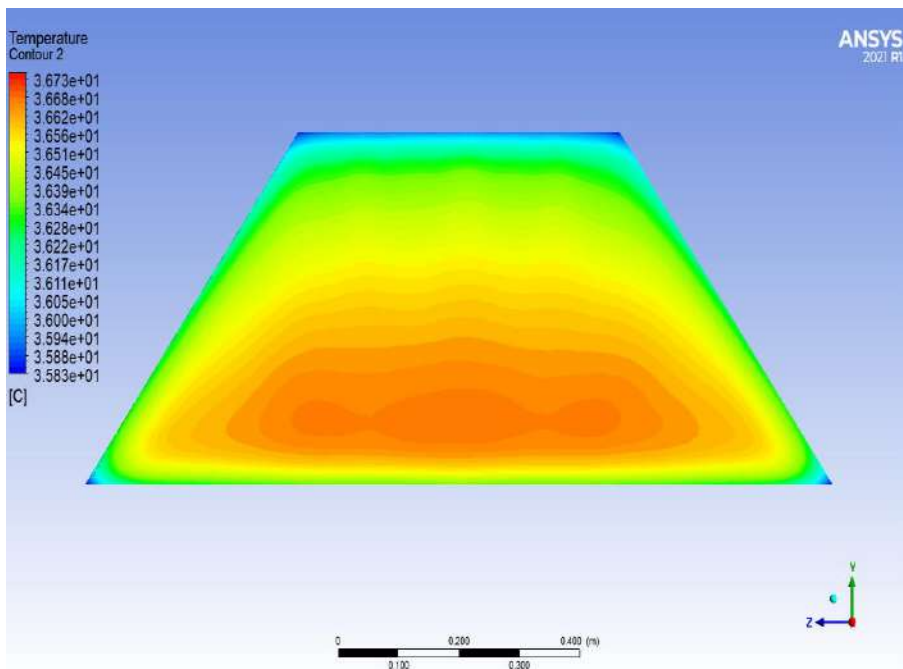
Figure (5.40) Temperature distribution when using solar still (GPLF and MSS$_{T3}$) at 11 am
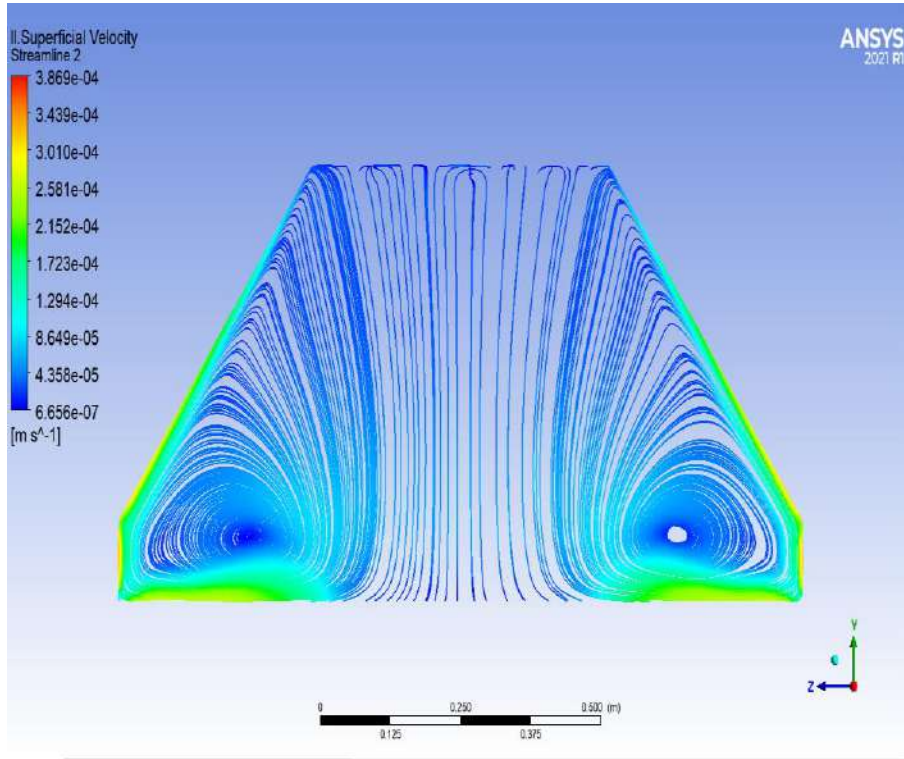
Figure (5.41) Streamline distribution when using solar still (GPLF and MSS$_{T3}$) at 11 am
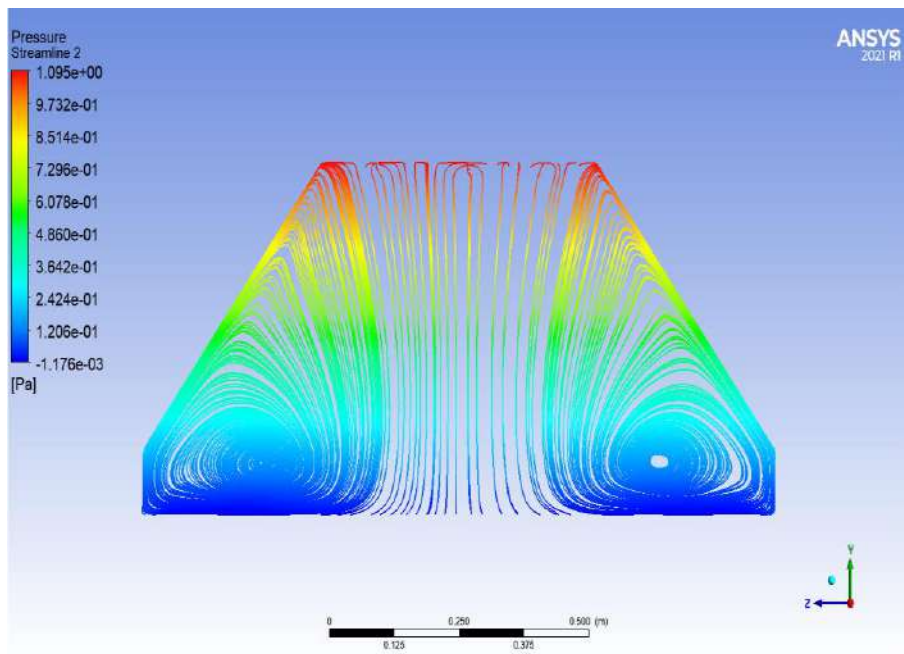
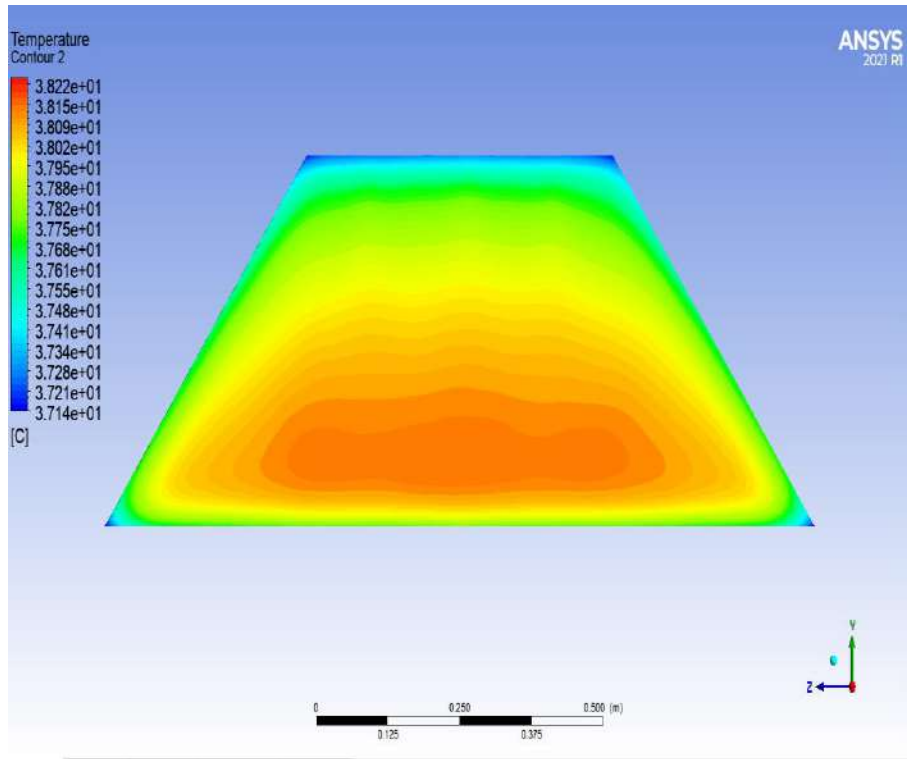Figure (5.42) Pressure streamline distribution when using solar still (GPLF and MSS$_{T3}$) at 11 am
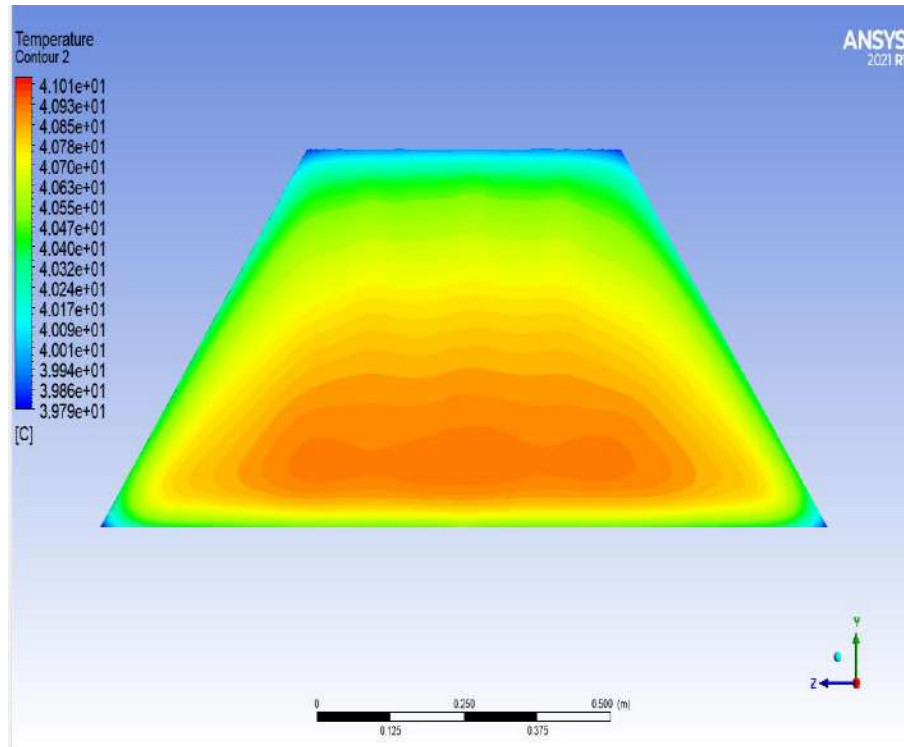
Figure (5.43) Temperature distribution when using solar still (GPLF and MSS$_{T3}$) at 1 pm
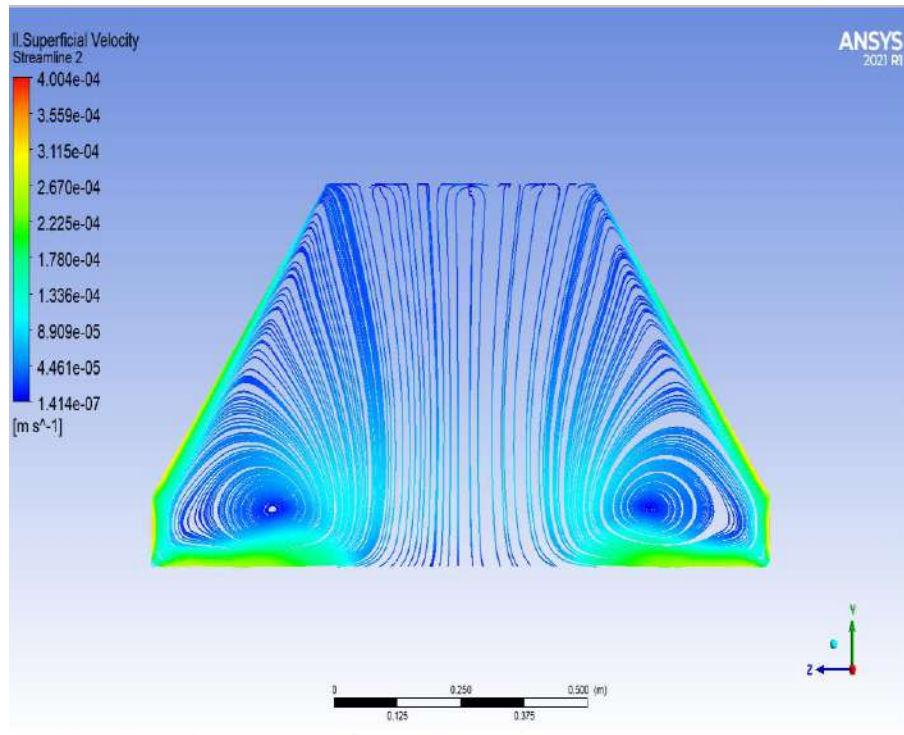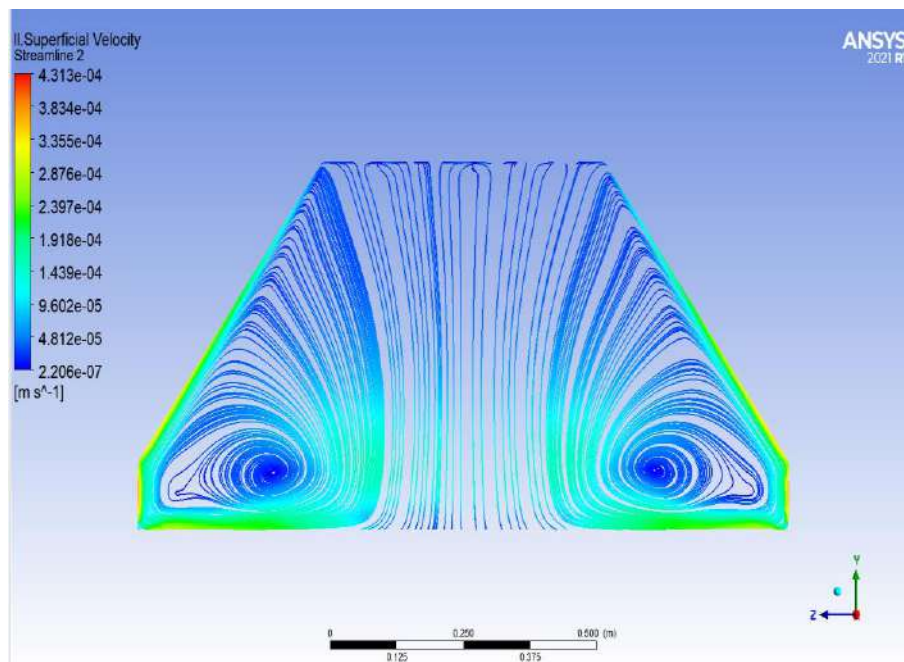

Figure (5.44) Streamline distribution when using solar still (GPLF and MSS$_{T3}$) at 1pm
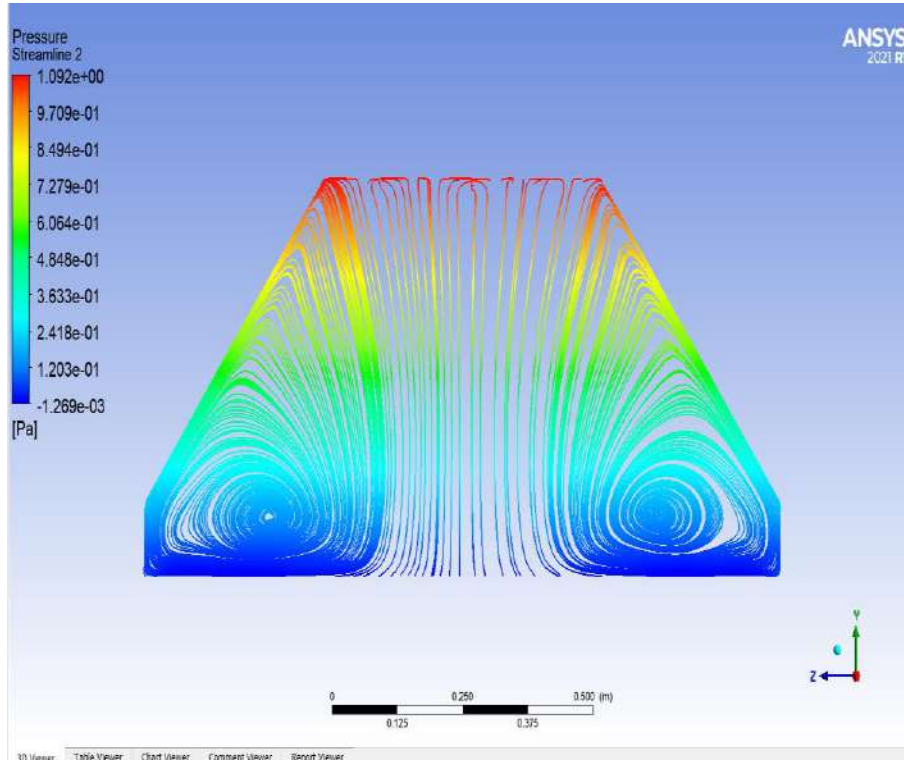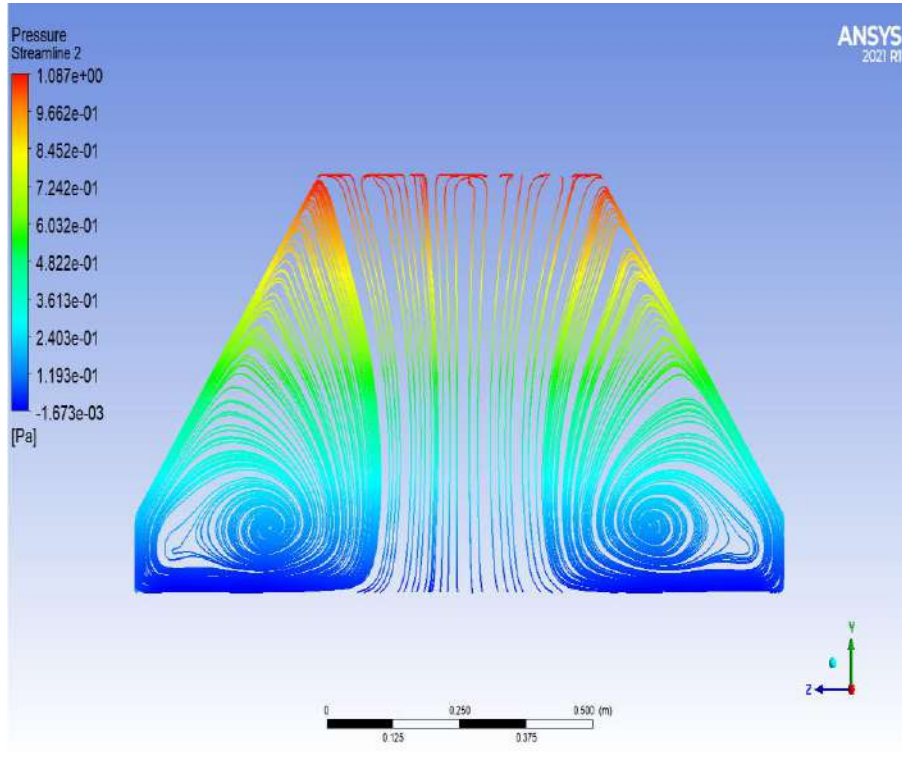
Figure (5.45) Pressure streamline distribution when using solar still (GPLF and MSS$_{T3}$) at 1 pm
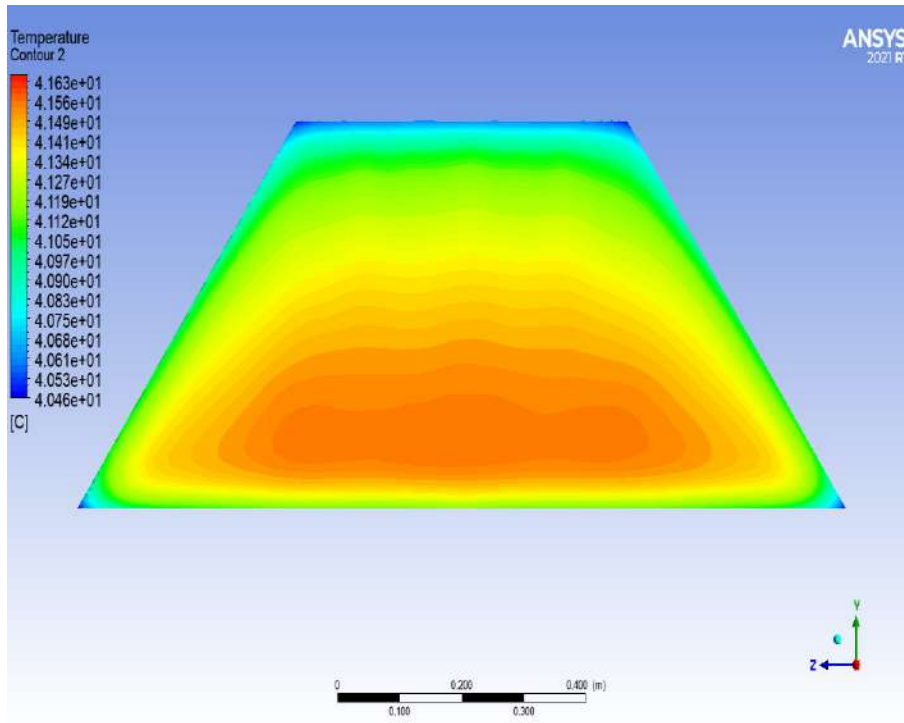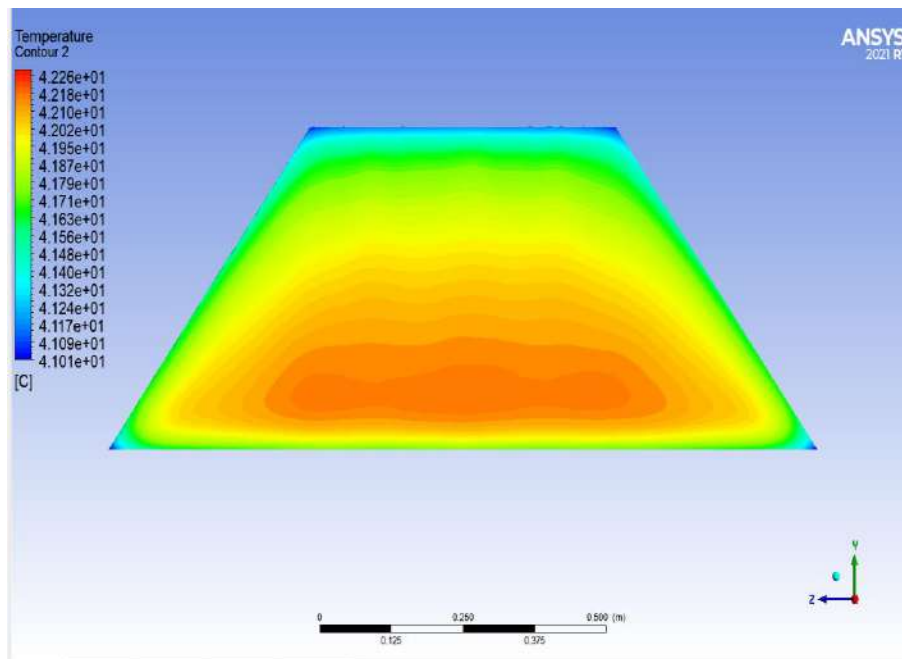

Figure (5.46) Temperature distribution when using solar still (GPLF and MSS$_{T3}$) at 3 pm
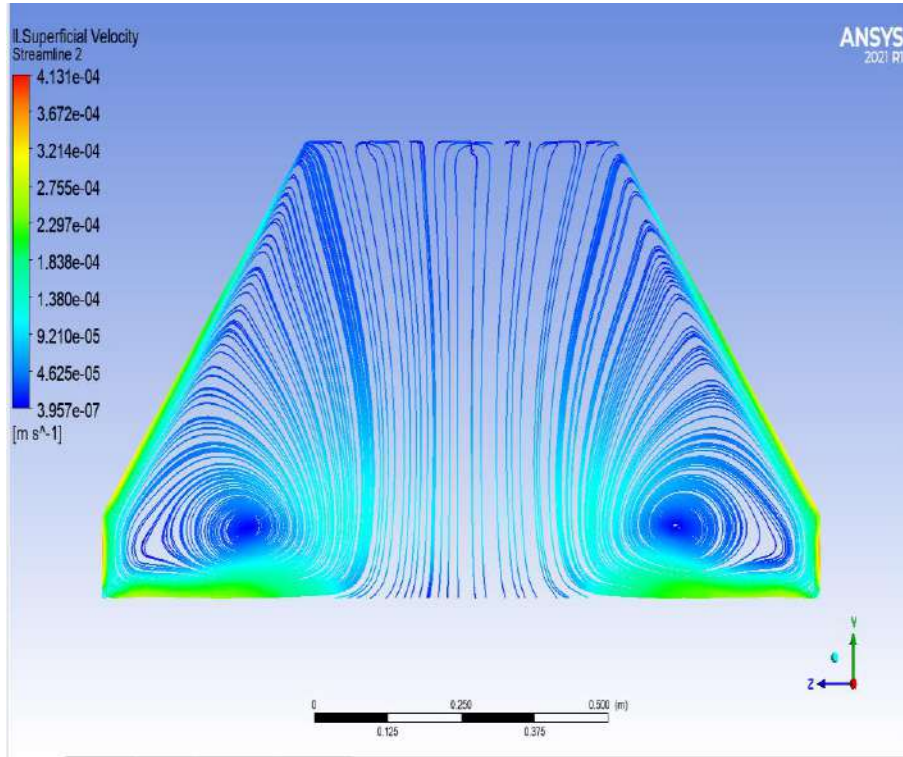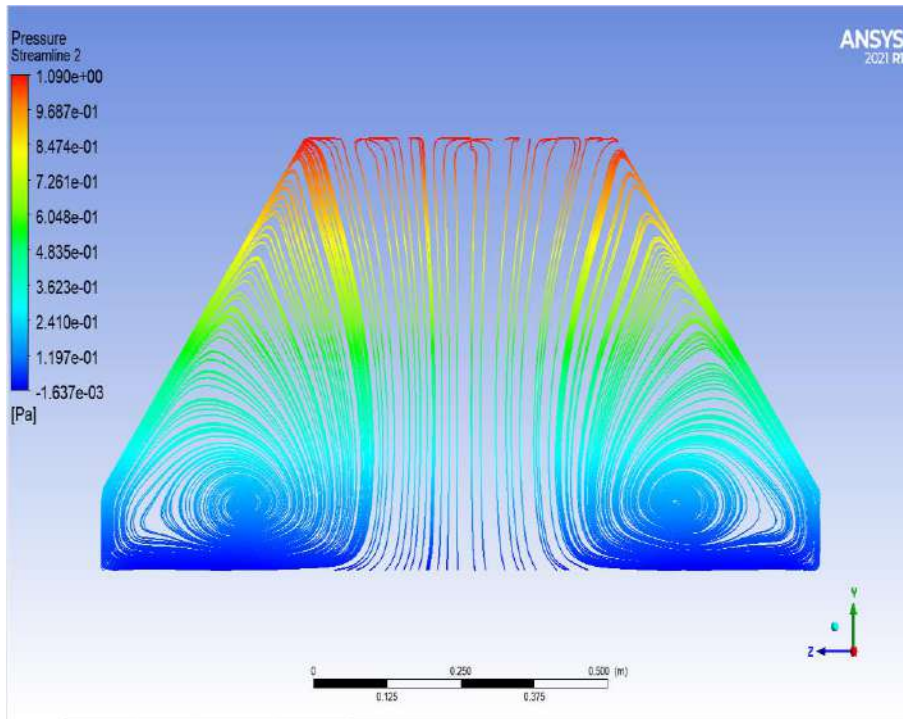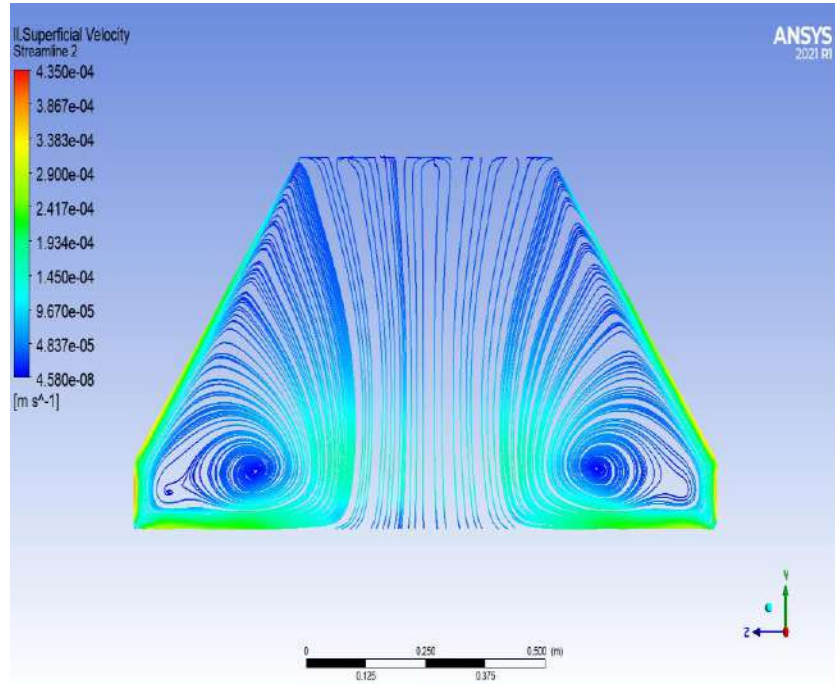
Figure (5.47) Streamline distribution when using solar still (GPLF and MSS_{T3}) at 3pm
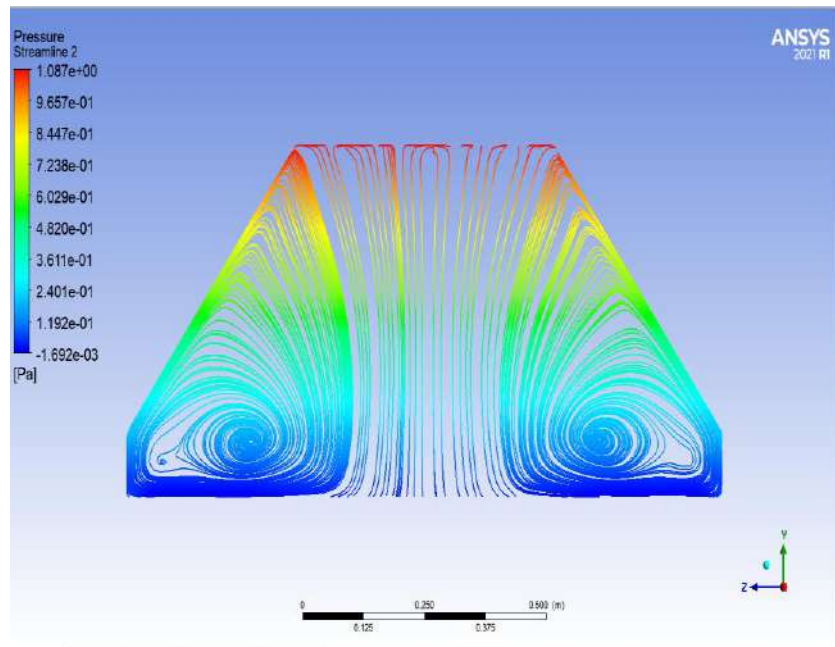
Figure (5.48) Pressure streamline distribution when using solar still (GPLF and MSS_{T3}) at 3 pm

5.3 Experimental Part Results

Experimental trials on the new distiller (15/10- 29/10) 2022 were conducted between the new distiller (with a single slope glass cover). In the circumstances of the city of Karbala, Iraq, at a 32-degree latitude angle. Each of these sub-sections show an effect of the followed techniques on the results. These techniques are: solar distilled only, solar distilled and magnets, a solar distilled and magnets with fin.

5.3.1 Intensity of Solar Radiation

Figures (5.49) to (5.52) show the solar radiation measurements collected from the weather at (the end of October 2022) for ten hours (8:00-5:00). Solar radiation changes because certain days have relatively few clouds throughout the test day, which is determined in situations when the sky can be clear. During the days of the experiment, the intensity of solar radiation reaches a maximum between 11:00 and 13:00 and then gradually decreases. The first figure shows the intensity of solar radiation when using the solar distillate only. While the other shows the intensity of the solar radiation for the distillate using different magnetic with different fins.
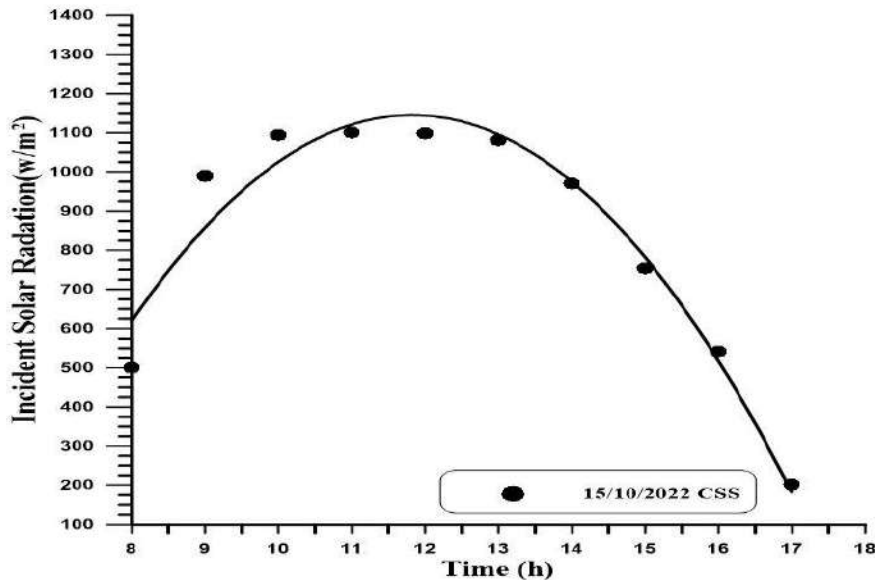
Figure (5.49) Intensity of solar radiation using (CSS)
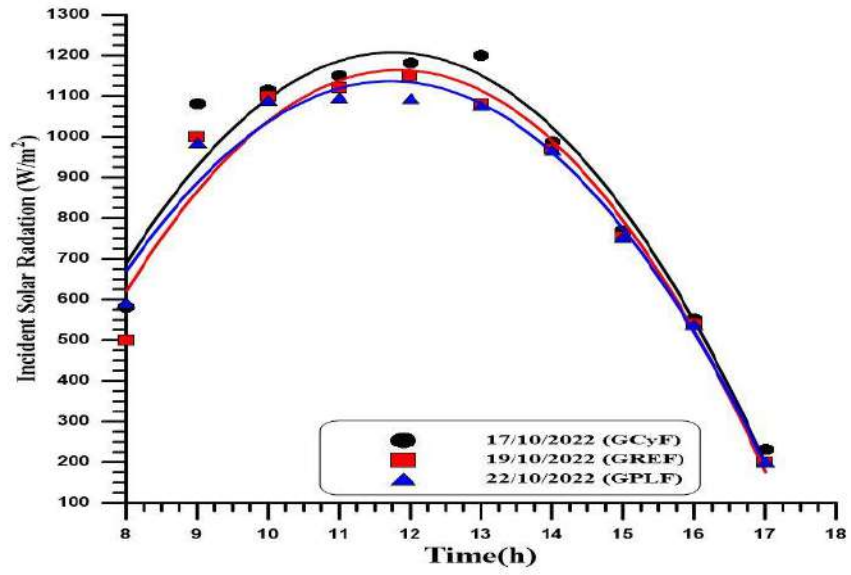
Figure (5.50) Incident solar radiation on the solar distiller with fin
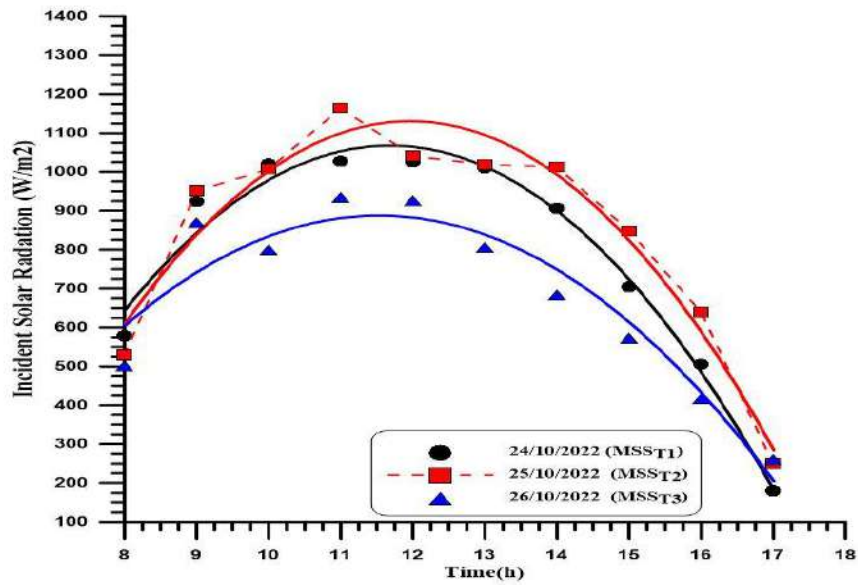
Figure (5.51) Incident solar radiation on the solar distiller with (MSS)
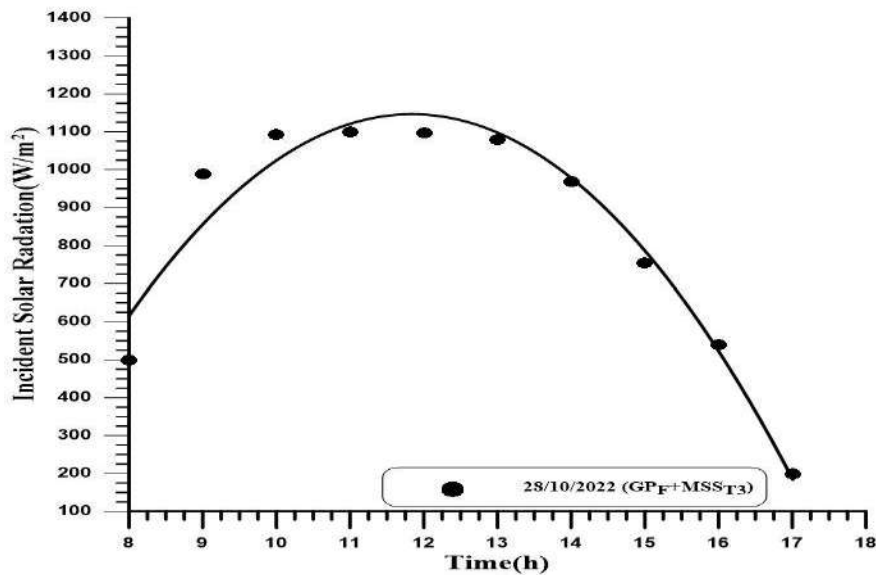
Figure (5.52) Incident solar radiation on the solar distiller with (GPLF and MSS)

5.3.2 The Impact of Magnetic Field and Fins on Temperature Distribution

The introduction of a magnetic field and fins in the solar distillation system has a significant impact on the fluid properties, leading to variations in temperature among different components. These components encompass the basin, the water inside the solar distiller, the inner and outer surfaces of the glass cover, and the temperature of the vapor. In the subsequent sections, we will present and elucidate the observed changes in temperature over time for all the investigated scenarios.

5.3.3 Temperature of Water in the Solar Still

The temperature of water in a solar distiller is influenced by various factors, such as solar radiation, water depth in the basin, and the concentration of impurities in the primary working fluid (water). In Figure (5.53), the experimental results of the water temperature in the solar distiller without any modifications or additions are depicted. The water temperature gradually rises until it reaches its peak value around 3:00 pm, after which it begins to decline. This pattern can be attributed to the maximum intensity of solar radiation during that time.

Figure (5.54) presents the experimental results of the solar distiller water temperature when using fins and magnetic flux. The introduction of fins has a positive effect on water temperature. Different types of fins were tested, and it was found that they increase the surface area available to absorb incident radiation, resulting in higher water temperature within the solar still and increased evaporation

and water production. Among the fin types, the flat plate fin demonstrated the most favorable performance due to its larger surface area compared to other types.

The presence of magnetic materials also has a discernible effect on the water temperature over time. When different strengths of magnets (T1, T2, and T3) were used, a minor increase in the temperature of the distiller water was observed. This slight rise in temperature can be attributed to the changes in water properties induced by the magnetic flux, which leads to alterations in the bonds between water molecules. This transformation enables the water to absorb heat energy more efficiently. Figure (5.55) showcases the experimental outcomes regarding the water temperature inside the solar distillation basin.

In our experiments, the strongest magnetic intensity (T3) and the optimal fin type (flat plate) were employed, resulting in higher water temperatures compared to previous experiments. The high magnetic flux contributes to transforming the water within the distiller into ionic water, enhancing heat absorption from incident radiation and leading to elevated water temperature and increased evaporation and water production within the distiller. The utilization of flat plate fins further increases the surface area available for absorbing incident radiation, resulting in higher water temperatures and enhanced evaporation. When comparing these methods with other experiments, this particular experiment stands out as one of the most successful practical demonstrations in our research. Combining all these techniques in the distillation system raises the water temperature inside it by approximately 24% compared to a standard distiller, as explained in the preceding sections.
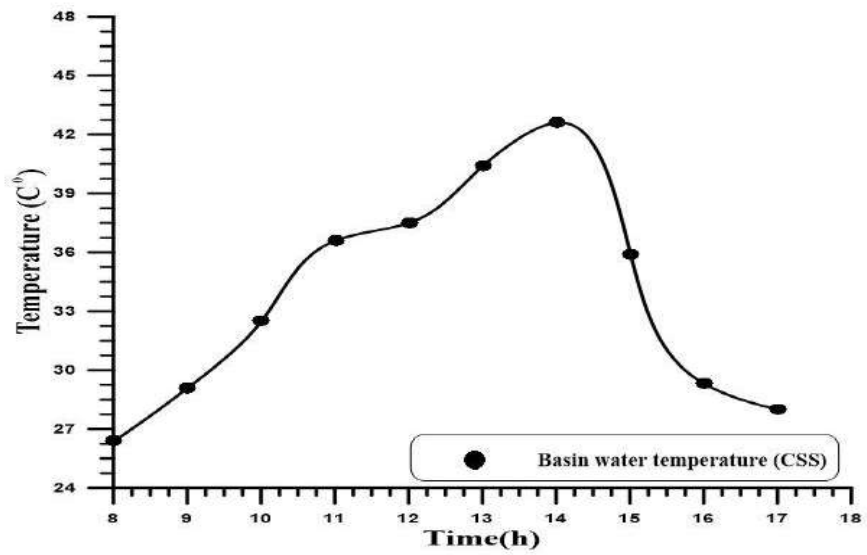
Figure (5.53) Ttemperature of the water inside the distiller (CSS)
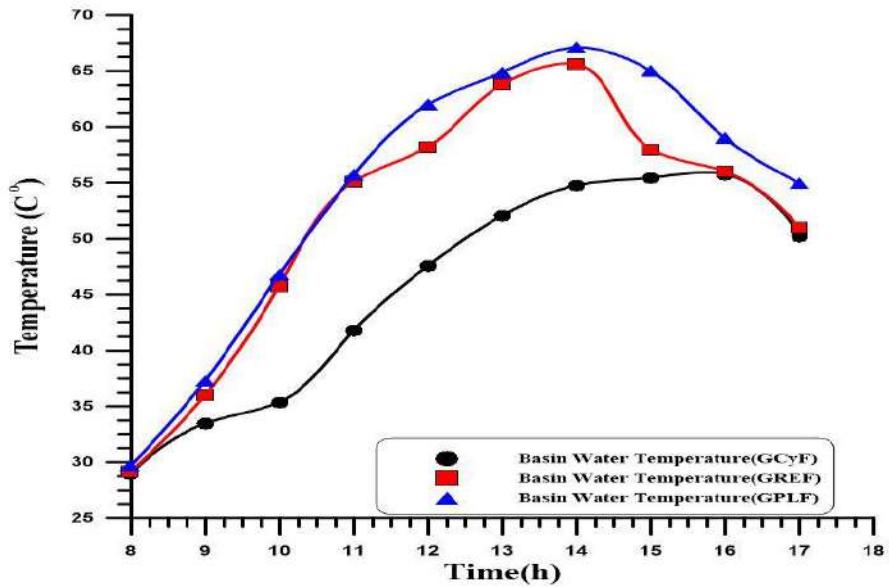
Figure (5.54) Temperature of the water inside the distiller Fin
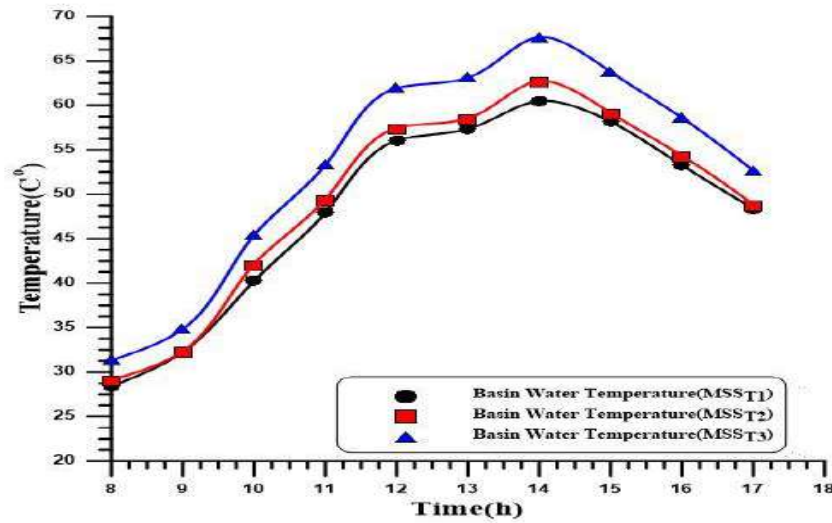
Figure (5.55) Temperature of the water inside the distiller MSS
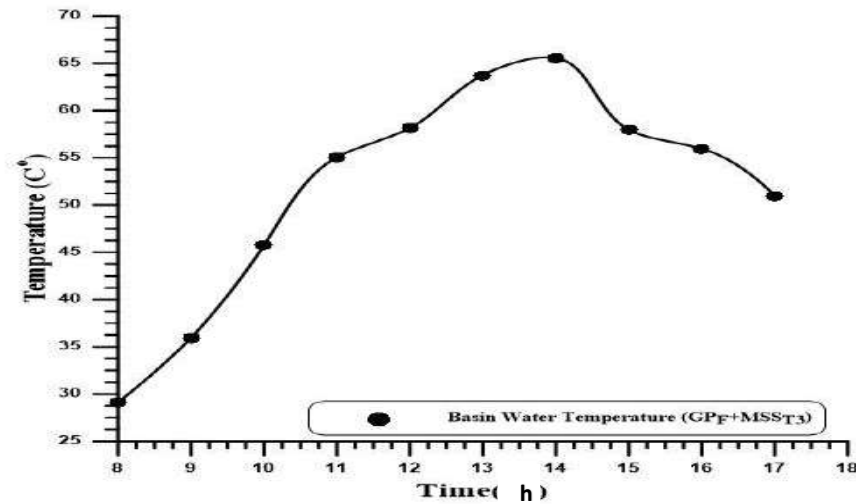
Figure (5.56) Temperature of the water inside the distiller (GPLF and MSS)

5.3.4 Solar Distiller Base Temperature

Figure (5.57) shows the temperature of the solar distiller base is directly affected by the temperature of the water inside this distiller. Figure (5.58) shows an effect of fins on the solar distiller base temperature experimentally from 8:00 am to 5:00 pm. The fins have a good effect on the last base temperature, which increases

by about 13% if compared with the case (distiller without modifications). This is because the fin more absorbable incident radiation heats the water in the distiller as a proactive stage. As mentioned in Figure (5.59), the magnetic flux positively affects the water temperature inside the solar distiller and positively affects the distiller base temperature. This is because of their directed relationship (water and distiller base temperature). Figure (5.60) shows that adding these techniques into the solar system individually increases the distiller base temperature and increases it when they are added collectively. In this case, it increases by more than 25% compared with the base case (distiller without additions).
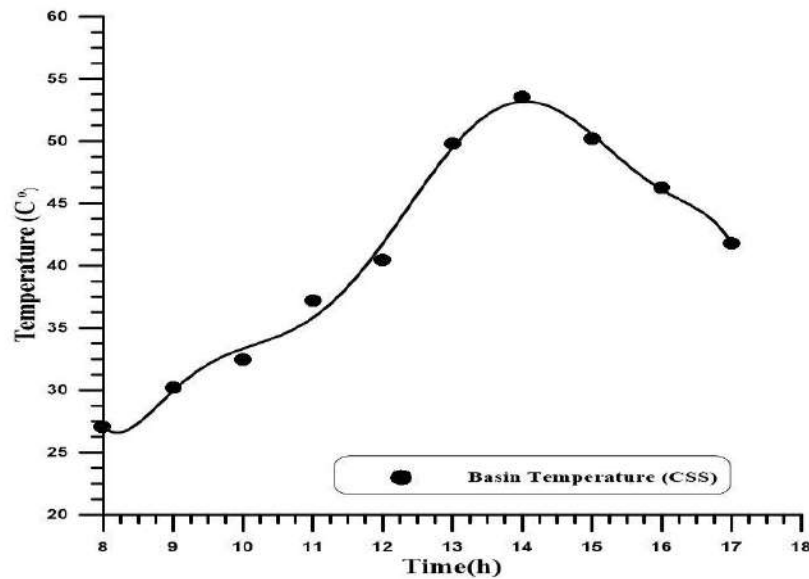
Figure (5.57) The solar distiller base temperature (CSS)
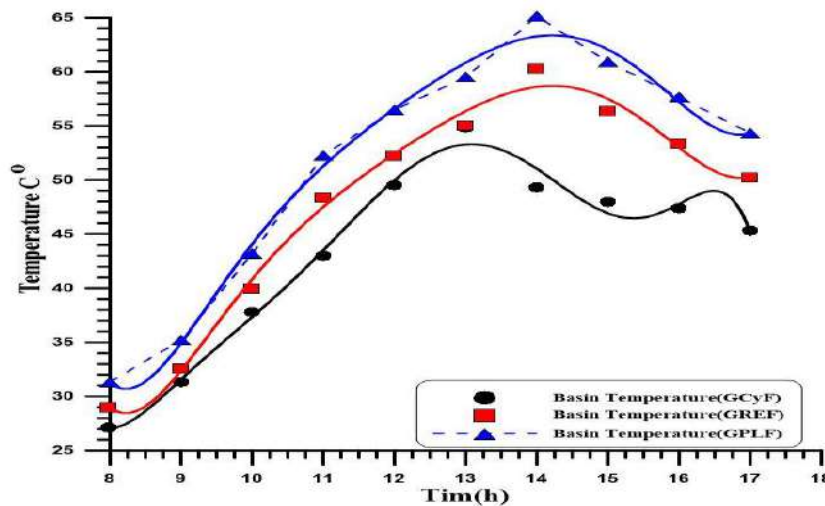
Figure (5.58) The solar distiller base temperature with fin
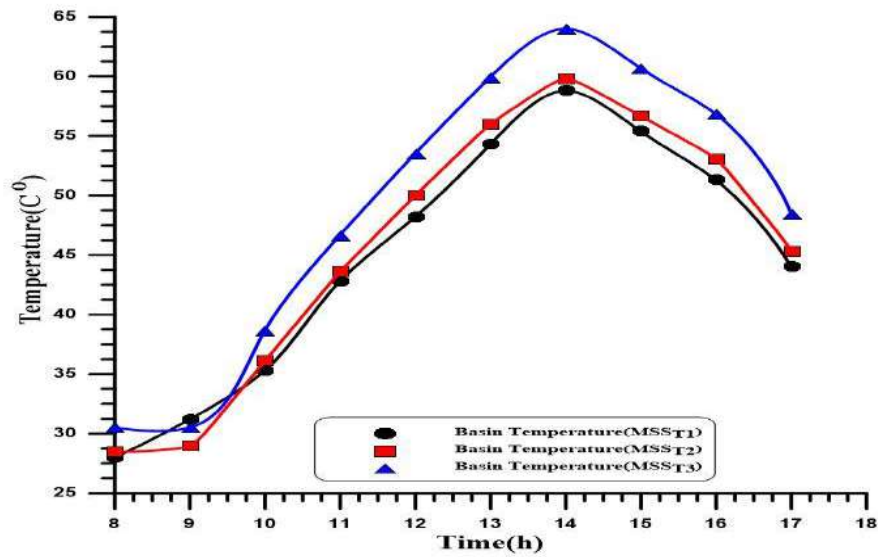
Figure (5.59) The solar distiller base temperature with (MSS)
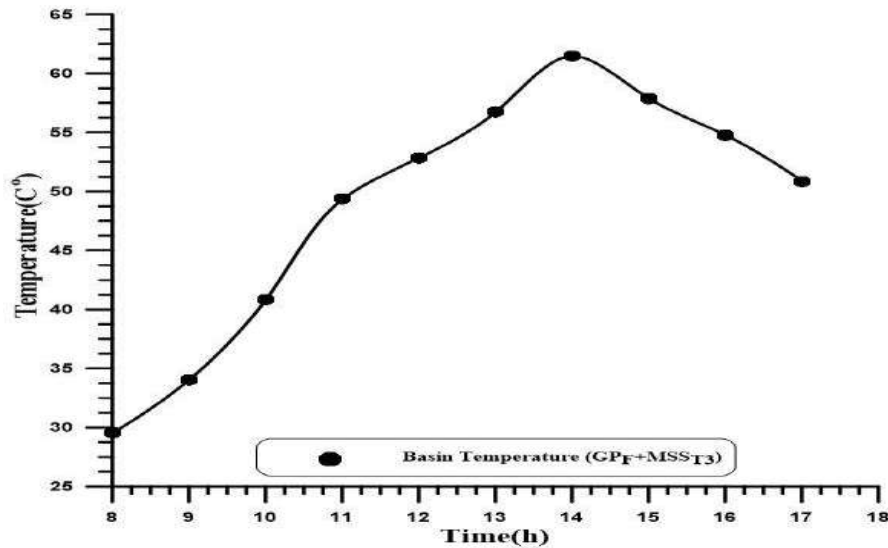
Figure (5.60) The solar distiller base temperature with (GPLF and MSS)

5.3.5 The Vapour Temperature

Figure (5.61) represents the temperature of the steam produced within the distillate during the experiment. Here, only solar power was utilized. The maximum temperature of the steam is found between the hours (13:00-15:00), as seen in the figure. The increase in solar radiation intensity and the high temperature of the water

inside the basin contribute to an increase in the evaporation process inside the distiller. Figure (5.62) shows the effect of fins on the steam temperature of the solar distiller has a positive effect on the steam temperature, where it increases with the use of CSS by about 8.5% compared to without it. This since the solar collector heats the water at a proactive stage. Figure (5.63) shows the temperature gradient of the steam generated within the distillate during the experiment period when three different concentrations of the magnetic field were employed. Figure (5.64) shows that adding these techniques collectively into the solar distillation system increases the water and steam temperature for the same reasons. When a magnetic field is applied, an increase in evaporation is observed in comparison without a magnetic field because of the kinetic energy of water molecules and the Lorentz force it weakens or breaks hydrogen bonds. After applying the magnetic field, it was observed that some properties of water and a change in the physical behavior of water. The magnetizing effects of water are related to magnetizing time, internally applied magnetic field strength, and water temperature, although these relationships are not linear. Experiments showed that reducing the volume of magnetic contact of water on the surface of the water-forming materials reduces the surface tensile strength of magnetized water.
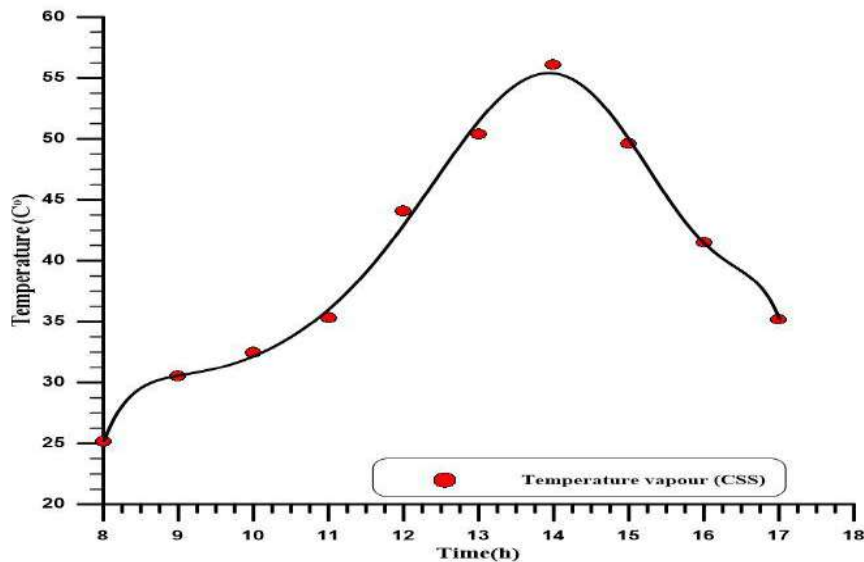
Figure (5.61) Temperature of the vapor as (CSS)
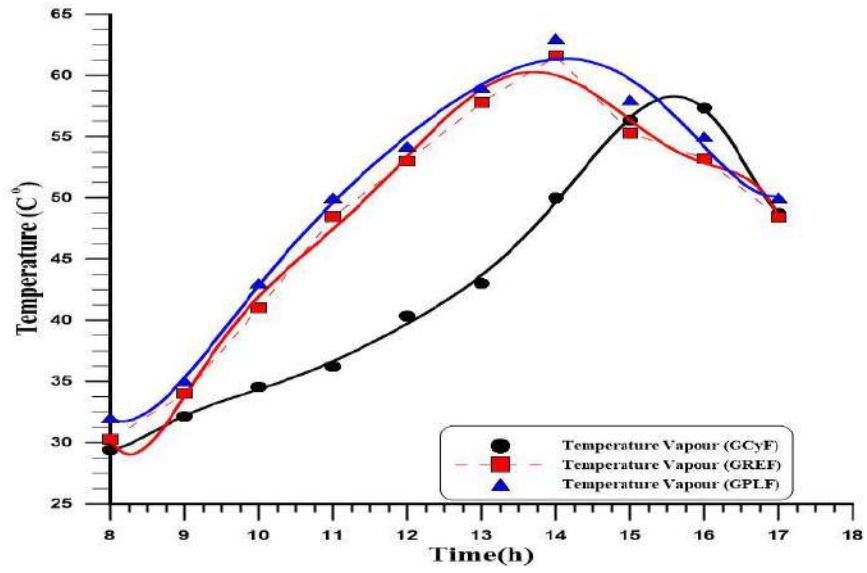
Figure (5.62) Temperature of the vapor as Fin
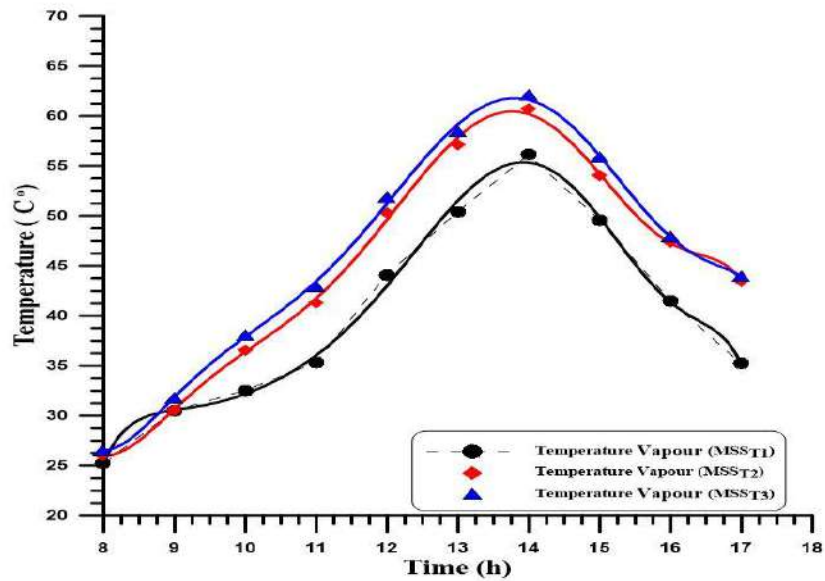
Figure (5.63) Temperature of the vapor as (MSS)
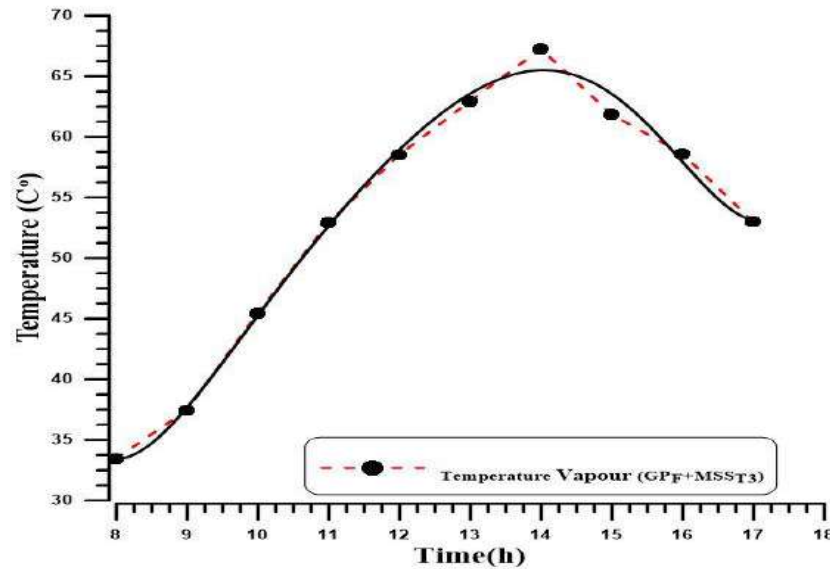
Figure (5.64) Temperature of the vapor (GPLF and MSS)

5.3.6 The Inside and Outside Temperature of Glass Cover

Figures (5.65) and (5.69) show the interior and external temperatures of the solar still's glass cover. The temperature difference between the inner and outer surfaces of the glazier cover generates more significant condensation between the two surfaces, which increases the amount of pure water produced. To create the greenhouse effect necessary as a driving force for pure water production, there must be a temperature difference between the inner and exterior solar distillers because of the flow of wind around the outside of the cover made of glass—the temperature decreases in this layer. The average temperature between the outside and interior glass was (15) °C. It is self-evident that the glazier lid's internal and exterior temperatures rise with increasing sun intensity, peaking at (12:00 to 15:00). The increased water vapor from the solar distilled basin influences the inner surface temperature of the glass cover. But has less of an impact on the glass cover's outer surface, which heats due to increased solar radiation and ambient temperature. Figures (5.66), (5.67) and (5.70), (5.71) show an effect of the fin and the magnetic field on the external and internal temperature of the solar distiller cover experimentally. Figure (5.66), (5.70) shows that the fin affects positively on the distiller cover's internal temperature as it increases by about 33%. This is because the fin heat of the water is at a proactive stage and leads to increasing the internal

temperature of the distiller cover. Figure (5.67), (5.71) shows that these techniques' effect is positive for the internal temperature of the solar distiller cover. It increases by about 20% compared with the typical case (distiller alone). Figure (5.68), (5.72) The addition of both fins and magnets to the distillation system enhances its performance. When both these components are incorporated, the system exhibits improved efficiency and effectiveness in the process of distillation. The difference in temperature between the inner and outer surfaces of the glass cover leads to increased condensation between the two surfaces and increased freshwater production. There is a discrepancy in the temperature between the surfaces of the internal and external solar distillation apparatus to achieve global warming. The reason for this is due to the movement of the wind on the glass cover from the outside, which leads to a decrease in the temperature on the outer surface. The figures also show that the glass cover's internal and external temperature increases with the sun's intensity and reaches a maximum between 2:00 and 3:00 hours. The increased water vapor from the basin from the solar still basin affects the surface temperature inside the glass cover. Its effect is less on the outer surface than the glass cover, which increases its temperature by increasing the intensity of solar radiation and the temperature of the surrounding environment.
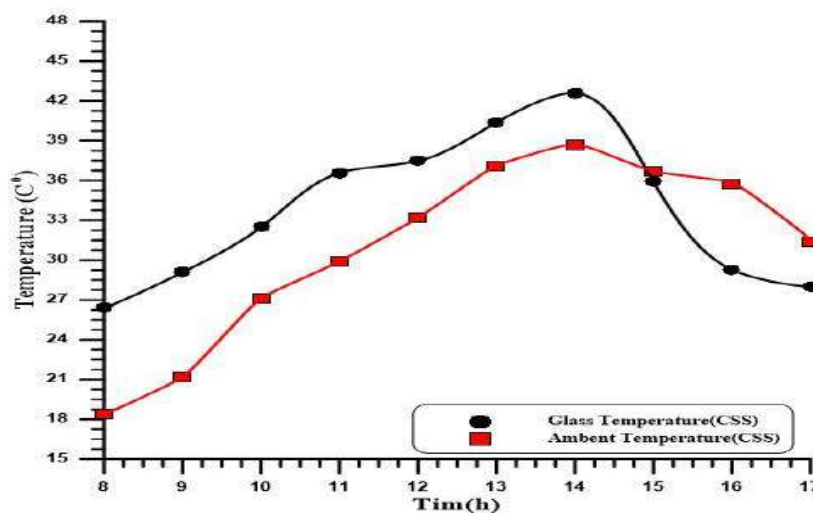
Figure (5.65) Outside temperature of glass cover with (CSS)
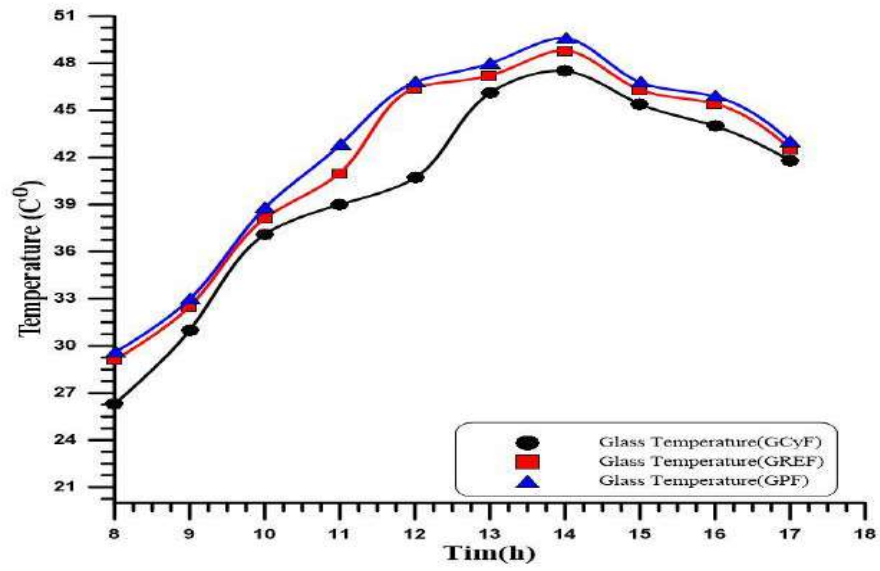
Figure (5.66) Outside temperature of glass cover with Fin
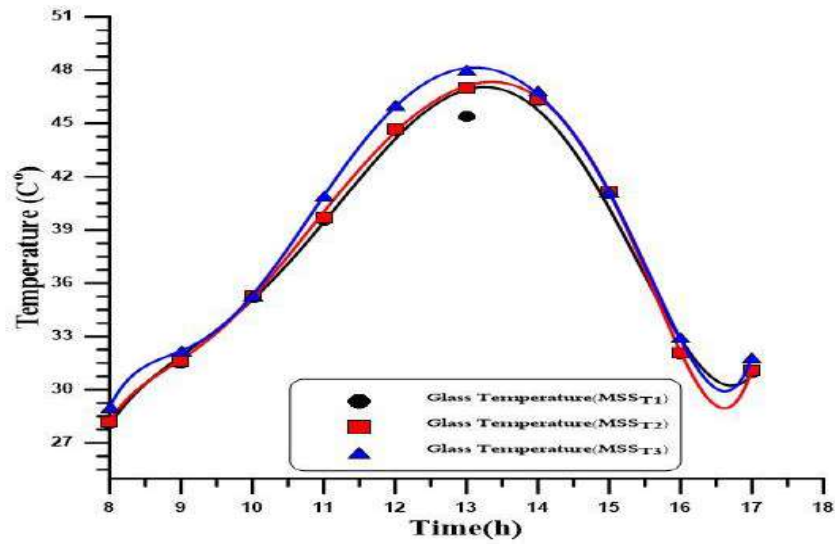
Figure (5.67) Outside temperature of glass cover with (MSS)
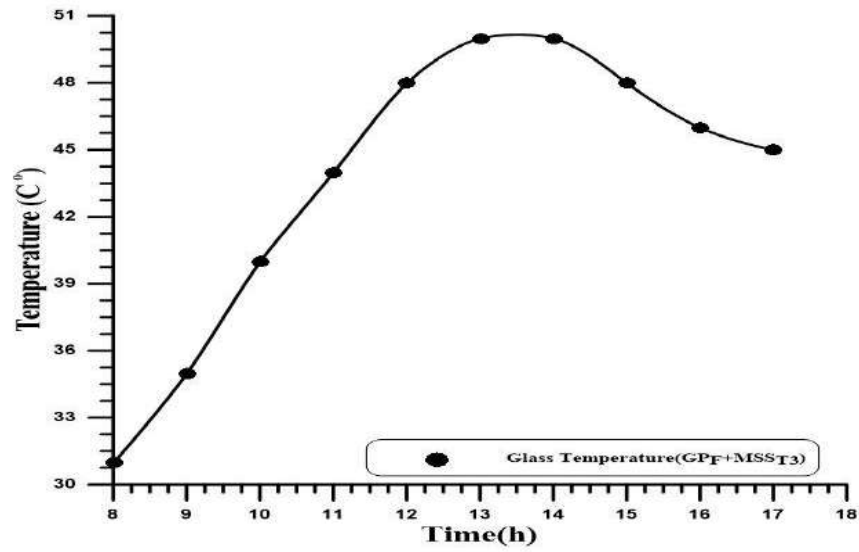
Figure (5.68) Outside temperature of glass cover with (GPLF and MSS)
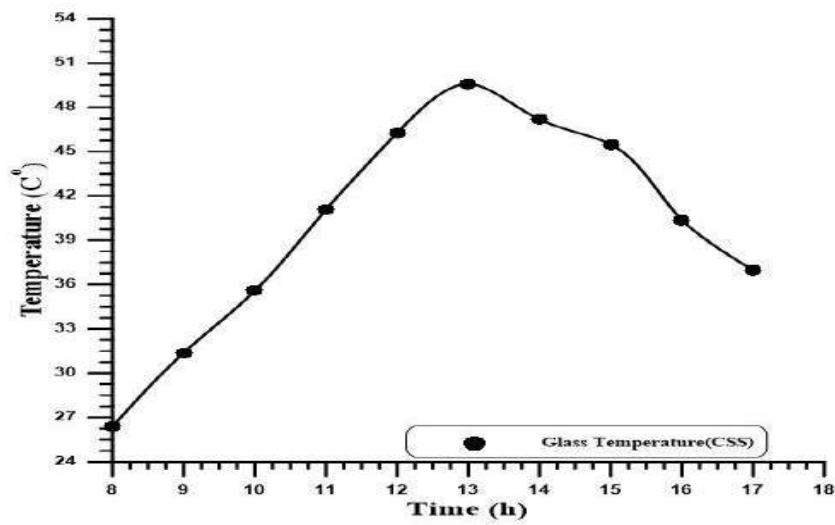
Figure (5.69) The temperature inside of glass cover with (CSS)
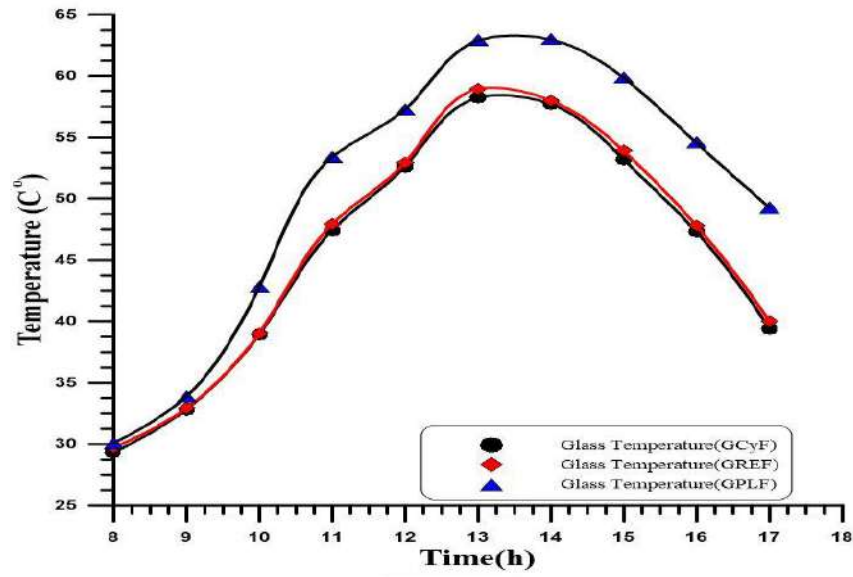
Figure (5.70) The temperature inside of the glass cover with fin
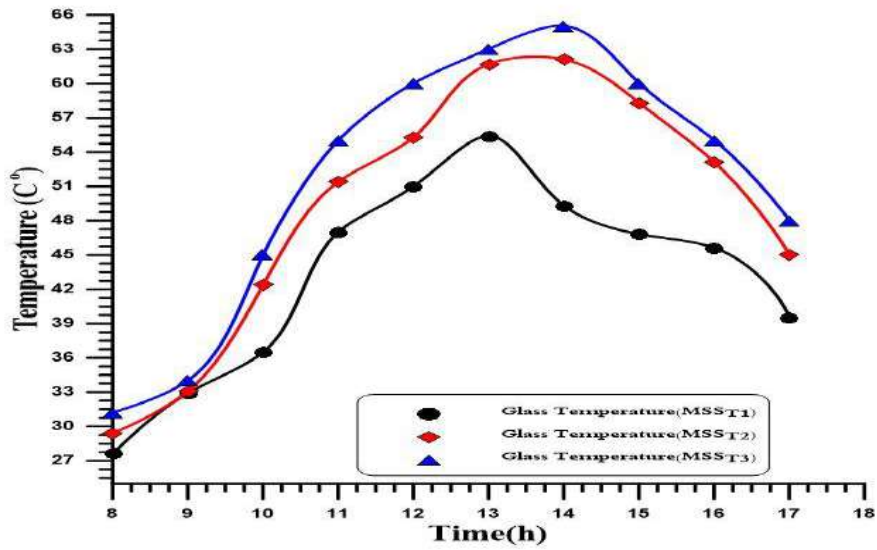
Figure (5.71) The temperature inside the glass cover with (MSS)
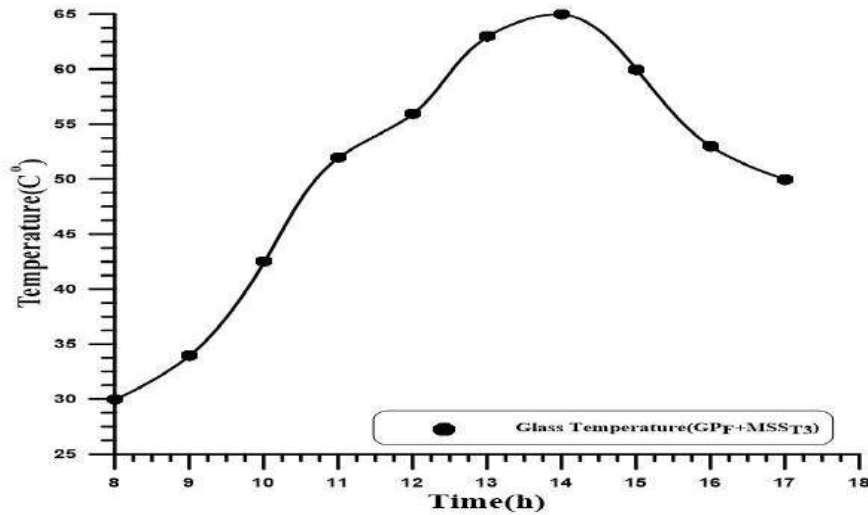
Figure (5.72) The temperature inside the glass cover with (GPLF and MSS)

5.3.7 The Optimum Temperature

Figures (5.73) to (5.76) depict the perfect temperature for the flat plate fin (GPLF), optimal magnetic field (MSS), conventional solar distillate (CSS) and (GPLF & MSS). These figures show that the vapor temperature at the glass's inner surface, which raises the glass's temperature from the internal surface, is the greatest temperature created in solar distillation. This causes a significant temperature difference between the inner and outer surfaces of the glass, which increases the process of condensation of steam on the inner side of the glass and increases system output and efficiency.
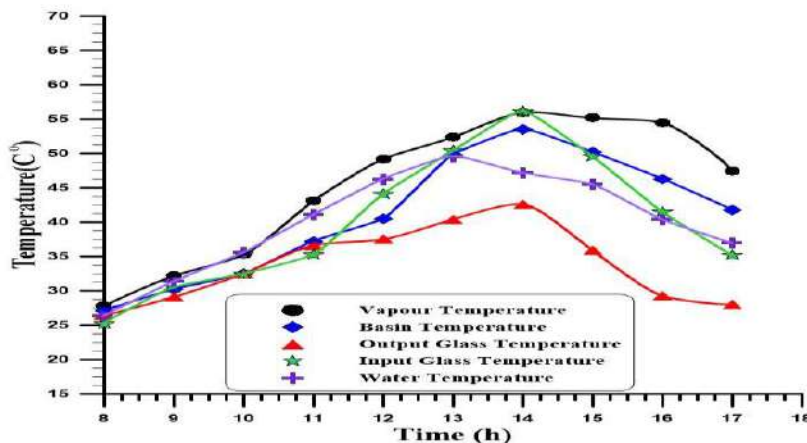
Figure (5.73) The temperature distribution in the conventional solar distillation (CSS)
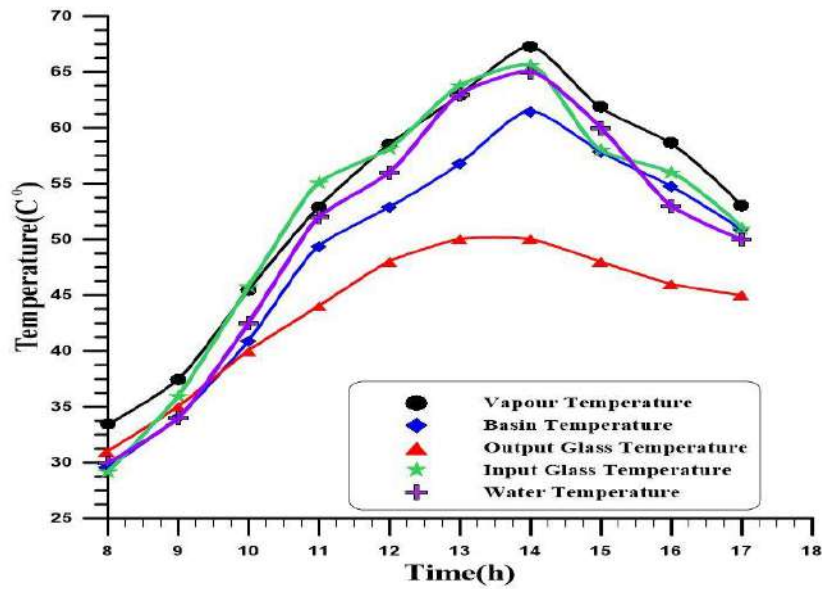
Figure (5.74) The temperature distribution in the solar distillation (GPLF and MSS)
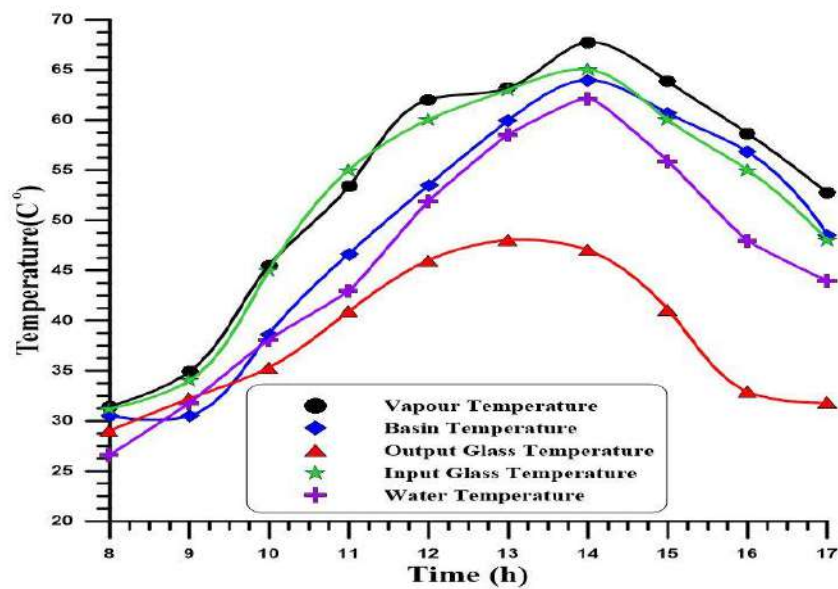
Figure (5.75) The optimization temperature in the (GPLF)
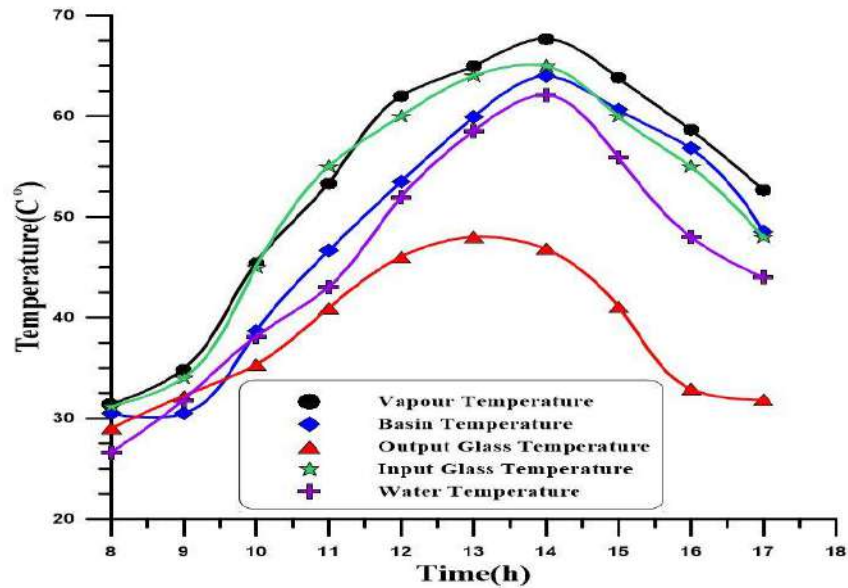
Figure (5.76) The optimization temperature in the (MSS$_{T3}$)

5.3.8 Water Distiller Hourly Productivity

Figure (5.77) shows that pure water production increases gradually until it reaches the peak at 3-4 pm. This is due to the graduate increase in water evaporation and condensation rates. They (evaporation and condensation) are affected by the temperature differential between the outside glass envelope and the aquarium water, which is the greatest at this time. Figures (5.78) and (5.79) show the effect of a fin and magnets field on the hourly productivity of the solar distiller experimentally from 8:00 am to 5:00 pm. As observed, fin positively influence hourly water productivity, which improves as the fin is used. Since the last one heats the water previously, increasing the water evaporation and condensation rate. Figures (5.80) and (5.81) using both the fin and the magnets simultaneously slightly increases the hourly water productivity. This is by comparing to using the solar collector only. This means that the magnets affect the hourly productivity of the water distiller.
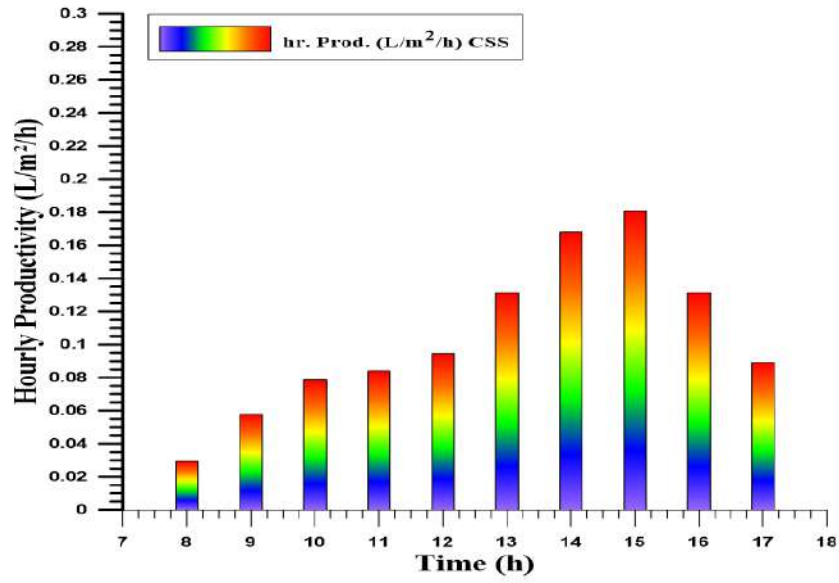
Figure (5.77) Daily productivity with (CSS)
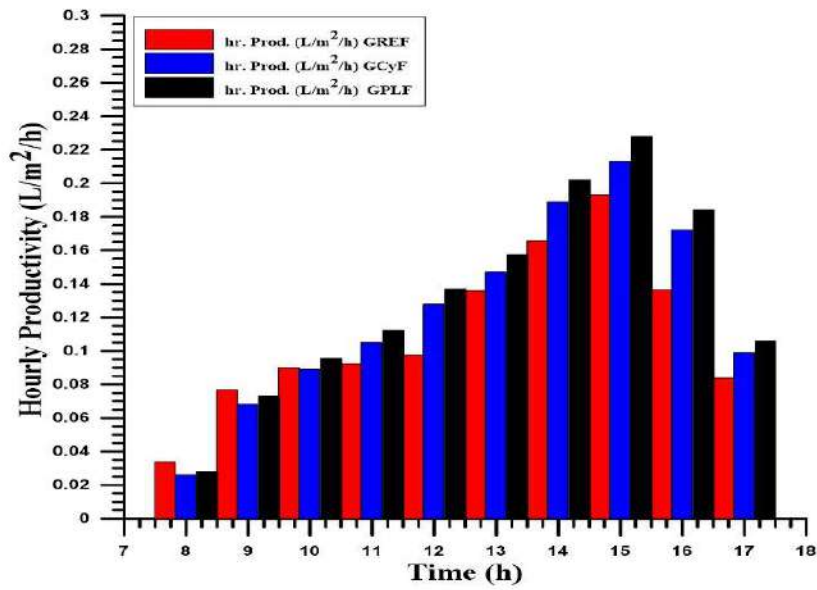
Figure (5.78) Daily productivity with fin
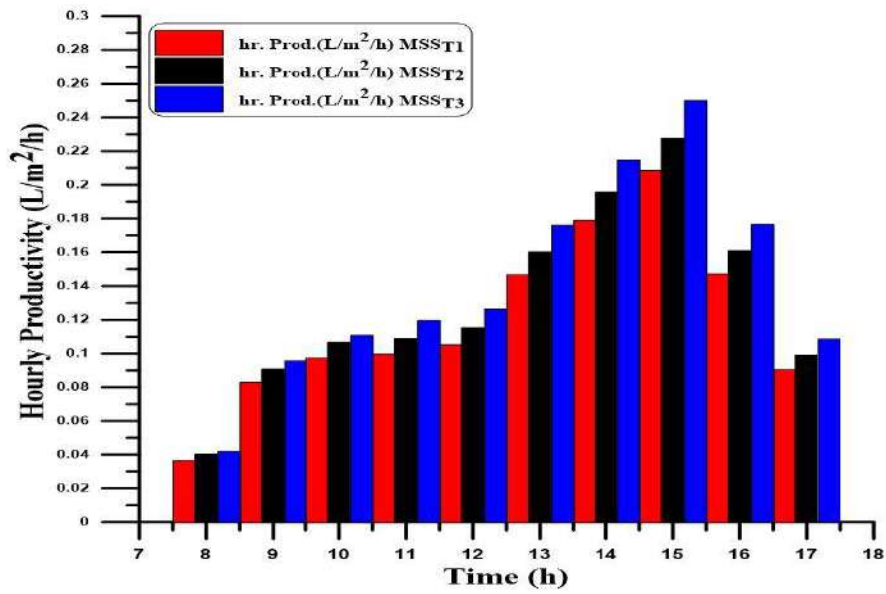
Figure (5.79) Daily productivity with (MSS)
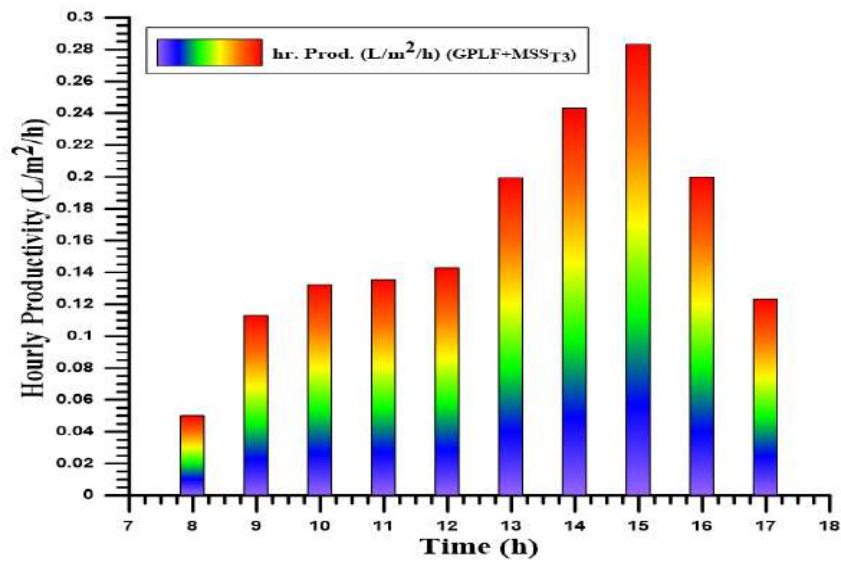
Figure (5.80) Daily productivity with (GPLF and MSS)
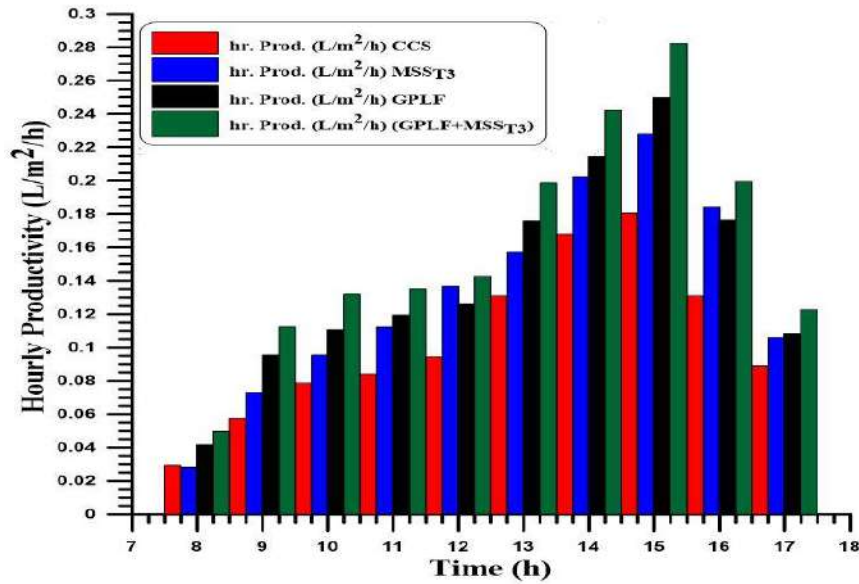
Figure (5.81) The optimization cases of the daily productivity

5.3.9 Solar Distiller Efficiency

Figure (5.82) shows the gradual increase in solar water distillation efficiency up to 3–4 pm peak hours. This is due to the graduate increase in water evaporation, condensation rate, and ambient temperature decrease. Figure (5.83) depicts the practical effect of a fin on the efficiency of a solar water distiller from 8:00 a.m. to 5:00 p.m. As observed, employing both the fin and the magnets simultaneously improves the solar water distiller's efficiency marginally. This is as compared to only using the CSS. This means that the fin greatly impacts the solar water distiller's efficiency. Figures (5.84) and (5.85) depict the effect of the fin and magnets on the efficiency of a solar water distiller over an 8:00 a.m. to 5:00 p.m. period. As illustrated in this diagram, the fin and magnetics have a major impact on the efficiency of the solar water distiller. However, if compared between the effect fin and magnets, the last has a minor impact because after applying the magnetic field, several properties of water changed, as well as a change in water's physical behavior. Although these relationships are not linear, the magnetizing effects of water are related to magnetizing time, externally applied magnetic field strength and water temperature.
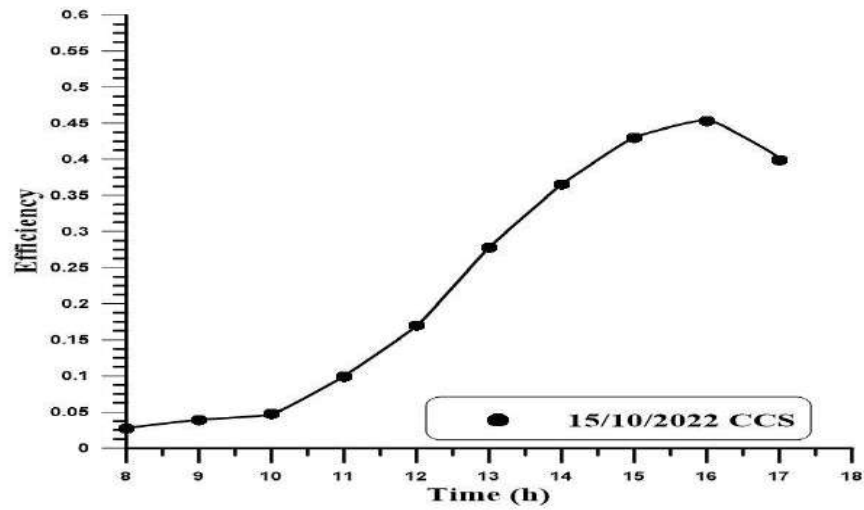
Figure (5.82) The efficiency of solar water distiller (CSS)
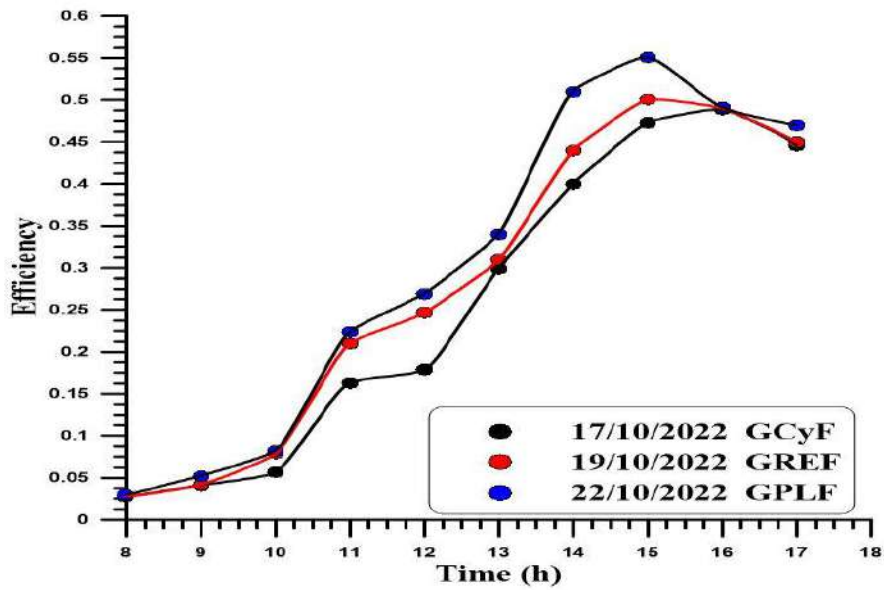
Figure (5.83) The efficiency of solar water distiller (fin)

109
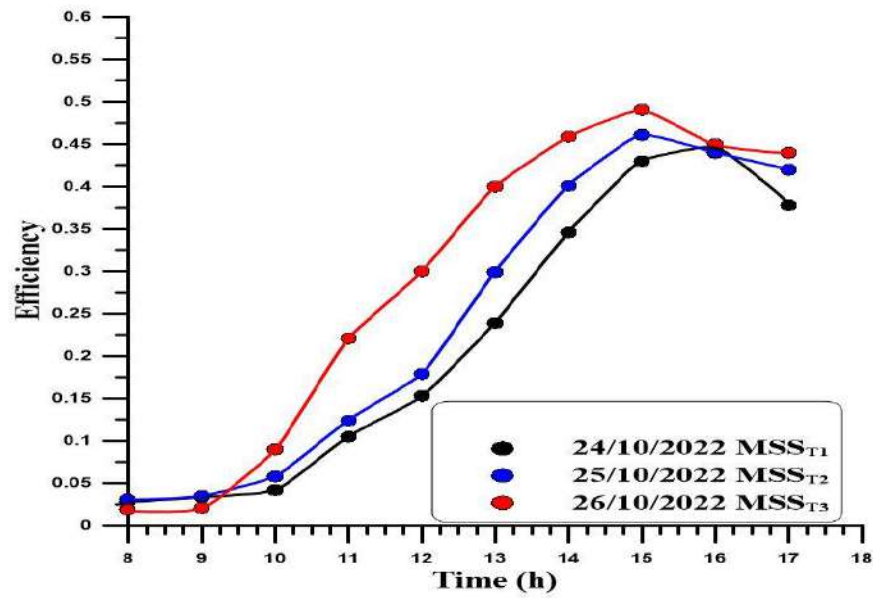
Figure (5.84) The efficiency of solar water distiller (MSS)
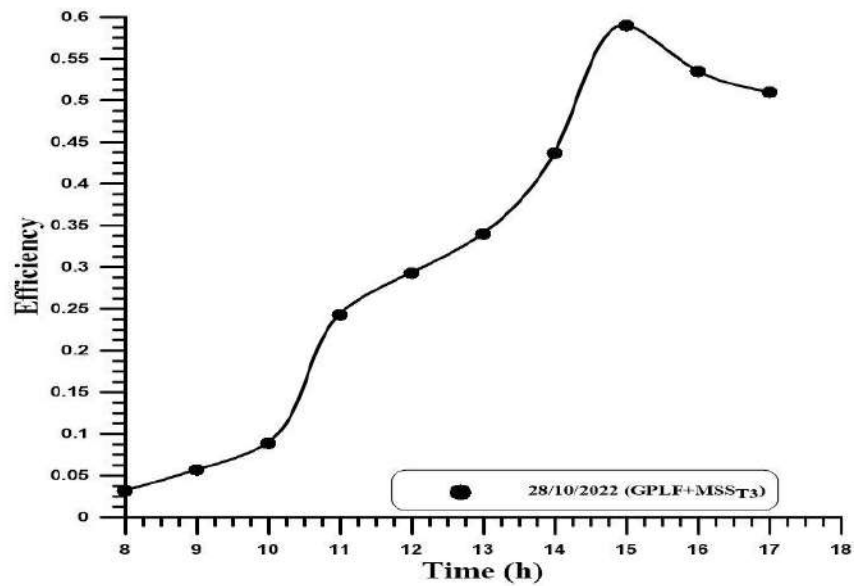
Figure (5.85) The efficiency of solar water distiller (GPLF and MSS)
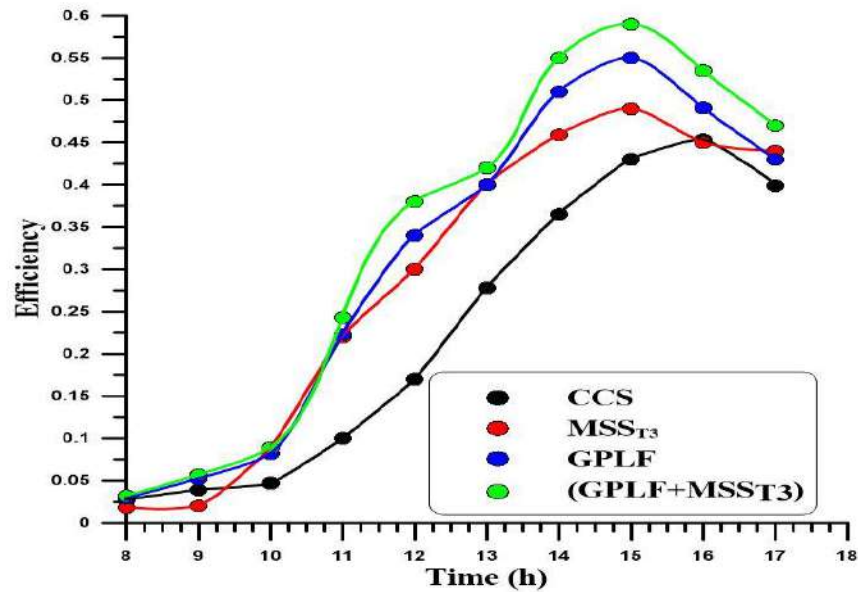
Figure (5.86) The optimization efficiency cases

5.4 Results Comparison

5.4.1 Comparison the Numerical Results with Experimental Work

Experimental work findings were used to validate the numerical results for the (3D) CFD model. The curves show that the CFD and experimental results for the temperature of the solar distillation basin, the water of the sun distillation basin, and the water vapor, as well as the internal and external temperature face of the glass, where the highest error was, are in agreement (11 percent). Figures (5.87) to (5.91) show comparisons between the current study's numerical and experimental results. This is for results of the water temperature, the basin temperature, the vapor temperature, the glass covers internal temperature and the glass cover external temperature, respectively. This is to show a deviation ratio of the experimental results compared to the numerical ones. As shown in these figures, there is a large agreement between them, which indicates that the present work was carried out according to what was planned. However, it is shown that there is a different ratio between them sometimes, but not large. This difference ratio is mainly due to assumptions considered in this study's numerical side. Other factors cause these differences, such as external conditions like wind speed, cloudiness and ambient temperature, etc., that cannot be controlled and the different measurement errors. To reduce this ratio, the experimental tests were repeated for several days. In addition,

the readings for each test were measured many times until stable and correct readings were obtained.

5.4.2 Validation of Results with Another Research

To guarantee the validity of our experimental research findings, the current work was compared to a similar experimental study conducted by Ramasamy Dhivagar [Ref.33], who worked on a solar water distillation using different GPLF and MSS, as shown in the Figures (5.92) and (5.93).
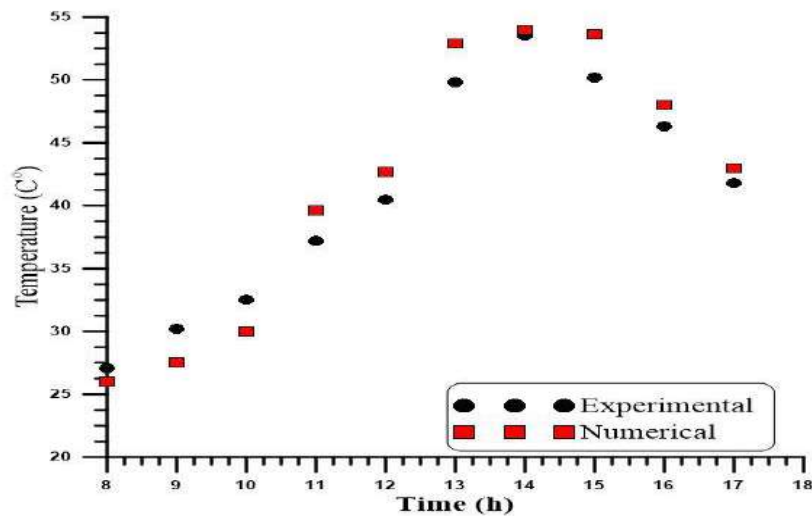
Figure (5.87) Comparison between the numerical results and the experimental results of the basin temperature
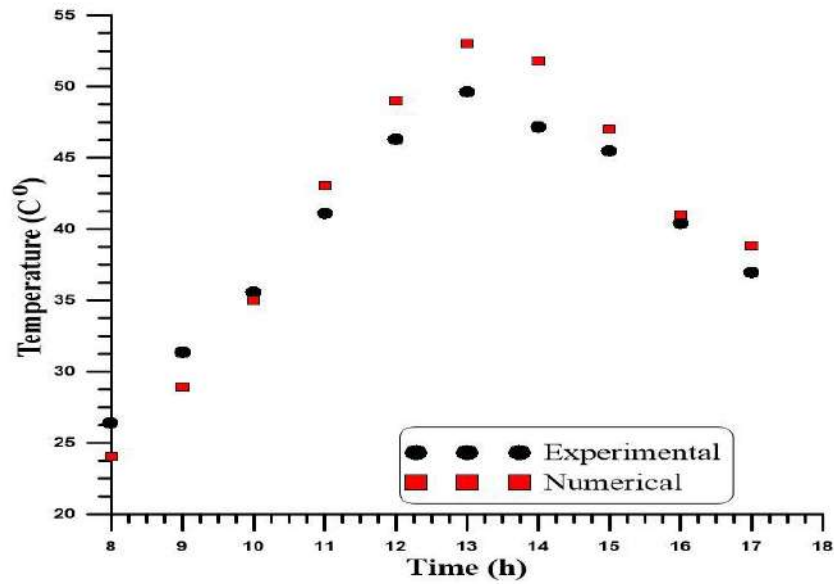
Figure (5.88) Comparison between the numerical results and the experimental
results of the glass cover internal temperature
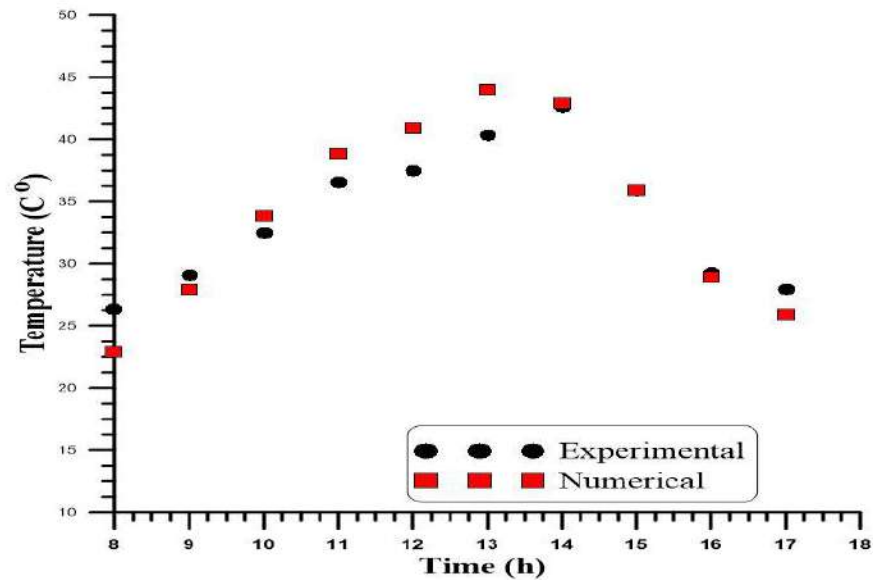
Figure (5.89) Comparison between the numerical results and the experimental
results of the glass cover external temperature
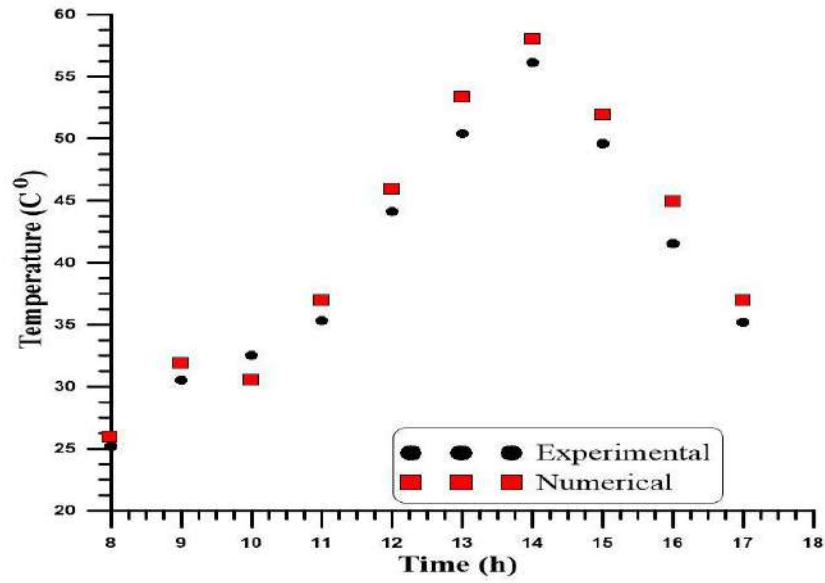
Figure (5.90) Comparison between the numerical results and the experimental results of the vapor temperature
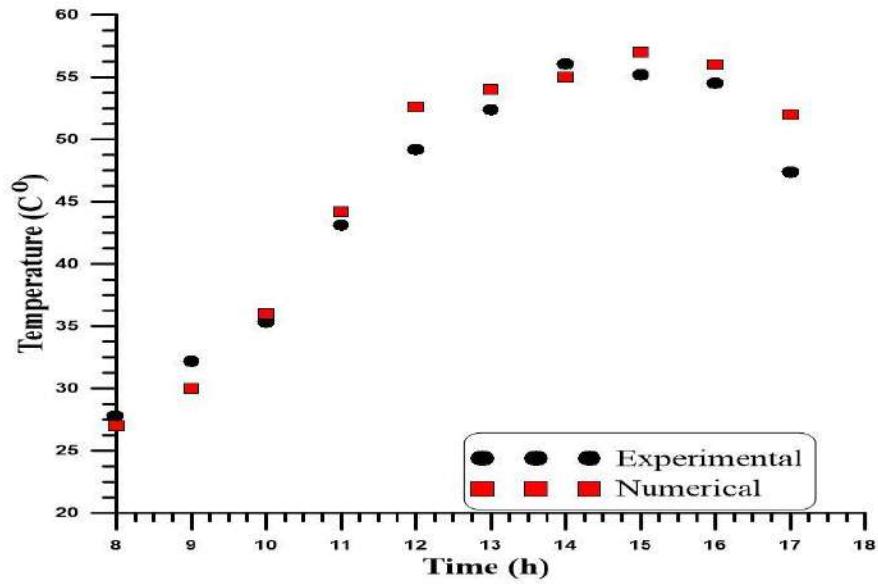
Figure (5.91) Comparison between the numerical results and the experimental results of the water temperature
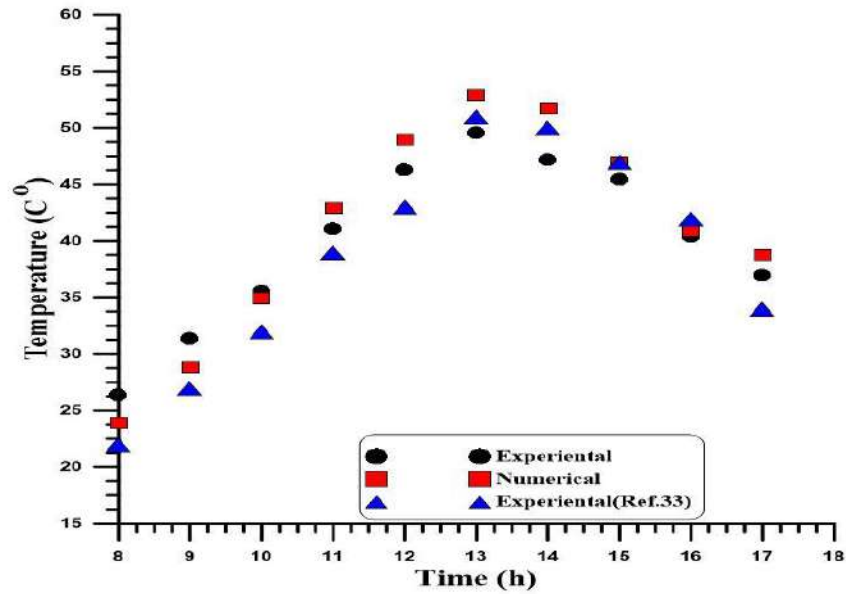
Figure (5.92) Water temperature (CSS) comparison between experimental,
numerical results and the researcher's experimental (Ramasamy Dhivagar Ref.33)
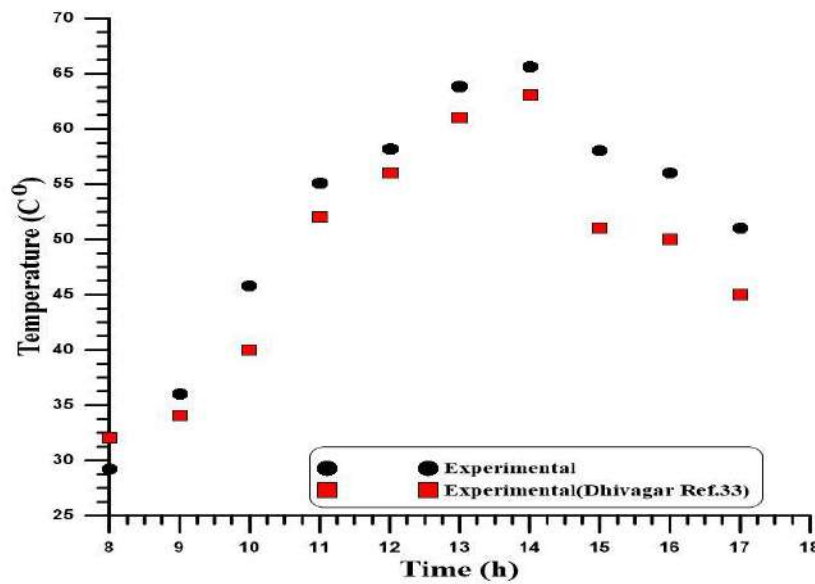
Figure (5.93) Water temperature (GPLF and MSS) comparison between
experimental results and the researcher (Ramasamy Dhivagar Ref.33)

6

Conclusions and Recommendations for Future Work

Chapter Six

Conclusions and Recommendations for Future Work

6.1 Conclusions

In this section, we present the conclusions drawn from the experimental investigation and analysis conducted in this study. The conclusions provide a summary of the key findings and outcomes, highlighting the significant contributions and implications of the research. The results obtained from the experiments are analyzed and interpreted to draw meaningful insights and draw a comprehensive understanding of the studied phenomenon. The following are the main conclusions derived from this study: 1- Enhancing the productivity and efficiency of the solar still by selecting the best possible design and materials.

2- Investigating the impact of weather conditions on the performance of the device.

3- Analyzing the temperature distribution inside and outside the device.

4- The effect of adding graphite fins to the device to increase the surface area exposed to solar radiation and selecting the material, dimensions, configuration, and shape of the fins to improve the device's performance.

5- Studying and understanding the effect of water magnetization on the device's productivity and consequently its efficiency, due to the influence of water's physical properties (viscosity, surface tension, boiling and evaporation temperature). This includes observing the importance of the method of placing magnets within the water, their quantity, and their strength. However, it should be noted that the full understanding of the effect of water magnetization remains incomplete.

6.2 Recommendations

Based on the findings and results of the experimental investigation, several recommendations can be made to enhance the productivity and efficiency of the solar water distillation system. These recommendations aim to optimize the system's performance and improve its overall effectiveness. The following areas can be considered for further improvements:

1. Enhancing Solar Radiation Concentration:

- Installing internal reflectors on the sides of the water distiller to increase the concentration of solar radiation.

- Exploring the use of reflective surfaces or mirrors to redirect and focus sunlight onto the distillation unit.

2. Incorporating Condensation Chambers:

- Adding a side or inner condensation chamber within the solar system to improve the condensation process and maximize water yield.

3. Utilizing Heat Exchangers:

- Introducing a heat exchanger to preheat the water before it enters the solar distillation device, increasing the temperature gradient and improving distillation efficiency.

4. Exploring Advanced Materials:

- Investigating the use of chemical solutions and organic compounds with high efficiency as phase change materials, which can enhance the heat transfer and evaporation rates.

By implementing these recommendations, it is expected that the solar water distillation system can achieve higher productivity and improved energy utilization, leading to more sustainable and effective water purification processes. Further research and development in these areas can contribute to the advancement of solar distillation technology and its practical applications.

References

[1] B. Gupta, A. Kumar, and P. V. Baredar, "Experimental investigation on modified solar still using nanoparticles and water sprinkler attachment," Front Mater, vol. 4, no. August, pp. 1–7, 2017, doi: 10.3389/fmats.2017.00023.

[2] A. K. Singh, "A review study of solar desalting units with evacuated tube collectors," J Clean Prod, vol. 279, p. 123542, 2021.

[3] H. Olfian, S. S. M. Ajarostaghi, and M. Ebrahimnataj, "Development on evacuated tube solar collectors: A review of the last decade results of using nanofluids," Solar Energy, vol. 211, pp. 265–282, 2020.

[4] A. M. Hamed, "Absorption–regeneration cycle for production of water from air-theoretical approach," Renew Energy, vol. 19, no. 4, pp. 625–635, 2000.

[5] A. H. Hassabou, "Experimental and Numerical Analysis of a PCM-Supported Humidification-Dehumidification Solar Desalination System," Institut für Energietechnik, München, 2011.

[6] T. Younos and K. E. Tulou, "Overview of desalination techniques," J Contemp Water Res Educ, vol. 132, no. 1, pp. 3–10, 2005.

[7] A. F. Muftah, K. Sopian, and M. A. Alghoul, "Performance of basin type stepped solar still enhanced with superior design concepts," Desalination, vol. 435, pp. 198–209, 2018.

[8] M. Shinde, R. Navthar, and S. M. Shinde, "Review on the types of solar stills," International Journal of Ambient Energy, vol. 43, no. 1, pp. 1420–1428, 2022.

[9] T.Suresh, A.Syed Abuthahir, A.Tamilazhagan, T.R.Sathishkumar, and S.Jegadeeswaran, "A Review on Modified Solar Stills with Thermal Energy Storage and Fins," International Research Journal of Engineering and Technology (IRJET), vol. 04, no. 10, Oct. 2017.

[10] A. F. Muftah, M. A. Alghoul, A. Fudholi, M. M. Abdul-Majeed, and K. Sopian, "Factors affecting basin type solar still productivity: A detailed review," Renewable and Sustainable Energy Reviews, vol. 32, pp. 430–447, 2014.

[11] P. M. Meena and A. P. Pannusa, "Different designs and parametric study of solar water distillation system," Int J Sci Eng Res, vol. 8, no. 4, 2017, [Online]. Available: http://www.ijser.org

[12] P. K. Ithape, S. B. Barve, and A. R. Nadgire, "CLIMATIC AND DESIGN PARAMETERS EFFECTS ON THE PRODUCTIVITY OF SOLAR STILLS: A REVIEW," 2017.

[13] S. W. Sharshir et al., "A mini review of techniques used to improve the tubular solar still performance for solar water desalination," Process Safety and Environmental Protection, vol. 124, pp. 204–212, 2019.

[14] J. C. Torchia-Núñez, J. Cervantes-de-Gortari, and M. A. Porta-Gándara, "Thermodynamics of a shallow solar still," Energy Power Eng, vol. 2014, 2014.

[15] Z. M. Omara, A. E. Kabeel, and A. S. Abdullah, "A review of solar still performance with reflectors," Renewable and Sustainable Energy Reviews, vol. 68, pp. 638–649, 2017.

[16] S. W. Sharshir, N. Yang, G. Peng, and A. E. Kabeel, "Factors affecting solar stills productivity and improvement techniques: a detailed review," Appl Therm Eng, vol. 100, pp. 267–284, 2016.

References

[17]   L. D. Jathar et al., "Effect of various factors and diverse approaches to enhance the performance of solar stills: a comprehensive review," J Therm Anal Calorim, vol. 147, no. 7, pp. 4491–4522, 2022.

[18]   A. Awasthi, K. Kumari, H. Panchal, and R. Sathyamurthy, "Passive solar still: recent advancements in design and related performance," Environmental Technology Reviews, vol. 7, no. 1, pp. 235–261, 2018.

[19]   P. Patel, A. S. Solanki, U. R. Soni, and A. R. Patel, "A review to increase the performance of solar still: make it multi-layer absorber," International Journal on Recent and Innovation Trends in Computing and Communication, vol. 2, no. 2, pp. 173–177, 2014.

[20]   M. O. Taiwo, "Improving the performance of solar stills using sun tracking," Master of Science Thesis, University of Strathclyde, UK, 2010.

[21]   T. R. Sathish Kumar, S. Jegadheeswaran, and P. Chandramohan, "Performance investigation on fin type solar still with paraffin wax as energy storage media," J Therm Anal Calorim, vol. 136, no. 1, pp. 101–112, 2019.

[22]   Pouya Jamzad, "Plate Heat Exchangers Using Natural Graphite Sheets," SIMON FRASER UNIVERSITY, 2017.

[23]   Y. Wang, H. Wei, and Z. Li, "Effect of magnetic field on the physical properties of water," Results Phys, vol. 8, pp. 262–267, 2018.

[24]   B. Patil, J. Hole, and S. Wankhede, "Parameters affecting productivity of solar still and improvement techniques: a detailed review," Int. J. Eng., Technol. Manage. Appl. Sci, vol. 5, no. 2, pp. 11–18, 2017.

[25]   S. A. Ghauri and M. S. Ansari, "Increase of water viscosity under the influence of magnetic field." American Institute of Physics, 2006.

[26]   Y. Fujimura and M. Iino, "The surface tension of water under high magnetic fields," J Appl Phys, vol. 103, no. 12, p. 124903, 2008.

[27]   Y.-Z. Guo et al., "Evaporation rate of water as a function of a magnetic field and field gradient," Int J Mol Sci, vol. 13, no. 12, pp. 16916–16928, 2012.

[28]   H. B. Amor, A. Elaoud, N. B. Salah, and K. Elmoueddeb, "Effect of Magnetic Treatment on Surface Tension and Water Evaporation (2017) Intern J Advan Ind Engin 5: 119-124."

[29]   M. Kuan, Y. Shakir, M. Mohanraj, Y. Belyayev, S. Jayaraj, and A. Kaltayev, "Numerical simulation of a heat pump assisted solar dryer for continental climates," Renew Energy, vol. 143, pp. 214–225, 2019.

[30]   R. S. Hansen, C. S. Narayanan, and K. K. Murugavel, "Performance analysis on inclined solar still with different new wick materials and wire mesh," Desalination, vol. 358, pp. 1–8, 2015.

[31]   A. E. Kabeel, K. Harby, M. Abdelgaied, and A. Eisa, "Performance of the modified tubular solar still integrated with cylindrical parabolic concentrators," Solar Energy, vol. 204, pp. 181–189, 2020.

[32]   M. Abu-Arabi, M. Al-harassed, H. Mousa, and Z. Alzghoul, "Theoretical investigation of solar desalination with solar still having phase change material and connected to a solar collector," Desalination, vol. 448, pp. 60–68, 2018.

[33]   D. W. Medugu and L. G. Ndatuwong, "Theoretical analysis of water distillation using solar still," International Journal of Physical Sciences, vol. 4, no. 11, pp. 705–712, 2009.

References

[34] O. Badran, "Theoretical analysis of solar distillation using active solar still," Int. J. of Thermal & Environmental Engineering, vol. 3, no. 2, pp. 113–120, 2011.

[35] K. S. Reddy and H. Sharon, "Performance Investigation of Combined Solar Desalination and Hot Water System; Performance Investigation of Combined Solar Desalination and Hot Water System," 2015.

[36] A.R. Abd Elbar, H. Hassan, and S. Ookawara, "Performance evaluation of a single-slope solar still with energy assessment techniques," Energy Conversion and Management, vol. 43, no. 4, pp. 523-537, 2002.

[37] A. K. Tiwari and G. N. Tiwari, "Annual performance analysis and thermal modelling of passive solar still for different inclinations of condensing cover," Int J Energy Res, vol. 31, no. 14, pp. 1358–1382, 2007.

[38] P. Dumka, A. Sharma, Y. Kushwah, A. S. Raghav, and D. R. Mishra, "Performance evaluation of single slope solar still augmented with sand-filled cotton bags," J Energy Storage, vol. 25, p. 100888, 2019.

[39] H. K. Jani and K. v Modi, "Experimental performance evaluation of single basin dual slope solar still with circular and square cross-sectional hollow fins," Solar Energy, vol. 179, pp. 186–194, 2019.

[40] M. Khandagre, B. Gupta, and J. Bhalavi, "Design parameters of Solar Still including application of phase change materials: A Review," 2019.

[41] K. Hidouri and M. Mohanraj, "Thermodynamic analysis of a heat pump assisted active solar still," Desalination Water Treat, vol. 154, pp. 101–110, 2019.

[42] P. Dumka, Y. Kushwah, A. Sharma, and D. R. Mishra, "Comparative analysis and experimental evaluation of single slope solar still augmented with permanent magnets and conventional solar still," Desalination, vol. 459, pp. 34–45, 2019.

[43] S. W. Sharshir, G. Peng, L. Wu, F. A. Essa, A. E. Kabeel, and N. Yang, "The effects of flake graphite nanoparticles, phase change material, and film cooling on the solar still performance," Appl Energy, vol. 191, pp. 358–366, 2017.

[44] H. Panchal, P. Patel, N. Patel, and H. Thakkar, "Performance analysis of solar still with different energy-absorbing materials," International Journal of Ambient Energy, vol. 38, no. 3, pp. 224–228, 2017.

[45] A. K. Kaviti, A. Yadav, and A. Shukla, "Inclined solar still designs: A review," Renewable and Sustainable Energy Reviews, vol. 54, pp. 429–451, 2016.

[46] W. M. Alaian, E. A. Elnegiry, and A. M. Hamed, "Experimental investigation on the performance of solar still augmented with pin-finned wick," Desalination, vol. 379, pp. 10–15, 2016.

[47] M. Montazeri, A. Banakar, and B. Ghobadian, "Enhancement of cascade solar still productivity with sloping absorber plate," Maejo International Journal of Science and Technology, vol. 11, no. 1, p. 35, 2017.

[48] M. C. Amiri and A. A. Dadkhah, "On reduction in the surface tension of water due to magnetic treatment," Colloids Surf A Physicochem Eng Asp, vol. 278, no. 1–3, pp. 252–255, 2006.

[49] R. Cai, H. Yang, J. He, and W. Zhu, "The effects of magnetic fields on water molecular hydrogen bonds," J Mol Struct, vol. 938, no. 1–3, pp. 15–19, 2009.

[50] E. Chibowski, A. Szcześ, and L. Hołysz, "Influence of magnetic field on evaporation rate and surface tension of water," Colloids and Interfaces, vol. 2, no. 4, p. 68, 2018.

[51] L. Holysz, A. Szczes, and E. Chibowski, "Effects of a static magnetic field on water and electrolyte solutions," J Colloid Interface Sci, vol. 316, no. 2, pp. 996–1002, 2007.

References

[52]   X. Pang and B. Deng, "Investigation of changes in properties of water under the action of a magnetic field," Science in China Series G: Physics, Mechanics and Astronomy, vol. 51, no. 11, pp. 1621–1632, 2008.

[53]   H. ben Hamouda et al., "Neonatal duodenal obstruction due to a preduodenal portal vein associated with intestinal malrotation: A case report," Pediatr Pol, vol. 92, no. 5, pp. 623–626, 2017.

[54]   S. J. P. Gnanaraj and V. Velmurugan, "An experimental study on the efficacy of modifications in enhancing the performance of single basin double slope solar still," Desalination, vol. 467, pp. 12–28, 2019.

[55]   S. Nazari, H. Safarzadeh, and M. Bahiraei, "Performance improvement of a single slope solar still by employing thermoelectric cooling channel and copper oxide nanofluid: an experimental study," J Clean Prod, vol. 208, pp. 1041–1052, 2019.

[56]   M. S. Yousef, H. Hassan, S. Kodama, and H. Sekiguchi, "An experimental study on the performance of single slope solar still integrated with a PCM-based pin-finned heat sink," Energy Procedia, vol. 156, pp. 100–104, 2019.

[57]   R. Dhivagar, M. Mohanraj, K. Hidouri, and Y. Belyayev, "Energy, exergy, economic and enviro-economic (4E) analysis of gravel coarse aggregate sensible heat storage-assisted single-slope solar still," J Therm Anal Calorim, vol. 145, pp. 475–494, 2021.

[58]   R. Dhivagar and M. Mohanraj, "Performance improvements of single slope solar still using graphite plate fins and magnets," Environmental Science and Pollution Research, vol. 28, pp. 20499–20516, 2021.

[59]   D. G. H. Samuel, P. K. Nagarajan, R. Sathyamurthy, S. A. El-Agouz, and E. Kannan, "Improving the yield of fresh water in conventional solar still using low cost energy storage material," Energy Convers Manag, vol. 112, pp. 125–134, 2016.

[60]   S. A. El-Agouz, "Experimental investigation of stepped solar still with continuous water circulation," Energy Convers Manag, vol. 86, pp. 186–193, 2014.

[61]   M. S. K. Tarawneh, "Effect of water depth on the performance evaluation of solar still," JJMIE, vol. 1, no. 1, 2007.

[62]   A. E. Kabeel, S. W. Sharshir, G. B. Abdelaziz, M. A. Halim, and A. Swidan, "Improving performance of tubular solar still by controlling the water depth and cover cooling," J Clean Prod, vol. 233, pp. 848–856, 2019.

[63]   A. A. Aljubouri, "Design and manufacturing of single sloped solar still: Study the effect of inclination angle and water depth on still performance," Al-Nahrain Journal of Science, vol. 20, no. 2, pp. 60–70, 2017.

[64]   H. Panchal, "Performance investigation on variations of glass cover thickness on solar still: experimental and theoretical analysis," Technology and Economics of Smart Grids and Sustainable Energy, vol. 1, pp. 1–11, 2016.

[65]   H. N. Panchal and P. K. Shah, "Effect of varying glass cover thickness on performance of solar still: in a winter climate conditions," International Journal of Renewable Energy Research, vol. 1, no. 4, pp. 212–223, 2012.

[66]   A. O. Edeoja, F. Unom, and J. A. Edeoja, "Investigation of the effect of cover thickness on the yield of a single basin solar still under Makurdi climate," International Journal of Engineering Science Invention, vol. 14, pp. 131–138, 2015.

References

[67]   A. S. Nafey, M. Abdelkader, A. Abdelmotalip, and A. A. Mabrouk, "Solar still productivity enhancement," Energy Convers Manag, vol. 42, no. 11, pp. 1401–1408, 2001.

[68]   F. L. Rashid, A. S. Shareef, and H. F. Alwan, "Performance enhancement of a new passive solar still design for water desalination," Journal of Mechanical Engineering Research and Developments, vol. 43, no. 3, pp. 75–85, 2020.

[69]   Z. Tigrine, H. Aburideh, F. Chekired, D. Belhout, and D. Tassalit, "New solar still with energy storage: application to the desalination of groundwater in the Bou-Ismail region," Water Supply, vol. 21, no. 8, pp. 4627–4640, 2021.

[70]   H. Panchal and P. Shah, "Modelling and verification of single slope solar still using ANSYS-CFX," International Journal of Energy and Environment, vol. 2, no. 6, pp. 985–998, 2011.

[71]   E. B. Moustafa, A. H. Hammad, and A. H. Elsheikh, "A new optimized artificial neural network model to predict thermal efficiency and water yield of tubular solar still," Case Studies in Thermal Engineering, vol. 30, p. 101750, 2022.

[72]   D. Mevada et al., "Investigation and performance analysis of solar still with energy storage materials: An energy-exergy efficiency analysis," Case Studies in Thermal Engineering, vol. 29, p. 101687, 2022.

[73]   R. N. Taqi, Z. A. Abdul Redha, and F. I. Mustafa, "Experimental Investigation of a Single Basin-Single Slope Solar Still Coupled with Evacuated Tube Solar Collector," J. Eng, vol. 27, pp. 16–34, 2021.

[74]   A. S. Abdullah, "Improving the performance of stepped solar still," Desalination, vol. 319, pp. 60–65, 2013.

[75]   V. Velmurugan, C. K. Deenadayalan, H. Vinod, and K. Srithar, "Desalination of effluent using fin type solar still," Energy, vol. 33, no. 11, pp. 1719–1727, 2008.

[76]   K. v Modi, S. R. Maurya, J. H. Parmar, A. B. Kalsariya, and P. B. Panasara, "An experimental investigation of the effectiveness of partially and fully submerged metal hollow-fins and jute cloth wick-fins on the performance of a dual-basin single-slope solar still," Clean Eng Technol, vol. 6, p. 100392, 2022.

[77]   K. M. Bataineh and M. A. Abbas, "Performance analysis of solar still integrated with internal reflectors and fins," Solar Energy, vol. 205, pp. 22–36, 2020.

[78]   A. Seyfi, R. Afzalzadeh, and A. Hajnorouzi, "Increase in water evaporation rate with increase in static magnetic field perpendicular to water-air interface," Chemical Engineering and Processing-Process Intensification, vol. 120, pp. 195–200, 2017.

[79]   A. Szcześ, E. Chibowski, L. Hołysz, and P. Rafalski, "Effects of static magnetic field on water at kinetic condition," Chemical Engineering and Processing: Process Intensification, vol. 50, no. 1, pp. 124–127, 2011.

[80]   M. Kamruzzaman, M. Wahiduzzaman, M. M. Alam, and L. Djenidi, "The effects of magnetic field on the fluid flow through a rotating straight duct with large aspect ratio," Procedia Eng, vol. 56, pp. 239–244, 2013.

[81]   B. K. Patil and S. Dambal, "Design and experimental performance analysis of solar still using phase changing materials and sensible heat elements," IJRMET, vol. 6, pp. 144–149, 2016.

[82]   André Bakker, " Applied computational fluid dynamics, mesh generation, computational fluid dynamics lectures. ," Pennsylvania, USA., 2006.

References

[83]   Solar Engineering of Thermal Processes, Third Edition by John A. Duffie and William A. Beckman.

Appendix (A)

A. The specification of drinking water:

A1. The standard specification for sater (IQS/417/2001) (ICS:13.060.20)

Table (A.1) The water standard specification

طرق الفحص*	المتطلبات الحد الاقصى ملغم/ لتر	الخصائص
وفق دليل رقم ٧٠٣	١...٠	الزرنيخ
وفق دليل رقم ٧٠٣	٣...٠	الكادميوم
وفق دليل رقم ٨٢٠	٥...٠	الكروم سداسي التكافؤ
راجع (٥-٩)	٢...٠	السيانيد
وفق دليل رقم ٥٤٧	١.٠	الفلوريد
وفق دليل رقم ٧٠٣	١...٠	الرصاص
وفق دليل رقم ٨٢٠	١....٠	الزئبق
وفق دليل رقم ٥٤٧	٥٠	النترات NO_3
راجع (٥-١٠)	٣	النتريت NO_2
وفق دليل رقم ٧٠٣	١...٠	السيلينيوم
راجع (٥-٧)	٢.٠	الالمنيوم
وفق دليل رقم ٦٧١	٢٥٠	الكلوريد
راجع (٥-١١)	١.٠	النحاس
راجع (٥-١٢)	٥٠٠ مسحوبة كـ $CaCo_3$	العسرة الكلية
وفق دليل رقم ٧٢٨	٣.٠	الحديد
وفق دليل رقم ٧٥٣	١.٠	المغنيز
راجع (٥-٧)	٢٠٠	الصوديوم
وفق دليل رقم ٢٠٥/ ج١	١٠٠٠	المواد الصلبة الذائبة
وفق دليل رقم ٦٧١	٢٥٠	الكبريتات
راجع (٥-١١)	٣	الزنك
وفق دليل رقم ٧٥٥	٥٠	الكالسيوم
راجع (٥-٧)	٥٠	المغنيسيوم
وفق دليل رقم ٨٢٠	٧.٠	الباريوم
راجع (٥-١١)	٢...٠	النيكل

٢-٢-١ المواد اللاعضوية

الجدول (٢) الخصائص الكيميائية (المواد اللاعضوية)

A2. Distilled sater tests

نتائج الفحوصات الكيمياوية

نوع العينة :   الجهه المستفيدة :

الموقع :   أسم جامع العينة :

Sample	طالب ماجستير ماء تقطير	طالب ماجستير ماء اساله		Unit
Date	12/08/2021	12/08/2021		
Temp.	31.5	30.80		C°
PH	7.41	7.90		
E.C	421	945		µs
T.D.S	27	618		mg/l
Turb.	3.5	43.55		NTU
T.S.S				mg/l
Alk. as CO₃⁻²				mg/l
C.O.D				mg/l
B.O.D				mg/l
T.H as caco₃	20	432		mg/l
Ca⁺² as co₃⁻²	3.38	138		mg/l
Mg⁺²	3	21		mg/l
Cl⁻				mg/l
SO₄⁻²	0.72	316.17		mg/l
NO₃⁻	13.67	6.84		mg/l
Na+	1.5	73.2		mg/l
K+	0.1	4.1		mg/l
Li+	0	0.1		mg/l
D.O				mg/l
PO₄⁻³				mg/l
Al				mg/l
O&G				mg/l
NH₃				mg/l

م.ز بكتريولوجي جنان حمود شنان

Appendix (B)

The calibration of instruments used in the thesis

B1.   The   temperature   meter,   Thermocouple,   and   solar   power   meter

REPUBLIC OF IRAQ

MINISTRY OF SCIENCE & TECHNOLOGY

RENEWABLE ENERGY DIRECTORATE

وزارة العلوم و التكنولوجيا
Ministry Of Science & Technology

جمهورية العراق

وزارة العلوم والتكنولوجيا

دائرة الطاقات المتجددة

العدد: ط م ٢٠٩

التأريخ: ١٩/ ٤ / ٢٠٢١

إلى/ جامعة كربلاء-كلية الهندسة

م/ معايرة أجهزة قياس

تحية طيبة

إشارة إلى كتابكم المرقم بالعدد (د.ع/١١٤٦/٦ في ٢٠٢١/٤/١٥)، بخصوص إبداء المساعدة لطالب الدراسات العليا / الماجستير (محمد محسن جاسم)، تم إجراء المعايرة للأجهزة والمعدات المدرجة تفاصيلها في أدناه في مختبراتنا بتأريخ ٢٠٢١/٤/١٩ وهي جاهزة للاستخدام.

شاكرين تعاونكم معنا .. مع فائق التقدير

الأجهزة التي تم معايرتها:

١-جهاز قياس شدة الإشعاع الشمسي العدد / ١

٢-جهاز قياس درجة الحرارة العدد /١

٣-جهاز قياس سرع الرياح العدد /١

٤-متحسس درجة الحرارة T/C k طول ١ متر العدد /١

دائرة
الطاقات المتجددة

وزارة العلوم و التكنولوجيا
Ministry Of Science & Technology

د. فلاح إبراهيم العطار

ع/المدير العام

٢٠٢١/٤/٩

نسخة منه إلى/

مركز تخطيط وإدارة الطاقة مع الأولوات .... للتفضل بالاطلاع مع التقدير

قسم التخطيط والمتابعة .... للتفضل بالاطلاع مع التقدير

·

3

Appendix C

C1. Sample of calculations

It is possible to take one of the numerical calculations as an example of how to find the values of the variables in the energy balancing equation, as well as the productivity and efficiency values, where the solution starts from the energy balancing equation, which is as follows:

$$q_{ga} = q_r + q_c + q_e + \alpha_g H$$

To find the value of q_{ga} from its equation:

$$q_{ga} = h_{ga}(T_g - T_a) + F_{g\text{-sky}}\, \sigma \left[(T_g + 273)^4 - (T_a + 273)^4 \right]$$

$$h_{ga} = a + b(v)^n$$

Where a=5.61, b= 1.09, n=1 for smooth surface of glass

V=21.66 km/hr. at 12:00 pm

Then $h_{ga} = 5.61 + 1.09(21.66)^1 = 29.22$ W/ m²°C

For Tg=67°C and Ta=41°C at 12:00 pm

So

$$q_{ga} = 29.22(67 - 41) + 0.94 * 5.67\, x\, 10^{-8} \left[(67 + 273)^4 - (41 + 273)^4 \right]$$

$$= 953.83 W/m2$$

$$q_C = ka \left(\frac{T_s - T_g}{\Delta y} \right)$$

$$T_s = T_b + \alpha_b \tau_g H \left(\frac{\delta_b}{2k_b}\right)$$

Where Tb= 106°C, H= 989 W/ m²at 12:00 pm

Then T_s=106+0.87*0.87*989*$\left(\frac{0.005}{2*204.2}\right)$=106.86°C

And q_C=0.03*$\left(\frac{106.86-67}{0.15}\right)$ =7,97 W/ m²

$$q_r = F_{bg}\sigma \left[(T_s + 273)^4 - (T_g + 273)^4\right]$$

Then $q_r = 0.9* 5.67$ x 10^-8 * [(106.86 + 273)^4 − (67 + 273)^4] =380,55 W/ m²

$\alpha_g H = 0,12 * 989 = 118,68$ W/ m²

Therefore, it is possible to find the value of q_e from the energy balance equation:

$$q_{ga} = q_r + q_c + q_e + \alpha_g H$$

953,83 = 380,55 + 7,97 + q_e+ 118,68

Then q_e= 446,63 W/ m²

The instantaneous productivity can be calculated from the following equation:

$$p = \frac{q_e}{L_b} \quad \text{where} \quad L_b = 10^3(2501.67 - 2.389T_b)$$

Then L_b= $10^3(2501.67 - 2.389106)$ =10^3 * 2245,7 J/kg

And $p = \frac{446.63}{10^3 * 2245.7}$ = 72 ml/ m².hr

The efficiency of the instantaneous system is according to the following equation:

$$\eta = \frac{q_e}{H} \ldots\ldots\ldots\ldots = \frac{446.63}{989} = 45\%$$

Table (C.1) The values of the constants used in the equations **[Ref 83]**

Design parameter	Symbol	Value
Constants	a	5.61
	b	1.09
	n	1
shape factor between glass and ambient	Fg-sky	0.94
shape factor between glass and bed	Fbg	0.9
glass absorptivity	α g	0.12
bed absorptivity	α b	0.87
Boltzmann constant	σ	5.67 x 10^-8
thermal conductivity of air	Ka	0.03 W/m-°C
thermal conductivity of galvanized	Kb	204.2 W/m-°C
the thickness of the layered absorbent	δb	0.005 m
glass transmissivity	τg	0.87
the thickness of the air gap for experiments (1,2,3)	Δy	0.15 m
the thickness of the air gap for experiments (3,4,5)	Δy	0.5 m

Appendix D

D1. Calculations table of MSST$_3$

Time	H, w m^2	V, km/hr	T ambient, C	P, experimental	P, theoretical	η, %	qc, wm^2	qr,w m^2	qe, w m^2	η total, %
08am	914	10.8	34	20	19	14	0.79	26.25	124	30
09am	938	10.8	37	20	24	17	2.81	105.57	155	
10am	963	10.8	39	30	33	22	3.54	142.3	212	
11am	988	10.8	40	45	46	3	4.77	209.3	292	
12pm	1002	10.8	41	54	55	34	5.39	249	345	
01pm	979	10.8	42	60	61	39	5.35	252	381	
02pm	953	10.8	42	65	63	42	5.25	248	397	
03pm	875	10.8	42	55	57	42	4.33	194	364	
04pm	673	10.8	43	36	35	33	3.56	147	222	
05pm	572	10.83	42	30	28	32	1.61	60	186	

Time	H, w/ m^2	V, km/hr	T ambient, C	P, experimental	P, theoretical	η, %	qc, w m^2	qr, w m^2	qe, w m^2	η total, %
08am	900	20.7	32.3	48.96	46.55	34.2	1.9	68.4475	308.4	42.24
09am	934	20.7	35.15	57.6	48.45	34.2	2.40	89.1005	319.008	

10am	965	20.7	36.1	61.44	57	3.8	5.04	210.482	367.5648	
11am	983	20.7	37.05	68.16	61.75	39.9	7.11	324.843	391.8144	
12pm	989	20.7	38.95	77.76	68.4	42.7	7.57	361.5225	428.7648	
01pm	914	20.7	39.9	67.2	76.95	53.2	6.63	312.4265	489.6768	
02pm	854	17.3	39.9	65.28	66.5	48.4	6.21	289.9685	421.4976	
03pm	784	17.3	39.9	43.2	64.6	52.2	5.99	275.8515	411.696	
04pm	686	17.3	39.9	38.4	43.7	40.8	3.31	132.848	282.1632	
05pm	556	17.3	39.9	26.88	37.05	43.7	0.28	86.45	244.8576	

D2. Calculations table of FLP$_{Rect.}$

Time	H, w m^2	V, km/hr	T ambient, C	P, experimental	P, theoretical	η, %	qc, w m^2	qr, w m^2	qe, w m^2	η total, %
08am	880	21.0	32.3	43.2	46.9	24.7	0.063	55.79	226.8	44
09am	885	21.0	34.2	52.8	57.5	29.8	0.0105	70.68	275.4	
10am	934	21.0	35.15	96	101.5	47.3	0.8925	112.7	467.64	

Time	H	V	T ambient	P exp	P theo	η	qc	qr	qe	η total
11am	951	21.0	38	120	124.2	56.6	1.3965	196.5	562.68	
12pm	965	17.5	38.95	124.8	128.7	56.6	1.6275	243.	576.72	
01pm	935	17.5	39.9	115.2	124.2	56.6	1.68	253.	560.52	
02pm	870	17.5	39.9	105.6	112.1	55.6	1.848	279.	506.52	
03pm	817	17.5	40.85	91.2	95.4	50.4	1.113	153.9	432	
04pm	727	17.5	40.85	48	53.0	31.9	0.651	82.1	244.08	
05pm	601	17.5	39.9	38.4	42.4	31.9	0.273	32.2	199.8	

D3. Calculations table of MSS$_{T3}$+FLP$_{Rect.}$

Time	H, w m^2	V, km/hr	T ambient, C	P, experimental	P, theoretical	η, %	qc, w m^2	qr, w m^2	qe, w m^2	η total, %
08am	747.74	6.7	32.98	42.75	46.55	39.7	0.874	119.04	310.66	47.47
09am	867.3	6.7	34.92	52.25	56.05	40.7	1.197	179.52	364.56	
10am	915.32	6.7	35.89	66.5	60.8	41.7	1.102	167.04	395.92	
11am	931.98	13.	38.8	71.25	68.4	46.5	1.311	195.84	448.84	

12pm	945.7	13.	39.77	76	80.75	53.3	1.349	210.24	523.32	
01pm	916.3	13.	40.74	71.25	73.15	50.4	1.1495	172.8	479.22	
02pm	852.6	13.5	40.74	66.5	71.25	53.3	1.0735	159.36	471.38	
03pm	800.66	13.5	41.71	66.5	64.6	51.4	0.874	125.76	425.32	
04pm	614.46	13.5	41.71	42.75	43.7	45.5	0.8835	120.96	288.12	
05pm	392.98	6.7	40.74	28.5	26.6	44.6	0.722	96	181.3	

الخلاصة

تم استخدام نظام معدل تم تصميمه وإنتاجه محليًا في التحقيق الحالي كإعداد تجريبي. المكون الرئيسي للنظام هو الجهاز الشمسي للتقطير، بالإضافة إلى المكونات الإضافية مثل أدوات القياس. تم إجراء التحقيق بشكل عددي باستخدام برنامج ANSYS. تم استخدام التقطير الشمسي بوجود المغناطيسات والزعانف لتحسين أداء الجهاز الشمسي للتقطير. تم إجراء التحقيقات التجريبية والرياضية لقياس درجات حرارة الماء وقاعدة الجهاز والبخار وغطاء الزجاج الداخلي والخارجي للجهاز. بالإضافة إلى كفاءة وإنتاجية الجهاز. أظهرت نتائج التجارب والتحليل الرياضي أن جميع الطرق المستخدمة في هذه الدراسة قد تحسن أداء الجهاز الشمسي للتقطير. يمكن زيادة درجة حرارة الماء في الجهاز لتوليد البخار بشكل أسرع. كان استخدام الزعانف أفضل من استخدام المغناطيسات في تحقيق هدف البحث. في الوقت نفسه، كان لاستخدام المغناطيسات دور أقل مقارنة بالزعانف. الأهم من ذلك، يمكن أن يرفع استخدام جميع هذه التقنيات مجتمعة (التقطير الشمسي مع الزعانف والزعانف مع المغناطيسات) درجة حرارة الماء وقاعدة الجهاز ودرجة حرارة البخار ودرجة حرارة الغطاء الداخلي للجهاز بنسبة تقدر بحوالي (24، 26، 34 و55) ٪. وبالتالي، يمكن أن يحسن استخدام جميع التقنيات مجتمعة كفاءة وإنتاجية الجهاز الشمسي للتقطير بنسبة 33٪، 38٪، و55٪ على التوالي مقارنة بالحالة العادية للجهاز الشمسي للتقطير (بدون أي تعديل). لإظهار درجة الموثوقية للبرنامج المستخدم في العمل الحالي ودقة وصحة النتائج العددية في هذه الرسالة، تم التحقق من النتائج عن طريق مقارنتها بالدراسات السابقة في نفس المجال وتحت ظروف مشابهة تقريبًا. تم الاستنتاج أن البرنامج تم بناؤه بشكل صحيح وأعطى نتائج مقبولة إلى حد كبير. وكانت نسبة الخطأ الأعلى بينها 10٪، وهو مقبول نسبيًا. من خلال مقارنة النتائج التجريبية للدراسة الحالية مع النتائج العددية، لوحظ وجود توافق جيد بينهما. وهذا يشير إلى أن العمل الحالي تم تنفيذه وفقًا للخطة المخطط لها وبطريقة تضمن تجنب الأخطاء قدر الإمكان. وتم تحقيق ذلك عن طريق تكرار الاختبارات التجريبية عدة مرات وأيام حتى تم الحصول على نتائج مستقرة وواقعية.

تحقيق تجريبي وعددي لتأثير زعانف الغرافيت والمغناط على الأداء الحراري لجهاز التبخير الشمسي ذو الميل الواحد

من قبل

علي باني خصاف

(بكالوريوس هندسة ميكانيكية/ الجامعة التكنلوجيا)

تحت أشراف

أ.د. عباس ساهي شريف   و   **أ.م. د. حيدر جبار كرجي**